

## ENDF/B-VII.1 Neutron Cross Section Data Testing with Critical Assembly Benchmarks and Reactor Experiments

A. C. Kahler,<sup>1,\*</sup> R. E. MacFarlane,<sup>1</sup> R. D. Mosteller,<sup>1</sup> B. C. Kiedrowski,<sup>1</sup> S. C. Frankle,<sup>1</sup> M. B. Chadwick,<sup>1</sup> R. D. McKnight,<sup>2</sup> R. M. Lell,<sup>2</sup> G. Palmiotti,<sup>3</sup> H. Hiruta,<sup>3</sup> M. Herman,<sup>4</sup> R. Arcilla,<sup>4</sup> S. F. Mughabghab,<sup>4</sup> J. C. Sublet,<sup>5</sup> A. Trkov,<sup>6</sup> T. H. Trumbull,<sup>7</sup> and M. Dunn<sup>8</sup>

<sup>1</sup>Los Alamos National Laboratory, Los Alamos, NM 87545, USA

<sup>2</sup>Argonne National Laboratory, Argonne, IL 60349, USA

<sup>3</sup>Idaho National Laboratory, Idaho Falls, ID 83415, USA

<sup>4</sup>Brookhaven National Laboratory, Upton, NY 11973, USA

<sup>5</sup>Culham Center for Fusion Energy, Abingdon, OX14 3DB, UK

<sup>6</sup>Jozef Stefan Institute, Jamova 39, 1000 Ljubljana, Slovenia

<sup>7</sup>Knolls Atomic Power Laboratory, Schenectady, NY 12309, USA

<sup>8</sup>Oak Ridge National Laboratory, Oak Ridge, TN 37831, USA

(Received 9 August 2011; revised received 21 September 2011; accepted 17 October 2011)

The ENDF/B-VII.1 library is the latest revision to the United States' Evaluated Nuclear Data File (ENDF). The ENDF library is currently in its seventh generation, with ENDF/B-VII.0 being released in 2006. This revision expands upon that library, including the addition of new evaluated files (was 393 neutron files previously, now 423 including replacement of elemental vanadium and zinc evaluations with isotopic evaluations) and extension or updating of many existing neutron data files. Complete details are provided in the companion paper [1]. This paper focuses on how accurately application libraries may be expected to perform in criticality calculations with these data. Continuous energy cross section libraries, suitable for use with the MCNP Monte Carlo transport code, have been generated and applied to a suite of nearly one thousand critical benchmark assemblies defined in the International Criticality Safety Benchmark Evaluation Project's International Handbook of Evaluated Criticality Safety Benchmark Experiments. This suite covers uranium and plutonium fuel systems in a variety of forms such as metallic, oxide or solution, and under a variety of spectral conditions, including unmoderated (i.e., bare), metal reflected and water or other light element reflected. Assembly eigenvalues that were accurately predicted with ENDF/B-VII.0 cross sections such as unmoderated and uranium reflected <sup>235</sup>U and <sup>239</sup>Pu assemblies, HEU solution systems and LEU oxide lattice systems that mimic commercial PWR configurations continue to be accurately calculated with ENDF/B-VII.1 cross sections, and deficiencies in predicted eigenvalues for assemblies containing selected materials, including titanium, manganese, cadmium and tungsten are greatly reduced. Improvements are also confirmed for selected actinide reaction rates such as <sup>236</sup>U, <sup>238,242</sup>Pu and <sup>241,243</sup>Am capture in fast systems. Other deficiencies, such as the overprediction of Pu solution system critical eigenvalues and a decreasing trend in calculated eigenvalue for <sup>233</sup>U fueled systems as a function of Above-Thermal Fission Fraction remain. The comprehensive nature of this critical benchmark suite and the generally accurate calculated eigenvalues obtained with ENDF/B-VII.1 neutron cross sections support the conclusion that this is the most accurate general purpose ENDF/B cross section library yet released to the technical community.

	<b>Contents</b>		<b>II. DATA TESTING</b>	<b>2</b>
<b>I. INTRODUCTION</b>		<b>2</b>	A. NJOY Processing	2
			B. ICSBEP Benchmark Overview	3
			C. Fast Systems	3
			D. Thermal Systems	9
			1. Solution Systems	9
			2. Low Enriched Lattice Systems	12
			E. <sup>233</sup> U/ <sup>232</sup> Th and Systems with Zr	15

\*Electronic address: [akahler@lanl.gov](mailto:akahler@lanl.gov)

F. Argonne ZPR Systems	16
1. Criticality Measurements	17
2. Beta-effective ( $\beta_{eff}$ ) Measurements	18
3. Measurements of Sodium Void Worth ( $\rho_{Na}$ )	19
4. Worth Measurements of Control Rods and Control Positions	20
G. Reaction Rate Studies	20
H. Rossi $\alpha$	25
I. Bethe Sphere Tritium-Production	26
<b>III. CONCLUSIONS</b>	27
<b>Acknowledgments</b>	27
<b>References</b>	27
<b>Appendix A</b>	28
<b>Appendix B</b>	30

## I. INTRODUCTION

The ENDF/B-VII.1 cross section library represents the latest advance in the United States' evaluated nuclear data file. This library builds upon the ENDF/B-VII.0 library that was released in 2006 [2]. Improvements in basic nuclear data that are embodied in this new library are discussed in the companion article to this paper [1]. This paper expands upon that report to describe how these new data perform when used in a Monte Carlo application library. Application libraries have been independently created with the NJOY Nuclear Data Processing System [3] by several of the co-authors and subsequently used with the continuous energy Monte Carlo MCNP code [4] in a variety of calculations to test the accuracy of the underlying nuclear data. These calculations are described below.

A broad outline of this paper begins with an overview of application library generation; a process used for all 423 of the ENDF/B-VII.1 neutron files whether they appear in a subsequent benchmark model calculation or not. The majority of data testing performed herein utilize critical benchmark models defined in the International Criticality Safety Benchmark Evaluation Project (ICSBEP) Handbook [5]. Additional calculations to predict measured reaction rate ratios and other selected reactor parameters are also documented. These calculations provide a broad test of the underlying nuclear data, as they involve a variety of fuel (fissile) nuclides under a variety of conditions (bare, moderated, and reflected). Specific benchmark attributes are given in subsequent sections.

There are notable improvements in selected benchmarks with ENDF/B-VII.1 cross sections compared to use of ENDF/B-VII.0 cross sections. Among these are reflected systems containing significant quantities of titanium and tungsten. Resolution of other long-standing biases such as the historical overprediction of Pu solution system eigenvalues remain for a future ENDF release. De-

tails of the successes, both new and continuing, for the ENDF/B-VII.1 library follow.

## II. DATA TESTING

Critical eigenvalue calculations, and in selected instances, reaction rate calculations have been performed for nearly one thousand critical benchmark assemblies. It is neither practical, nor necessary, to describe these benchmarks in detail, nor to analyze the calculated results of every benchmark in order to assess the ENDF/B-VII.1 cross section library. Rather, this section is divided into logical partitions that describe (i) the processing of these data into an application library for MCNP with NJOY; (ii) an overview of the International Criticality Safety Benchmark Evaluation Project Handbook for which most of the benchmarks are described; (iii) several sections of benchmarks grouped by common attributes such as spectrum or fuel type; (iv) specialized calculations that yield C/E results for reaction rates or Rossi- $\alpha$ .

### A. NJOY Processing

The NJOY Nuclear Data Processing System has been used to create ACE formatted files for all neutron evaluations of the ENDF/B-VII.1 library. While significant additional quality checks are needed before such files are formally released to the broader technical community, sufficient internal checking has been done to allow their use in the validation calculations of ICSBEP benchmarks with MCNP that follow.

NJOY is a modular program, with a variety of subprograms each performing a unique task in a multistep sequence that starts from the original ENDF-formatted file and ends with an ACE file suitable for use in a MCNP calculation. The ENDF/B-VII.1 files processed here used NJOY's RECONR, BROADR, UNRESR, HEATR, PURR, GASPR and ACER modules. RECONR is used to create a unionized energy grid for all cross sections of a given evaluated file. If resolved resonance parameters are present, they are expanded into the appropriate pointwise cross sections, typically scattering, capture and possibly fission. Also, with the Limited Reich-Moore (LRF=7) format, there may be resonant charged particle and/or inelastic scattering cross sections. In the ENDF/B-VII.1 library  $^{35}\text{Cl}$  uses the LRF=7 format. Linear interpolation is used for intervening energy points, and the density of energy points is sufficient to assure that this interpolation is accurate to within a user specified tolerance. For the files generated herein that tolerance is 0.1%. The output from RECONR is passed to BROADR, where the cross sections are Doppler broadened to 293.6 °K. NJOY allows the user to specify a different linear interpolation tolerance as part of its BROADR input, but in most instances (including here) we choose to maintain the same linear interpolation tolerance as used in RECONR. UNRESR and

HEATR which follow are not necessarily needed for the MCNP transport calculations performed herein, but they are important and necessary steps to create a complete processed file and so we include these steps in our generic NJOY processing. PURR is used to create unresolved resonance probability tables. Our standard PURR job uses 32 probability bins and computes 64 ladders. GASPR is used to accumulate the various cross sections that produce charged particles (p, d, t,  $^3\text{He}$  and  $\alpha$ ) into a single cross section. It is not necessary for transport calculations, but is often used for calculating production of the particle of interest. Finally, ACER is used to accumulate the various quantities into MCNP's ACE format.

## B. ICSBEP Benchmark Overview

As noted in the Introduction, the vast majority of benchmark results presented herein come from models defined by the International Criticality Safety Benchmark Evaluation Project in the International Handbook of Evaluated Criticality Safety Benchmark Experiments. Evaluations in this Handbook are defined using an XXX-YYY-ZZZ-aaa.b nomenclature system. The XXX designator defines the fuel system and includes Pu for  $^{239}\text{Pu}$  fueled systems, and HEU, IEU and LEU for highly-enriched, intermediate-enriched and low-enriched  $^{235}\text{U}$  fuel systems. Highly enriched systems contain at least 90%  $^{235}\text{U}$ , low-enriched systems contain less than 10%  $^{235}\text{U}$  while intermediate-enriched systems cover the intervening range. Other XXX designators include U233 for  $^{233}\text{U}$  fueled systems and MIX which is used for systems with both  $^{235}\text{U}$  and  $^{239}\text{Pu}$ . The YYY designator defines the chemical form of the fuel, with MET meaning a metal system, SOL being a solution and COMP a compound. ZZZ is used to define the average fission energy. FAST is used when more than 50% of the fissions occur above 100 keV and THERM is used if more than 50% of the fissions occur below 0.625 eV. INTER is used when 50% or more of the fissions occur between these energy limits, and MIXED is used when no energy interval has 50% or more fissions. Finally, aaa.b is a simple numerical index, and .b represents one of the individual case numbers when multiple experiments are described in a single evaluation. As it can be unwieldy to cite the complete evaluation name, we often can use only the first initial of each designator to uniquely specify a benchmark; for example the HEU-MET-FAST-001 benchmark, is abbreviated HMF1 in this paper.

The ICSBEP Handbook contains hundreds of evaluated experiments, representing several thousand critical configurations. The Handbook is re-issued annually and usually contains several dozen new evaluations in each issue. It is neither necessary, nor practical, to perform calculations for all of these benchmarks to validate the ENDF/B-VII.1 library. However, over the years we have created MCNP models for nearly one thousand of these benchmarks. Many are discussed in the ensuing sections,

and we summarize the calculated eigenvalues for all of them in Appendix B.

One particularly valuable aspect of the Handbook is the occurrence of many related experiments that utilize similar or identical materials with only small changes. While the information gleaned from analyzing any individual experiment is valuable in its own right, the added information obtained from extracting correlated information over a wider range of parameters allows one to have greater confidence in the resulting conclusions about the accuracy of the underlying nuclear data and its overall range of applicability. The HMF7 experiment is one such example. These experiments were performed at Oak Ridge National Laboratory (ORNL) and utilize the same fuel material, but include varying amounts of polyethylene. This series of experiments, while categorized as "FAST actually has a fission energy of average lethargy that varies from 830 keV to a low of 34 eV. Of course the assembly spectrum is not a delta function at this average energy, but this is still a useful metric to indicate how the spectrum changes as a function of materials, and in this case where the change covers several orders of magnitude it is clear that the underlying nuclear data are being tested over a broad energy range. Another example is the suite of experiments scattered throughout the HEU-MET-FAST and HEU-MET-MIXED categories from RFNC-VNIITF (Russian Federal Nuclear Center at the All-Russian Institute of Technical Physics) that use the same HEU fuel plates but include a variety of materials placed as axial reflectors, axial and radial reflectors or as diluent material placed between individual HEU slabs. Among the non-fissile materials used are aluminum, titanium, vanadium, iron and tungsten. These experiments include increasing amounts of the various materials in an axial reflector configuration, or various combinations of these materials and polyethylene. Again we have multiple arrangements with a common fuel material that then allows for testing the cross section adequacy of the substituted materials over a wide range of some parameter such as average fission energy or material thickness. ICSBEP users will quickly find other examples.

## C. Fast Systems

The historical Los Alamos National Laboratory (LANL) suite of FAST experiments represents a simple subset of the ICSBEP FAST benchmark category that is easily calculated to obtain an initial indication of the high energy cross section data for the important uranium and plutonium isotopes. These experiments include Godiva (HMF1), Flattop (HMF28), Jezebel and dirty Jezebel (PMF1, PMF2), Flattop-Pu (PMF6), Thor (PMF8), Big-Ten (IMF7), plus Jezebel-23 and Flattop-23 (UMF1, UMF6). Details of these assemblies are summarized in Table I.

Calculated eigenvalues with ENDF/B-VII.1 cross sections are shown in Fig. 1. There are several features of

TABLE I: Attributes of traditional LANL critical assemblies and their corresponding ICSBEP Benchmark Name.

ICSBEP Benchmark	Traditional Name	Geometry	Material
HMF1	Godiva	Bare Sphere	HEU
HMF28	Flattop	Reflected Sphere	HEU (core) <sup>nat</sup> U (refl)
PMF1	Jezebel	Bare Sphere	<sup>239</sup> Pu+4.5 a/o <sup>240</sup> Pu
PMF2	“dirty” Jezebel	Bare Sphere	<sup>239</sup> Pu+20.1 a/o <sup>240</sup> Pu
PMF6	Flattop-Pu	Reflected Sphere	<sup>239</sup> Pu (core) <sup>nat</sup> U (refl)
PMF8	Thor	Reflected Sphere	<sup>239</sup> Pu (core) <sup>232</sup> Th (refl)
IMF7	Big-Ten	Cylinder	Heterogeneous mix of uranium plates with varying <sup>235</sup> U content
UMF1	Jezebel-23	Bare Sphere	<sup>233</sup> U
UMF6	Flattop-23	Reflected Sphere	<sup>233</sup> U (core) <sup>nat</sup> U (refl)

this figure common to many that will appear in this paper. First, the ordinate is commonly labeled  $k_{\text{eff}}$  C/E. This means that the plotted data are the MCNP calculated eigenvalue divided by the expected model eigenvalue. There are innumerable approximations that might cause the model of a critical system to yield a non-unit eigenvalue and so for consistency when comparing multiple benchmarks we normalize calculated eigenvalues to expected eigenvalue for that model. Also, our MCNP kcode calculations often track 50 million histories, or more when obtaining reaction rate tallies. This means the stochastic uncertainty on the eigenvalue calculation is often only a few pcm. This uncertainty is comparable to the size of the plotted datum and so we do not include it in our figures. We do however include the inferred experimental eigenvalue uncertainty that is published in the ICSBEP evaluation. These uncertainties are included in the figures as error bars centered on unity. Finally, the ordinate range is often defined as 0.975 to 1.025. The plotted data may be situated much closer to unity, but 5% is an important interval in many safety analyses and we find it informative to illustrate the accuracy of our eigenvalue calculations on such a scale.

For the traditional LANL assemblies, the calculated eigenvalues are all close to unity, and virtually identical to the accurate eigenvalue results obtained previously with ENDF/B-VII.0 cross sections. The only calculated eigenvalue that is clearly outside the experimental uncertainty is the Thor benchmark. The published experimental uncertainty in the ICSBEP Handbook for this benchmark is 60 pcm, and is likely underestimated as the mass uncertainty that is also given suggests the uncertainty

is more likely closer to 150 pcm. The calculated Thor eigenvalue is near 0.998, yielding a C/E value which is only slightly larger than one standard deviation removed from this more realistic uncertainty estimate. Nevertheless, calculated  $k_{\text{eff}}$  for this assembly is somewhat lower than that of the other traditional LANL assemblies, suggesting that an unknown aspect of the current <sup>232</sup>Th cross sections remain to be improved. Observing virtually no change in calculated eigenvalues with ENDF/B-VII.1 cross sections, compared to those obtained with ENDF/B-VII.0, is expected since only minimal changes to the delayed neutron data (reverting back to the values from ENDF/B-VI.8) have been made for the primary fissile nuclides in ENDF/B-VII.1.

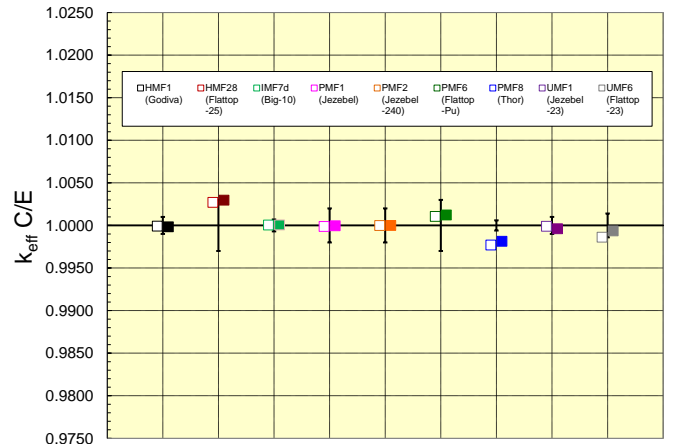


FIG. 1: Calculated eigenvalues with ENDF/B-VII.0 (closed symbols) and ENDF/B-VII.1 (open symbols) cross sections for a selection of LANL critical assemblies. Error bars represent the reported experimental uncertainty.

There are many other FAST system benchmarks for which eigenvalue calculations have been performed. Among these are a series of Russian experiments consisting of a sequence of cylindrical HEU plates approximately 20 cm in diameter and approximately 1 cm tall each. These plates are stacked in two sub-critical assemblies that are moved together to create a critical or near critical assembly. Permutations on these assemblies involve the placement of extra material at the ends of these assemblies (i.e., axial reflectors), placement of extra material between the individual HEU plates (i.e., insertion of diluents or moderators) and further combinations that also include the use of radial reflector material. Various combinations of HEU and these extra materials allow for testing of those extra material’s nuclear data. For example, HMF79 consists of five configurations with a central HEU core region and varying thicknesses of Ti axial reflectors (approximately 1 cm, 2 cm, 4 cm, 10 cm and 20 cm thick, respectively). The central region consists of ten or eleven HEU plates. Criticality is controlled by fixing five or six of these plates plus upper reflector in place and slowly moving the near mirror image lower half of the assembly toward the fixed material. Depending upon

the specific materials criticality is obtained when the gap between fixed and movable sections is less than a few centimeters, and often only a few millimeters. The average fission energy is little changed in an experiment such as this that only involves heavy materials, but being able to accurately calculate the critical eigenvalue as a function of reflector thickness provides confidence that the high energy scattering cross sections and their associated angular distributions are accurate. A variation of these experiments is to then place the axial reflector material between the individual HEU plates to act as a diluent, or to increase the average energy variation through use of a combination of diluents and polyethylene. Some structural materials of interest that have been used in these types of experiments are noted in Table II.

TABLE II: Summary list of fast ICSBEP benchmarks with common fuel plates and varying reflector and/or diluent materials.

Benchmark	Axial Reflector	Diluent	Radial Reflector
HMF15	—	—	—
HMF65	—	—	—
HMF82	CH <sub>2</sub> (top)	—	—
HMF91	CH <sub>2</sub>	—	—
HMF44	Al	—	—
HMF89	—	Al	—
HMF34.2	—	Al/CH <sub>2</sub>	CH <sub>2</sub>
HMF79	Ti	—	—
HMF34.1	—	Ti/CH <sub>2</sub>	Ti/CH <sub>2</sub>
HMM1	—	Ti/CH <sub>2</sub>	Ti/CH <sub>2</sub>
HMM15	—	Ti/CH <sub>2</sub>	Ti/CH <sub>2</sub>
HMF25	V	—	—
HMF40	—	V	—
HMM16	CH <sub>2</sub>	V/CH <sub>2</sub>	CH <sub>2</sub>
HMF43	Fe (steel)	—	—
HMF87	—	Fe (steel)	—
HMF33	—	Fe (steel)/CH <sub>2</sub>	—
HMF34.3	—	Fe (steel)/CH <sub>2</sub>	—
HMF49	W	—	—
HMF50	—	W	—
HMM17	CH <sub>2</sub>	W/CH <sub>2</sub>	CH <sub>2</sub>

Additional experimental evaluations for these and other materials will be introduced into the ICSBEP Handbook in future years. For example, an experiment similar to HMF89 that uses Al as a diluent and also includes both axial and radial polyethylene reflectors has been designated HMF90 and is currently undergoing final review with the expectation of being published in the next edition of the ICSBEP Handbook. Aluminum and iron are two important structural materials noted in the above tabulation of measurements, but there has been little or no change in these cross sections between ENDF/B-VII.0 and ENDF/B-VII.1, and so we expect little change in calculated eigenvalues for HEU benchmarks with only these materials. Such is the case, as shown in the Table III; the

calculated ENDF/B-VII.0 and ENDF/B-VII.1 eigenvalues are nearly identical and close to unity. Also shown in Table III is the energy corresponding to the average lethargy causing fission (EALF). This is a common measure of the average assembly energy (although the reader is reminded that the actual energy distribution about this average is very broad), and can vary from a high in excess of 800 keV for unmoderated systems to low keV values or eV values depending upon the degree of moderation in any given critical assembly.

TABLE III: Calculated eigenvalues for various bare and reflected benchmark assemblies with common fuel plates. Benchmark attributes are summarized in Table II. Multiple values for selected assemblies indicate differing material arrangements. Refer to the ICSBEP Handbook for details.

Benchmark	ENDF/B-VII.0 $k_{\text{eff}} C/E^*$	ENDF/B-VII.1 $k_{\text{eff}} C/E^*$	EALF, MeV**
HMF15	0.99510(9)	0.99485(9)	0.831
HMF65	0.99860(9)	0.99868(9)	0.831
HMF82	0.99727(10)	0.99708(10)	0.187
	0.99721(10)	0.99714(10)	0.119
	0.99956(10)	0.99926(11)	0.080
HMF91	1.00009(11)	1.00003(11)	0.0085
HMF44	1.00049(9)	1.00044(9)	0.820
	1.00008(9)	0.99999(9)	0.814
	1.00030(9)	1.00048(9)	0.805
	0.99996(9)	0.99984(9)	0.798
	1.00050(9)	1.00045(9)	0.796
HMF89	1.00102(9)	1.00094(9)	0.771
HMF34.2	0.99949(11)	0.99985(11)	0.0140
HMF43	0.99955(9)	0.99954(9)	0.821
	0.99860(9)	0.99853(9)	0.813
	0.99916(9)	0.99921(9)	0.805
	0.99787(9)	0.99784(9)	0.793
	0.99892(9)	0.99902(9)	0.791
HMF87	0.99989(9)	0.99979(9)	0.751
HMF33	0.99998(11)	1.00010(11)	0.0138
	0.99847(12)	0.99840(12)	0.0019
HMF34.3	0.99843(11)	0.99827(11)	0.0130

\* Values in parenthesis represent the uncertainty in the corresponding least significant digits.

\*\* EALF = Energy of average lethargy causing fission. The ENDF/B-VII.1 value is given but the results are virtually identical for ENDF/B-VII.0.

Other materials, most notably titanium and tungsten, have seen significant changes in their cross sections between ENDF/B-VII.0 and ENDF/B-VII.1. These changes were motivated by the large  $k_{\text{eff}} C/E$  deviations from unity for ENDF/B-VII.0 based calculations. The observed variation in predicted  $k_{\text{eff}} C/E$  values with recent ENDF/B cross sections is illustrated in Fig. 2.

Measurements have been made for eight assemblies using the same HEU fuel and varying amounts of Ti or a

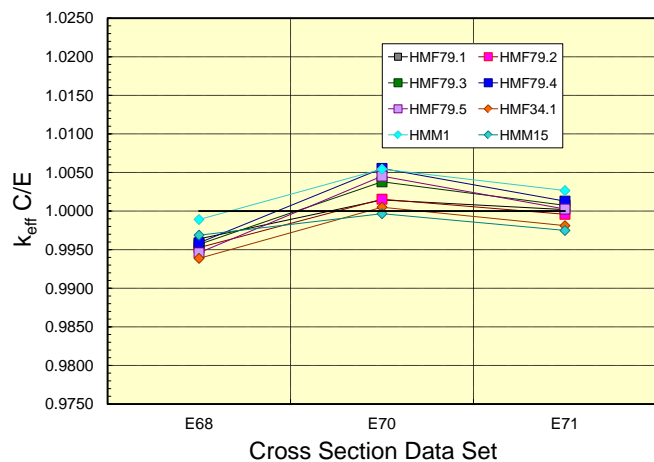


FIG. 2: Calculated eigenvalues for Titanium bearing HEU benchmarks with ENDF/B-VI.8 (E68), ENDF/B-VII.0 (E70) and ENDF/B-VII.1 (E71) cross sections.

combination of Ti and polyethylene. With ENDF/B-VI.8 cross sections the average calculated eigenvalue is too low by just over 400 pcm and there is a 500 pcm variation from the minimum to maximum calculated eigenvalue; a result that is actually better than it might first appear as the bare ENDF/B-VI HEU calculated eigenvalues were also biased low by 0.2%. However, with ENDF/B-VII.0 cross sections the average calculated eigenvalue is too large by almost 300 pcm, there appears to be a systematic increase of nearly 400 pcm in calculated eigenvalue with increasing reflector thickness and there is a 600 pcm variation from the minimum to maximum calculated eigenvalue. Clearly the cross section changes embodied in moving from ENDF/B-VI.8 to ENDF/B-VII.0 did not yield an improvement in critical eigenvalue calculations for Ti bearing systems. With ENDF/B-VII.1 cross sections the average eigenvalue is virtually unity and the eigenvalue trend with reflector thickness has been reduced by nearly 50%. The overall minimum to maximum variation, now 530 pcm, remains large.

Fig. 3 illustrates these same calculated eigenvalues, now plotted against EALF. The ENDF/B-VII.1 calculated eigenvalues are seen to fluctuate above and below unity versus energy, indicating no trend in calculated eigenvalue versus energy. Overall we conclude that the titanium isotopic cross section data in ENDF/B-VII.1 is superior to that available from earlier ENDF/B libraries.

Another structural material of importance whose cross sections have been revised for ENDF/B-VII.1 is tungsten. A suite of critical experiments using tungsten as an axial reflector of varying thickness or as a diluent were noted above (HMF49 and HMF50). In addition, diluent tungsten plus polyethylene (HMM17) has been used to test the cross section accuracy in the presence of a softer spectrum. Finally, critical systems using  $^{239}\text{Pu}$  or  $^{233}\text{U}$  (PMF5, UMF4) have also been modeled. Calculated eigenvalues, with cross sections from ENDF/B-VI.8 for-

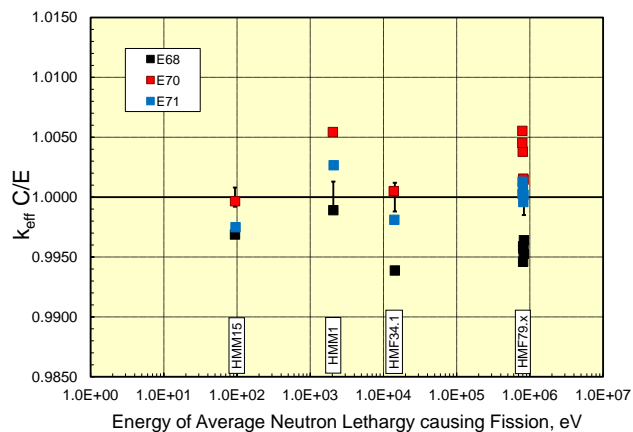


FIG. 3: Calculated eigenvalues for titanium bearing critical assemblies, shown as a function of average fission energy for that assembly. The near unity eigenvalues obtained support the conclusion that these new titanium cross sections are more accurate than those previously available and they do not exhibit an eigenvalue trend as a function of assembly energy.

ward, are shown in Fig. 4.

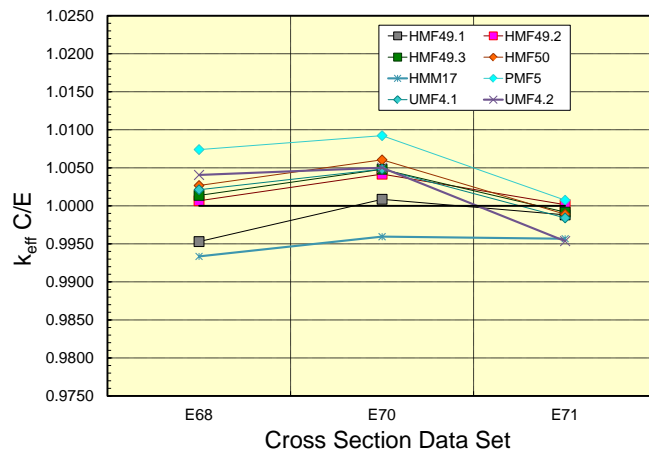


FIG. 4: Calculated eigenvalues for Tungsten bearing critical assemblies. The reduced spread in calculated eigenvalues with the latest cross sections compared to previous ENDF/B generations indicates a significant improvement in these latest evaluated files.

Going back to ENDF/B-VI.8, the average calculated multiplication factor was biased high by approximately 0.1%; a seemingly reasonable result. However, bare ENDF/B-VI.8 HEU system eigenvalues were biased low by nearly 0.2 %, suggesting a bias of nearly 0.3% rather than 0.1% for tungsten bearing systems. ENDF/B-VII.0 failed to improve these calculated eigenvalues as average tungsten bearing system eigenvalues increased to a bias of nearly 0.4%. In addition, there was a large spread in calculated eigenvalues, varying by over 1% from a low of 0.996 to a high of 1.009. The revised tungsten cross sections appearing in ENDF/B-VII.1 are a significant im-

provement. The average calculated eigenvalue is now 0.9985; a marginally low but reasonable value in light of experimental uncertainties that are up to 160 pcm. Of greater importance is the reduced spread in calculated eigenvalues, as the minimum to maximum variation now only spans an interval of 0.995 to 1.001. A more complete discussion of the improvements made to these cross sections is provided in our companion paper [1].

Accurate calculated eigenvalues are obtained for systems with iron (HMF43, HMF87, HMF33 and HMF34.3) and aluminum (HMF44, HMF89 and HMF34.2). These elements are typically found in shipping containers or in structural materials surrounding fissile materials and so it is important that their nuclear data be accurately known. We will also show accurate calculated eigenvalues for iron in a thermal environment in a later section where LEU-COMP-THERM assembly results are presented.

Another material of interest and importance in reactor physics is beryllium. There are a large number of beryllium bearing benchmarks in the ICSBEP Handbook. Several of them represent systematic studies with a varying Be reflector thickness surrounding either HEU, <sup>239</sup>Pu or mixed HEU/Pu cores. These are geometrically simple systems, consisting of nested spheres. Some of their characteristics are summarized in Table IV.

Unfortunately, the calculated eigenvalues from these benchmarks yield conflicting interpretations. Figs. 5 through 9 include calculated eigenvalues for ENDF/B-VI.8, ENDF/B-VII.0 and ENDF/B-VII.1 cross sections. Figs. 5, 6 and 7 display calculated eigenvalues for the HMF41, HMF58 and MMF7 benchmarks. These benchmarks had been most closely studied during the interim between ENDF/B-VI.8 and ENDF/B-VII.0. They generally exhibit a positive calculated eigenvalue bias with some evidence for an increasing bias with increasing reflector thickness when calculated with ENDF/B-VI.8 cross sections.

These observations lead to a re-evaluation of the <sup>9</sup>Be cross sections for ENDF/B-VII.0 which tended to yield calculated eigenvalues significantly closer to unity with little or no evidence for a trend in calculated eigenvalue versus reflector thickness. Unfortunately, during the closing months prior to the release of ENDF/B-VII.0 new microscopic experimental data became available from RPI [7], and the HMF66 and HMF77 benchmarks were approved for publication in the ICSBEP Handbook. The new RPI data tended to be in better agreement with the ENDF/B-VI.8 <sup>9</sup>Be evaluation, and the calculated eigenvalues for HMF66 and HMF77 tended to be closer to unity with ENDF/B-VI.8 cross sections compared to ENDF/B-VII.0 (see Figs. 8 and 9), in direct contrast to the apparently more accurate calculated eigenvalues obtained with ENDF/B-VII.0 cross sections for the HMF41, HMF58 and MMF7 benchmarks. At that time it was decided to retain the revised ENDF/B-VII.0 Be evaluation, but it was clear that additional work on the <sup>9</sup>Be cross section file was warranted.

The revised <sup>9</sup>Be evaluation that appears in ENDF/B-

TABLE IV: Characteristics for a selection of ICSBEP benchmarks that contain varying amounts of Beryllium. Multiple configurations for a given benchmark indicated that the combined arrangement of fuel and material differs, generally a decrease in the amount of fuel and an increase in reflector thickness. See the ICSBEP Handbook for details.

Benchmark	Materials	Be Shell Thickness, cm	Summary Description
HMF41	HEU/Be	4.6	External radial reflector
		11.8	
HMF58	Be/ HEU/ Be	0.5//20.3	Internal and external radial reflector
		0.5//9.3	
		0.5//5.4	
		0.5//3.3	
		0.5//2.2	
HMF66	Be/ Be/ HEU/ Be	0.5/2.6//8.7	Two nested internal Be shells and variable HEU shells plus an external Be reflector
		0.5/2.6//5.3	
		0.5/2.6//3.9	
		0.5/3.5//13.2	
		0.5/3.5//7.8	
		0.5/3.5//5.6	
		0.5/4.2//7.7	
0.5/4.2//10.6			
HMF77	Void/ HEU/ Be	9.3	Variable central void and variable HEU shells plus an external Be reflector
		5.7	
		14.7	
		8.6	
		6.3	
		8.8	
		4.5	
6.9			
MMF7	Pu/ HEU/ Be	20.0 - 1.36	Fixed Pu + increasing HEU + decreasing Be; repeat for five Pu cores
		17.3 - 0.67	
		10.2 - 1.23	
		3.57 - 0.66	
		2.66 - 1.50	

VII.1 includes the new RPI data and, not surprisingly, the cross sections and calculated eigenvalues are similar to those of ENDF/B-VI.8. However, the <sup>9</sup>Be cross section file adopted for ENDF/B-VII.1 remains a work in progress. The basic cross section re-evaluation is believed to be complete, but a re-assessment of the scattering angular distributions has not been performed. This will be a future task, and if warranted such new distributions will be incorporated into a future ENDF beryllium release. Regardless of future revisions to the evaluated Be file, the current file yields predicted critical eigenvalues that are generally accurate to within ±0.5%.

The HMF7 benchmark suite provides the opportunity to test cross section data over a broad energy range. This

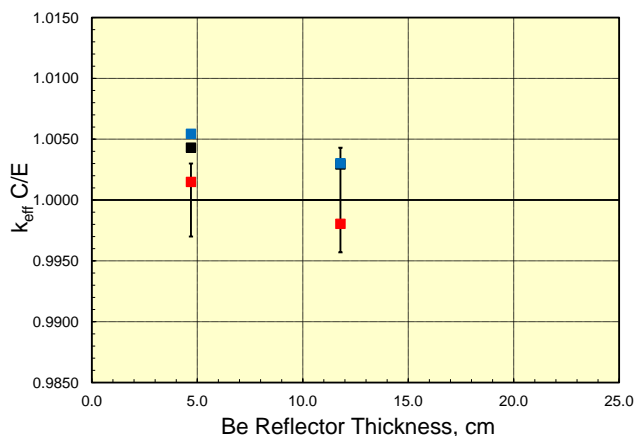


FIG. 5: Calculated eigenvalues with recent ENDF/B cross section libraries (black symbol is ENDF/B-VI.8; red symbol is ENDF/B-VII.0 and blue symbol is ENDF/B-VII.1) for the HMF41 benchmark. Note that Figs. 5 through 9 use the same ordinate axis to portray to total range of beryllium reflector thicknesses over the entire benchmark suite.

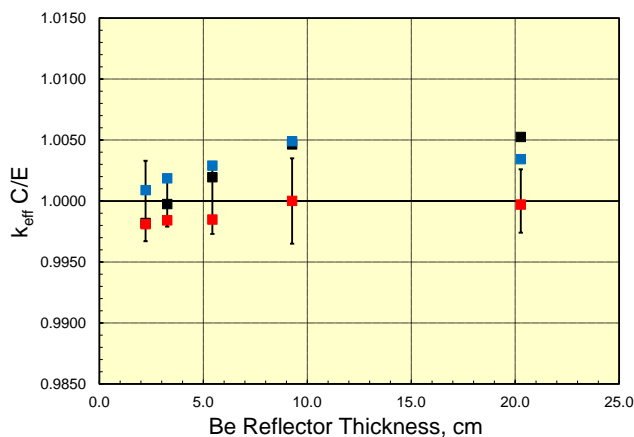


FIG. 6: Calculated eigenvalues with recent ENDF/B cross section libraries (black symbol is ENDF/B-VI.8; red symbol is ENDF/B-VII.0 and blue symbol is ENDF/B-VII.1) for the HMF58 benchmark.

benchmark contains HEU and polyethylene. The HEU consists of 2.5 cm thick rectangular plates, either 25.4 cm x 25.4 cm or 12.7 cm x 25.4 cm in size. Various combinations of the HEU and similarly sized polyethylene plates are stacked into otherwise bare critical assemblies. A further softening of the spectrum is obtained by surrounding the 12.7 cm x 25.4 cm plates with a 12.7 cm thick external radial and axial polyethylene reflector. In summary, there are three broad classes of assemblies, (i) 25.4 cm x 25.4 cm HEU plates with or without interleaved polyethylene and no external reflector, (ii) 12.7 cm x 25.4 cm HEU plates with or without interleaved polyethylene and no external reflector and (iii) 12.7 cm x 25.4 cm HEU plates with or without interleaved polyethylene plus a 12.7 cm thick reflector on all sides. The ENDF/B-VII.1 calculated eigenvalues are illustrated in Fig. 10.

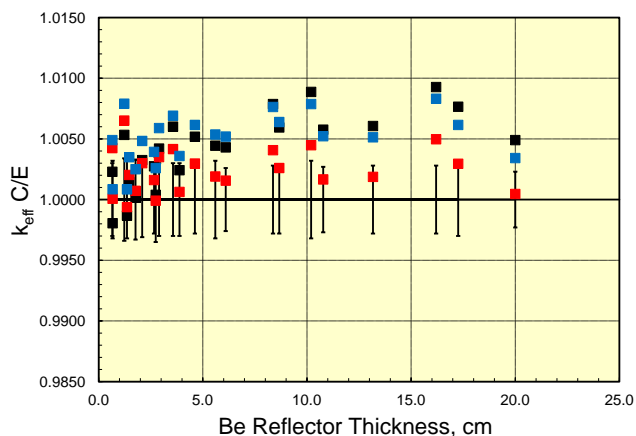


FIG. 7: Calculated eigenvalues with recent ENDF/B cross section libraries (black symbol is ENDF/B-VI.8; red symbol is ENDF/B-VII.0 and blue symbol is ENDF/B-VII.1) for the MMF7 benchmark.

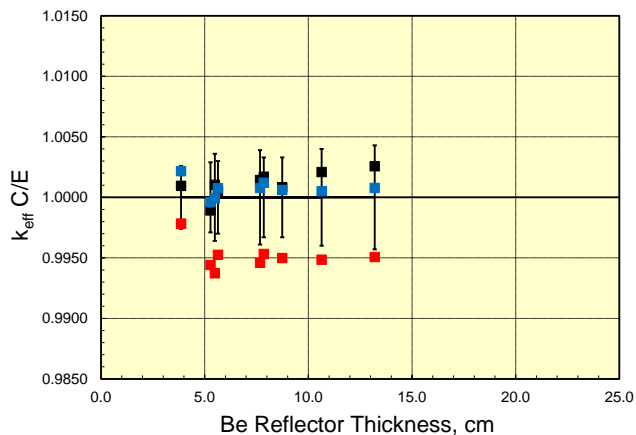


FIG. 8: Calculated eigenvalues with recent ENDF/B cross section libraries (black symbol is ENDF/B-VI.8; red symbol is ENDF/B-VII.0 and blue symbol is ENDF/B-VII.1) for the HMF66 benchmark.

This benchmark suite has been calculated previously with ENDF/B-VI.8 and ENDF/B-VII.0 cross sections. As the hydrogen, carbon and  $^{235}\text{U}$  cross sections are little changed going from ENDF/B-VII.0 to ENDF/B-VII.1 there is correspondingly little change in the calculated eigenvalues. In general the calculated eigenvalues are within 200 pcm of unity, with no statistically significant difference between the three configuration categories noted above. There is a possible small bias in calculated eigenvalues through the low to several hundred keV energy range but these data are not conclusive, as model simplifications introduce a bias of up to 200 pcm that is normalized away in the C/E plots and the overall experimental uncertainty ranges from  $\sim 120$  pcm to  $\sim 240$  pcm

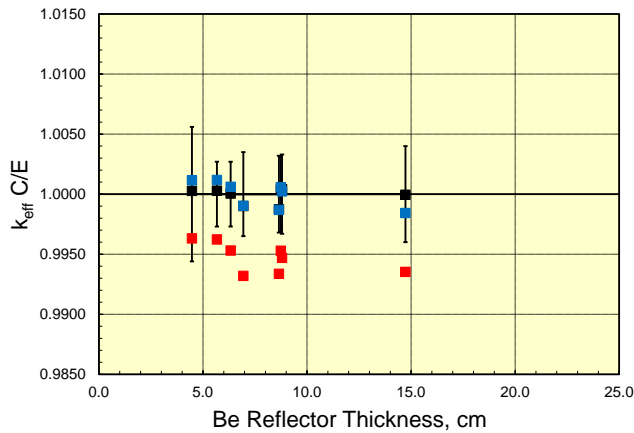


FIG. 9: Calculated eigenvalues with recent ENDF/B cross section libraries (black symbol is ENDF/B-VI.8; red symbol is ENDF/B-VII.0 and blue symbol is ENDF/B-VII.1) for the HMF77 benchmark.

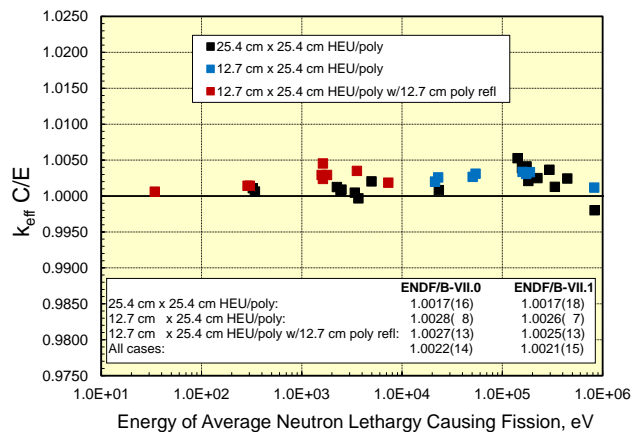


FIG. 10: ENDF/B-VII.1 calculated eigenvalues for the HMF7 benchmark suite. The variable amount of polyethylene appearing in the many configurations of this suite allow for cross section data testing over a wide energy range.

#### D. Thermal Systems

The ICSBEP Handbook contains many moderated assemblies suitable for cross section data testing. The simplest systems are solution assemblies in simple geometry; generally spheres or cylinders that contain little more than the fissile material of interest, hydrogen and oxygen. Nitrogen or fluorine are also typically present but are often of limited neutronic importance. More complex systems include arrays of fuel rods, typically  $\text{UO}_2$  fueled. These arrays can be of various sizes, including groups of clusters or a single large rectangular or hexagonally oriented lattice. Reactivity control is maintained through various means, including cluster separation, water height, total number of fuel rods or the presence of soluble poison. Most of the benchmarks reported below are water reflected, but we also provide limited results for lattice

assemblies in the presence of lead, depleted uranium or steel (mostly iron) reflecting walls as well as for configurations with soluble boron, cadmium and gadolinium. An experiment containing  $^{103}\text{Rh}$ , an important fission product, is also noted.

#### 1. Solution Systems

The HEU-SOL-THERM (HST) benchmark class allows testing of thermal  $^{235}\text{U}$ , hydrogen and oxygen data. Calculated eigenvalues are typically correlated against calculated Above Thermal Leakage Fraction, ATLF. This parameter varies significantly as a function of assembly geometry, and can serve as a qualitative measure of fission spectrum moderation. For geometrically large systems the fission neutrons are both born and moderated in the fissile solution, leading to a small ATLF value. For geometrically small systems the fission neutrons have a higher probability of escaping the solution, leading to a large ATLF. Until the early 1990s these benchmarks exhibited a significant bias in  $k_{\text{eff}} C/E$  and a large positive trend with increasing ATLF. These issues were largely resolved due to Lubitz [6] in ENDF/B-VI.3 and since then testing of this benchmark class is performed with the aim of verifying that the most recent upgrades to the underlying nuclear data retain the now accurate  $k_{\text{eff}} C/E$  predictions.

Calculations with ENDF/B-VII.1 are shown in Fig. 11. Included are the results of a linear least squares fit of calculated eigenvalues correlated against ATLF. The regression analysis takes the form of  $k_{\text{predicted}} = A_0 + B_0 * ATLF$ . Absence of a bias is signified when  $A_0$  is found to be unity, or more specifically when its absolute value plus or minus its uncertainty encompasses unity. In the analyses reported here we report the 95% confidence interval (95CI) as the uncertainty used to assess whether the regression coefficient is statistically significant. The  $B_0$  term is a measure of whether a trend in  $k_{\text{eff}} C/E$  exists versus that regression parameter. Once again, the absolute value plus or minus the 95CI in that parameter prediction is used to conclude whether the postulated parameter trend is significant.

The HST benchmark suite contains 45 specific assemblies from ten HST benchmarks. These present experiments performed at either Oak Ridge National Laboratory or at Rocky Flats during the 1950s and 1960s. The assembly models are geometrically simple, consisting of spheres or cylinders and include unreflected and water reflected configurations. The resulting regression coefficients when using ENDF/B-VII.1 cross sections are  $A_0 = 1.0007 \pm 0.0032$  and  $B_0 = -0.0010 \pm 0.0084$ . Since  $A_0$  and its 95CI bracket unity and  $B_0$  and its 95CI also bracket zero, we conclude that there is neither a bias nor a trend versus ATLF in our reactivity calculations for this benchmark class. For ENDF/B-VII.0 we determined virtually identical regression coefficients,  $A_0 = 1.0007 \pm 0.0032$  and  $B_0 = -0.0010 \pm 0.0085$ . The

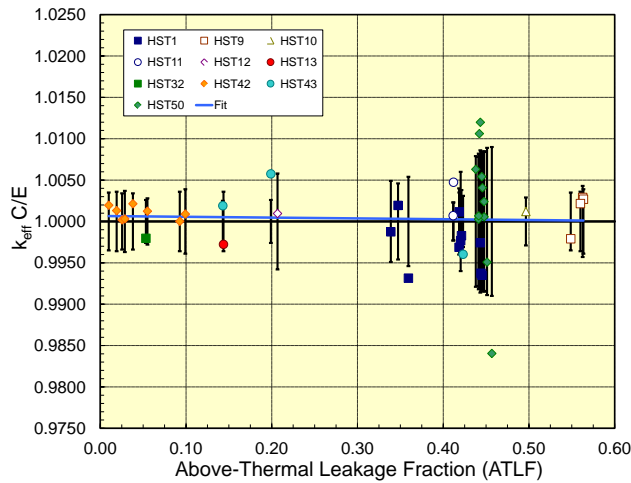


FIG. 11: Calculated eigenvalues for a suite of HEU-SOL-THERM benchmarks. This benchmark suite has been used for many years to validate thermal uranium critical assembly benchmark eigenvalue predictions. Results with ENDF/B-VII.1 cross sections are little changed from ENDF/B-VII.0, as expected, given that there has been minimal change in the underlying  $^{235}\text{U}$ , hydrogen and oxygen evaluated cross section data.

lack of change from ENDF/B-VII.0 to ENDF/B-VII.1 is not surprising. As noted previously, these are simple systems consisting primarily of HEU, oxygen and hydrogen. As the underlying cross section data is little changed, we expect and have confirmed that the performance of these data in criticality simulations is little changed. However, expansion of this benchmark suite is warranted in the hope that further experiments can be used to reduce the  $B_0$  regression coefficient uncertainty. Alternatively, one might reassess the HST50 benchmark evaluation to see whether additional information can be extracted from the original log books to allow for a more consistent model with smaller uncertainties. Currently the large variation in  $k_{\text{eff}} C/E$  values among the 11 cases of this series of experiments are a significant contributor to the large 95CI for this parameter.

The HST49 experiment differs from those considered above in that it contains Cd. A variety of configurations exist with varying amounts of Cd either in the fuel solution, the reflector or both. Cadmium is an important thermal absorber, and its presence in an HEU solution system is an excellent medium to test its thermal reactivity impact. Results from 20 configurations are displayed in Fig. 12. In general, the ENDF/B-VII.1 results are a significant improvement over ENDF/B-VII.0, as the average ENDF/B-VII.0  $k_{\text{eff}} C/E$  is 0.9930 while the average ENDF/B-VII.1  $k_{\text{eff}} C/E$  is 0.9977. This improvement is gratifying, but is tempered by the realization that there is considerable variation in the individual  $k_{\text{eff}} C/E$  results. The reported experimental uncertainties are around 200 to 300 pcm, but the minimum-to-maximum variation in  $k_{\text{eff}} C/E$  for these 20 configura-

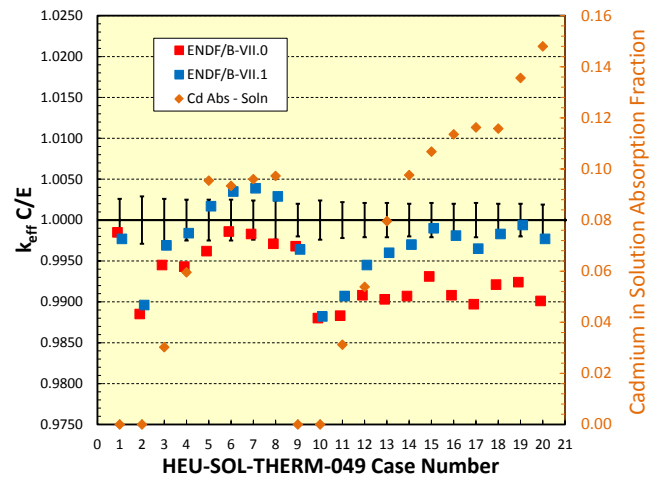


FIG. 12: Calculated eigenvalues (left hand axis) and Cadmium absorption fractions (right hand axis) for the HEU-SOL-THERM-049 benchmark. See the ICSBEP Handbook for additional details.

tions is nearly 1600 pcm with ENDF/B-VII.1, and just over 1000 pcm with ENDF/B-VII.0 cross sections. There is a clear need to analyze additional Cd bearing critical experiments, and to that end we note that the LCT28 benchmark provides a low-enriched fuel rod lattice configuration with Cd. However, at this time, we are unaware of any analyses of this benchmark beyond the sample ENDF/B-VI based results that are typical of an ICSBEP evaluation.

A suite of more than 150 PU-SOL-THERM benchmarks have been calculated in recent years with various cross section libraries. These benchmark models are geometrically simple and the only significant materials beside those needed to represent the thin-walled containers are plutonium, hydrogen, oxygen and nitrogen. Calculated eigenvalues for this class of benchmark have been biased high by approximately 0.5% in past ENDF/B libraries and this situation is unchanged for ENDF/B-VII.1 as the average  $C/E k_{\text{eff}}$  for these benchmarks is 1.0046. The individual  $C/E k_{\text{eff}}$  values vary from 0.9934 to 1.0193 and the population standard deviation is 0.0046. Corresponding values for ENDF/B-VII.0 were an average  $k_{\text{eff}} C/E$  of 1.0047 and a population standard deviation of 0.0046.

Past analyses of HEU-SOL-THERM experiments have correlated  $C/E k_{\text{eff}}$  versus ATLF. That correlation for the Pu-SOL-THERM experiments is shown in Fig. 13. We note in Table V the slope and intercept terms for this regression, and for linear regression fits of  $C/E k_{\text{eff}}$  versus other parameters. As with the HST results, the uncertainty value cited here is actually the 95CI. The calculated slope and its associated 95CI in  $k_{\text{eff}} C/E$  versus ATLF is  $+0.0038 \pm 0.0075$ . Again, as noted in the HST discussion, since the magnitude of the 95CI exceeds the magnitude of the slope we conclude that this slope value is statistically insignificant. This means there is no trend in calculated eigenvalue versus this parameter; a con-

clusion similar to that noted for the HST benchmark class. The other key regression coefficient is the intercept,  $1.0034 \pm 0.0026$ . In contrast to HST benchmarks, this intercept is significantly different from unity and is consistent with the 0.5% C/E  $k_{\text{eff}}$  bias noted in the previous paragraph.

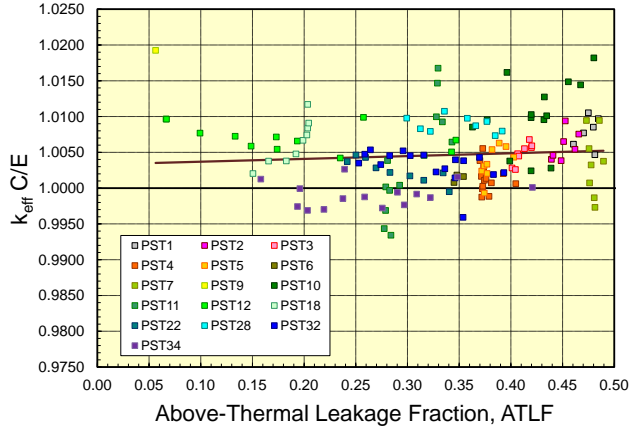


FIG. 13: Calculated eigenvalues for a suite of Pu-Sol-Therm benchmarks and the resulting correlation (solid brown line) with ATLF. Calculated regression coefficients are an intercept of 1.0034(26) and slope of +0.0038(75), where the values in parenthesis are 95% confidence intervals on the predicted coefficient. The slope is statistically insignificant but the intercept clearly deviates from unity by nearly 0.5%. This bias has been observed in past ENDF/B cross section libraries, and remains in ENDF/B-VII.1.

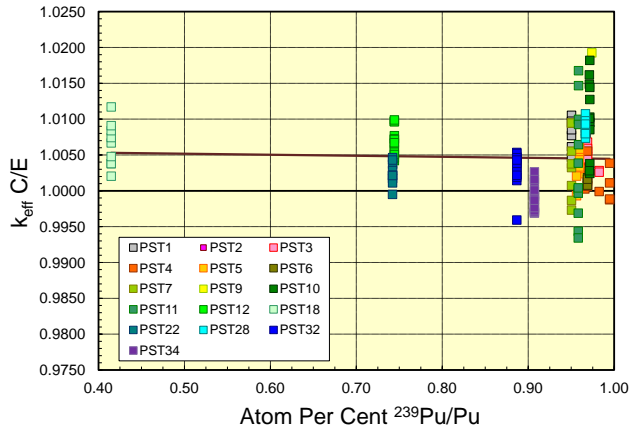


FIG. 14: Calculated eigenvalues for a suite of Pu-Sol-Therm benchmarks and the resulting correlation (solid brown line) with  $^{239}\text{Pu}$  atom fraction. Calculated regression coefficients are an intercept of 1.0061(47) and slope of -0.0016(50), where the values in parenthesis are 95% confidence intervals on the predicted coefficient. The slope is statistically insignificant but the intercept clearly deviates from unity by nearly 0.5%. This bias has been observed in past ENDF/B cross section libraries, and remains in ENDF/B-VII.1.

There are other parameters that could be considered

for regression analysis in the hope that a statistically significant trend is observed that could be related to some aspect of the underlying nuclear data. Among the other possible regression parameters noted in Table V is the  $^{239}\text{Pu}/\text{Pu}$  atom fraction, which varies from a low of 0.4 to  $>0.99$ . C/E  $k_{\text{eff}}$  values are plotted against this parameter in Fig. 14. Once again no trend is observed, as the  $^{239}\text{Pu}/\text{Pu}$  atom fraction slope parameter is determined to be  $-0.0016 \pm 0.0053$ . The intercept term,  $1.0061 \pm 0.0047$  is consistent with an overall bias for this benchmark class. Note however even the absence of a trend in the face of a constant bias provides important information. In this instance, lack of a trend in C/E  $k_{\text{eff}}$  suggests that the underlying bias is not due to a unique aspect of  $^{239}\text{Pu}$  nuclear data since the observed bias remains constant despite the significant variation in  $^{239}\text{Pu}$  content.

Other parameters that have been studied include Above Thermal Fission Fraction, ATFF; g Pu per liter; different measures of the average fission energy; or various calculated reaction fractions including  $^{239}\text{Pu}$  capture or fission and hydrogen capture. Regression coefficients for these parameters are summarized in Table V.

TABLE V: Calculated regression coefficients for a suite of PST benchmark assemblies, correlated against various critical assembly parameters.

Parameter	Intercept & 95% CI*	Slope & 95% CI*
Above Thermal Leakage Fraction, ATLF	1.0034(26)	+0.0038(75)
Above Thermal Fission Fraction, ATFF	1.0059(9)	-0.0188(90)
$^{239}\text{Pu}/\text{Pu}$ atom fraction	1.0061(47)	-0.0016(53)
g Pu/liter	1.0058(10)	-1.5(8.6)e-6
Energy of average lethargy causing fission, EALF, eV	1.0053(8)	-0.0037(15)
Average fission energy, eV	1.0057(9)	-6.8(3.3)e-8
$^{239}\text{Pu}$ production fraction	1.0106(116)	-0.0061(119)
$^{239}\text{Pu}/\text{Pu}$ capture fraction	1.0030(37)	+0.0021(45)
Hydrogen (in solution) capture	1.0037(13)	+0.0109(118)
H/Pu number density ratio	1.0037(13)	-1.6(1.8)e-6

\* Values in parenthesis represent the 95CI in the corresponding least significant digits.

The ATFF and EALF correlations, both measures of average fission energy, indicate a possible trend. However, these results must be viewed with caution as they are largely driven by the PST34 benchmark series.

This series contains significant quantities of gadolinium (more than 20% gadolinium absorption in PST34.6) and changes to the important  $^{155,157}\text{Gd}$  cross sections can easily shift these C/E  $k_{\text{eff}}$  values by several tenths of a percent. Recent RPI experimental results, [8], would support a decrease in the low energy gadolinium absorption cross section that would increase the average PST34 C/E  $k_{\text{eff}}$  values and eliminate this trend. However C/E  $k_{\text{eff}}$  for the PST34 benchmarks with the highest calculated gadolinium absorption fractions will increase to beyond 1.01 when calculated with a  $^{157}\text{Gd}$  file using RPI thermal data. Also, the impact upon other gadolinium bearing benchmarks, such as LCT5 (discussed below), is to significantly worsen the C/E  $k_{\text{eff}}$ . In contrast, the gadolinium bearing LCT35.3 benchmark's C/E  $k_{\text{eff}}$  (also noted below) improves with the RPI file. Therefore, in the absence of definitive integral data testing support the ENDF/B-VII.1 gadolinium cross sections are little changed from those in ENDF/B-VII.0. Further study of the underlying microscopic data and these integral benchmark results is warranted.

All-in-all, we conclude that there is no single experimental parameter that easily accounts for the PST C/E  $k_{\text{eff}}$  bias. Alternatively, lack of a trend in  $k_{\text{eff}}$  C/E supports the argument that the underlying nuclear data behind that parameter are likely not the cause of this bias. Specifically lack of a trend in  $k_{\text{eff}}$  C/E when correlated with calculated  $^{239}\text{Pu}$  capture,  $^{239}\text{Pu}$  fission and hydrogen capture all indicate that these data are reasonably accurate. Also, lack of a trend in  $k_{\text{eff}}$  C/E versus a basic benchmark model parameter such as g Pu per liter or H/Pu number density ratio suggests that these fundamental solution characteristics are properly defined.

It is a simple fact that an eigenvalue bias exists for the PST benchmark class. This bias has been present through all generations of ENDF/B libraries, and it remains so with these latest data.

### 2. Low Enriched Lattice Systems

LEU-COMP-THERM (LCT) is an important benchmark class, as these benchmarks span the range of nuclear parameters, particularly uranium enrichment, moderation and soluble or lumped poisons that are important to the commercial reactor industry. The ICSBEP Handbook contains nearly 100 LCT evaluations. Those that have been calculated with the new ENDF/B-VII.1 library are summarized in Table VI.

Resolution of the longstanding negative calculated eigenvalue bias for  $\text{UO}_2$  fuel systems was an ENDF/B-VII.0 success story. With essentially no change in the uranium or oxygen cross sections for ENDF/B-VII.1 we expect to retain this good calculated eigenvalue performance. Fig. 15 displays the calculated eigenvalues for a selection of the ICSBEP LEU benchmarks. These systems encompass experiments from throughout the world, including the United States, France, Russia and Japan.

TABLE VI: Selected attributes for a suite of LEU-COMP-THERM benchmarks. Further details are available from the ICSBEP Handbook.

Benchmark	Fuel	Comment
LCT1	U(2.35)O <sub>2</sub>	Water moderated and reflected.
LCT2	U(4.31)O <sub>2</sub>	Water moderated and reflected.
LCT5	U(4.31)O <sub>2</sub>	Water moderated and reflected. Includes dissolved Gd, same fuel as LCT1 or LCT2.
LCT6	U(2.6)O <sub>2</sub>	Water moderated and reflected.
LCT7	U(4.738)O <sub>2</sub>	Water moderated and reflected.
LCT8	U(2.459)O <sub>2</sub>	Borated water moderated and reflected; also may include water holes and poison rods.
LCT10	U(4.31)O <sub>2</sub>	Water moderated with Lead, Uranium or steel plus water reflectors. Same fuel as LCT2.
LCT11	U(2.5)O <sub>2</sub>	Borated water moderated and reflected; also includes water holes.
LCT17	U(2.35)O <sub>2</sub>	Water moderated with Lead, Uranium or steel plus water reflectors. Same fuel as LCT1.
LCT22	U(10.0)O <sub>2</sub>	Water moderated and reflected.
LCT24	U(10.0)O <sub>2</sub>	Water moderated and reflected.
LCT25	U(7.5)O <sub>2</sub>	Water moderated and reflected.
LCT27	U(4.738)O <sub>2</sub>	Water moderated with Lead plus water reflectors. Same fuel as LCT7.
LCT35	U(2.6)O <sub>2</sub>	Water moderated and reflected, includes either soluble boron or gadolinium. Same fuel as LCT6.
LCT39	U(4.738)O <sub>2</sub>	Water moderated and reflected. Same fuel as LCT, now including water holes.
LCT79	U(4.31)O <sub>2</sub>	Water moderated and reflected. Includes $^{103}\text{Rh}$ foils. Same fuel as LCT2.

It is clear from the figure that accurate eigenvalue calculations for this class of benchmark are obtained with ENDF/B-VII.1 cross sections, although both the uncertainty and  $k_{\text{eff}}$  C/E variation for the 9.8 w/o Russian experiments is large.

These experiments are all water moderated, but span a range of enrichments (from  $\sim 2.3$  w/o to  $\sim 10$  w/o), and

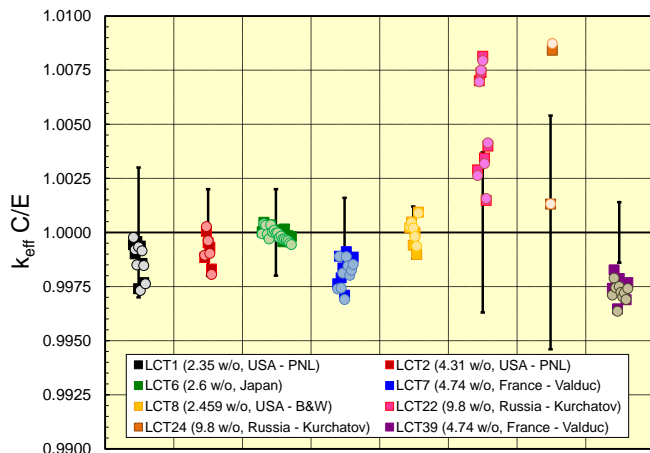


FIG. 15: Calculated eigenvalues (solid squares are ENDF/B-VII.0, lighter circles are ENDF/B-VII.1) for a suite of LEU-COMP-THERM benchmarks. ENDF/B-VII.1 results are virtually identical to ENDF/B-VII.0, as expected, and are generally within the experimental uncertainty.

span a range of moderations. They are all thermal systems, but the combination of fuel diameter, rod diameter and lattice pitch, or presence of soluble poison, yield all combinations of undermoderated, near optimally moderated and overmoderated systems. These benchmarks range in size from small arrays of clusters containing as few as a hundred rods each to large single clusters with more than 4900 rods. Regardless of the degree of moderation, accurate eigenvalue calculations are obtained, as the majority of the calculated eigenvalues are within the one sigma experimental uncertainty and it is apparent that all are within the two sigma uncertainty.

Calculations of the LCT10, LCT17 and LCT27 benchmarks are another example where a previous benchmark from the ICSBEP Handbook serves as a base case. LCT10 utilizes the same fuel rods as were present in the water moderated LCT2 benchmark, but now includes large reflecting walls of either Lead, <sup>depl</sup>U or steel (mostly Iron) aligned along two sides of these clusters. Similarly LCT17 uses these same reflecting materials plus LCT1 fuel while LCT27 places large Lead blocks radially around a lattice consisting of the same fuel as used in LCT7. Multiple configurations where the reflector walls are positioned immediately adjacent to the lattice, then moved perpendicularly away from the fuel, thereby allowing for varying amounts of water between the fuel and reflector are defined.  $k_{\text{eff}}$  C/E results for ENDF/B-VII.0 and ENDF/B-VII.1 calculations are illustrated in Fig. 16.

There are six sets of calculated eigenvalues portrayed here. The leftmost set, LCT2, serves as a base case for the LCT10 results that appear next. Both LCT2 and LCT10 use the same fuel, arranged in virtually identical configurations. The lattice pitch is 2.54 cm for both and the cluster arrangement is a triplet of 13 x 8 clusters arranged along the 13 rod row. The reflecting walls are positioned parallel to the 13 rod row and vary in location

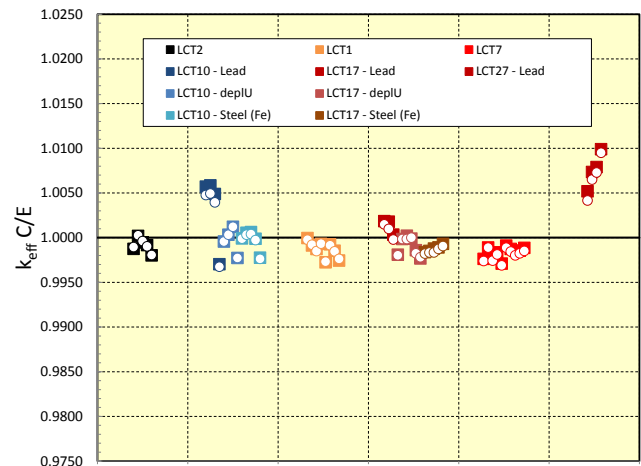


FIG. 16: Calculated eigenvalues (solid squares are ENDF/B-VII.0, open circles are ENDF/B-VII.1) for LEU-COMP-THERM benchmarks with water only or water plus one of lead, depleted uranium or steel (iron) reflectors. LCT2 and LCT10 contain the same fuel and cluster/lattice geometry, with LCT2 serving as a water reflector only base case. Metallic reflector walls were placed in multiple locations, leading to 3 or more critical assembly configurations for each material. See the ICSBEP Handbook for additional details.

from immediately against the lattice or pulled away by up to 5.4 cm. The rods and walls are immersed in water and cluster separation, varying from 20 cm to less than 10 cm is used to attain criticality. For LCT10 there are four discrete measurements with Lead and <sup>depl</sup>U walls and five measurements with steel. All but three of the calculated LCT10 eigenvalues are tightly clustered and in good agreement with the LCT2 values. Three configurations, for lead walls immediately adjacent to the clusters, or pulled back by either 0.66 cm or 1.32 cm yield high calculated eigenvalues. For the fourth lead configuration the wall to lattice separation is  $\sim 5.4$  cm, a distance large enough that Lead reflection has little impact upon the calculated eigenvalue. The next two sets of calculations in Fig. 16 are for the LCT1 (base case) and LCT17 benchmarks. Once again the base geometry is a set of three clusters, now 19 x 16 rods set on a 2.03 cm pitch, with the reflecting wall located immediately adjacent the assembly and then moved perpendicularly away. Three measurements were made with a Lead wall, six measurements with <sup>depl</sup>U and five with steel. All reflected configuration calculated eigenvalues are in reasonable agreement with the base case, although close examination of these calculated eigenvalues still reveals a small bias for the Lead reflector case. That this bias is much smaller is likely a consequence of a larger lattice compared to LCT10 and so the production coming from interior lattice rods that are farther away from the reflector are not affected. The rightmost two sets of  $k_{\text{eff}}$  C/E are for the LCT7 (base case) and LCT27 (Lead reflected) experiments. In LCT27 the lead walls are posi-

tioned radially adjacent to a 14 x 14 rod lattice, and then successively pulled back in 0.5 cm steps to a maximum separation of 1.5 cm from the lattice. Once again a large calculated eigenvalue bias is observed. Lead cross sections are virtually unchanged in ENDF/B-VII.1 compared to ENDF/B-VII.0, but it seems clear that there have been and there remain deficiencies in one or more of the isotopic Lead evaluations that produce an overprediction in calculated eigenvalues. While an overprediction may be viewed by some in the criticality safety community as better than an underprediction, the opposite conclusion would be drawn by the shielding community since a consequence of calculating too much reflection back into the assembly means that a prediction of shield effectiveness would likely underpredict the number of neutrons (and therefore the dose) due to neutrons that penetrate that shield. Clearly further evaluation work on the Lead cross sections is needed.

The accurate  $k_{\text{eff}}$  C/E results for  $^{\text{depl}}\text{U}$  and steel, coupled with the previously obtained accurate  $k_{\text{eff}}$  C/E results for these materials in FAST systems indicate that their basic nuclear data are accurate over the entire energy range defined within their respective ENDF evaluations.

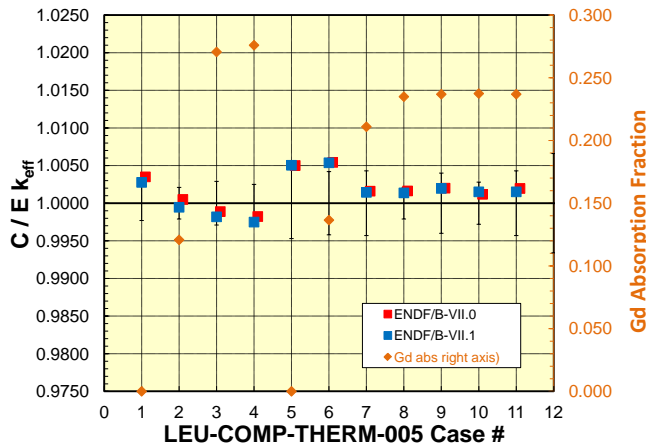


FIG. 17: Calculated eigenvalues (left hand axis) and Gadolinium absorption fractions (right hand axis) for the LEU-COMP-THERM-005 benchmark. See the ICSBEP Handbook for additional details.

The LCT5 benchmark, coupled with the LCT2 base case, provide a thermal system test of the important isotopic gadolinium cross section evaluations, particularly  $^{155,157}\text{Gd}$ . We have modeled 11 cases from this benchmark, consisting of varying amounts of dissolved Gd for assemblies with three basic lattice pitch values. Assembly size varied from a minimum of 132 rods to more than 1500 rods, arranged in an hexagonal pattern. Individual  $k_{\text{eff}}$  C/E values are shown in Fig. 17 and suggest a small positive bias, though mostly within the experimental error, for Gd poisoned systems compared to the unpoisoned base case. The overall average  $k_{\text{eff}}$  C/E though is 1.0015, a result about 0.2% higher than the average

LCT2  $k_{\text{eff}}$  C/E. We have already noted the recent  $^{157}\text{Gd}$  measurements by RPI [8] which suggest that these capture cross sections are too high. These results have not been included in the current  $^{157}\text{Gd}$  evaluation, but if they were the resulting LCT5  $k_{\text{eff}}$  C/E would increase by more than 0.5%, leading to a significant increase in the current LCT5-to-LCT2 bias. Another LCT benchmark with soluble gadolinium is LCT35.3, with about 10% Gd absorption. C/E  $k_{\text{eff}}$  for this assembly is low, 0.99507(10), and would increase and therefore improve by approximately 250 pcm with the RPI data. We previously stated that C/E  $k_{\text{eff}}$  results for PST34 are also sensitive to gadolinium cross section data and that those results were significantly worse when calculated with a  $^{157}\text{Gd}$  file derived from the RPI data. As noted in the PST discussion, in view of these conflicting results the ENDF/B-VII.1  $^{157}\text{Gd}$  evaluation is little changed from that of ENDF/B-VII.0. See the companion paper [1] for further discussion.

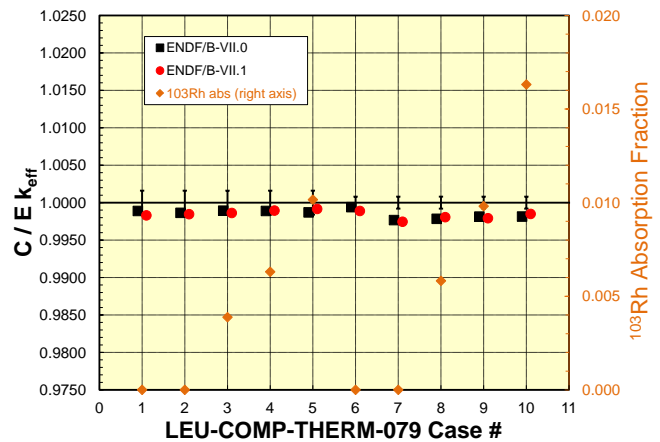


FIG. 18: Calculated eigenvalues (left hand axis) and  $^{103}\text{Rh}$  absorption fractions (right hand axis) for the LEU-COMP-THERM-079 benchmark. See the ICSBEP Handbook for additional details.

Finally, we note the results for the LCT79 benchmark. This is a series of assemblies with varying quantities of  $^{103}\text{Rh}$  foils placed among the  $\text{U}(4.31)\text{O}_2$  fuel pellets. There are typically 36 “poisoned” fuel rods centered in the assembly and surrounded by  $\sim 100$  to  $\sim 250$  “driver” rods - the exact number varying due to a combination of changing the amount of  $^{103}\text{Rh}$  or the lattice pitch. These “driver” rods contain the same fuel but lack the  $^{103}\text{Rh}$  foils. Calculated eigenvalues are illustrated in Fig. 18 and we note that the overall  $k_{\text{eff}}$  C/E results for both ENDF/B-VII.0 and ENDF/B-VII.1 are very good. For the base (LCT2) system, the average  $k_{\text{eff}}$  C/E is 0.9992 with either ENDF/B-VII.0 or ENDF/B-VII.1 cross sections while the LCT79  $k_{\text{eff}}$  C/E averages are 0.9988 and 0.9987 for ENDF/B-VII.0 and ENDF/B-VII.1 cross sections, respectively. The individual  $k_{\text{eff}}$  C/E values are tightly clustered, with a minimum-to-maximum span of less than 200 pcm. Although there have been revisions to the resolved resonance parameters in  $^{103}\text{Rh}$  for ENDF/B-

VII.1 the thermal capture cross section is essentially unchanged. The thermal assembly  $k_{\text{eff}}$  C/E results reported here support this evaluation.

### E. $^{233}\text{U}/^{232}\text{Th}$ and Systems with Zr

$^{233}\text{U}$  is little changed from that in ENDF/B-VII.0, and in fact the majority of data testing performed during the beta evaluation phase of ENDF/B-VII.1 used the  $^{233}\text{U}$  ENDF/B-VII.0 file. At a recent International Atomic Energy Agency (IAEA) Consultants meeting [9] on the adequacy of  $^{233}\text{U}$  cross section data for the  $^{233}\text{U}/\text{Th}$  fuel cycle it was noted that the low energy inelastic scattering cross section displayed a seemingly unphysical bump; an artifact of the earlier ENDF/B-VI based evaluation that had been carried forward into ENDF/B-VII.0. Recent calculations, described in [1] have reduced this feature and represents the only cross section change to the evaluated  $^{233}\text{U}$  file in going from ENDF/B-VII.0 to ENDF/B-VII.1.

$^{233}\text{U}$  bearing benchmarks from the ICSBEP Handbook that have been calculated include ten FAST systems. Among these are a bare sphere, UMF1, a  $^{nat}\text{U}$  reflected sphere, UMF6, as well as  $^{233}\text{U}$  spheres reflected by varying amounts of uranium, tungsten or beryllium. Calculated eigenvalues for ENDF/B-VII.0 and ENDF/B-VII.1 are shown in Table VII.

TABLE VII: Calculated eigenvalues for a suite of ICSBEP Handbook U233-MET-FAST benchmarks.

Benchmark	ENDF/B-VII.0 $k_{\text{eff}}$ C/E*	ENDF/B-VII.1 $k_{\text{eff}}$ C/E*	Comment
UMF1	0.99961(8)	0.99990(8)	Jezebel-23
UMF2	0.99906(8)	0.99894(8)	HEU reflector
	1.00056(9)	1.00024(8)	
UMF3	0.99948(9)	0.99928(9)	$^{nat}\text{U}$ reflector
	1.00010(9)	0.99970(9)	
UMF4	1.00482(9)	0.99841(9)	W reflector
	1.00501(9)	0.99536(9)	
UMF5	0.99440(10)	0.99611(9)	Be reflector
	0.99259(10)	0.99537(9)	
UMF6	0.99936(10)	0.99862(10)	Flattop-23

\* Values in parenthesis represent the uncertainty in the corresponding least significant digits.

As with all data testing results reported throughout this paper there are two questions to answer. First, are those benchmarks that are accurately calculated with ENDF/B-VII.0 cross sections still accurately calculated with the latest cross sections, and secondly, are those benchmarks that exhibited significant ENDF/B-VII.0 based C/E  $k_{\text{eff}}$  deviations from unity now calculated more accurately?

From Table VII we note that those UMF benchmarks whose reactivity was accurately calculated with

ENDF/B-VII.0 continue to be accurately calculated, as the near unity C/E  $k_{\text{eff}}$  values for UMF1, UMF2, UMF3 and UMF6 are retained. As noted previously, in the discussion of HMF systems, a significant revision to the W cross sections has occurred and we continue to see their impact upon calculated reactivity, with the previous 500 pcm overprediction now being a 100 to 400 pcm underprediction. Also, the Be reflected systems exhibit a reactivity increase consistent with that observed for other (HEU, Pu and MIX) FAST systems. In general the average C/E  $k_{\text{eff}}$  value is improved. For the benchmark configurations tabulated above the average C/E  $k_{\text{eff}}$  and the standard deviation of the ten sample population for ENDF/B-VII.0 and ENDF/B-VII.1 are 0.9989(42) and 0.9982(19), respectively. Although the average eigenvalue for ENDF/B-VII.1 has decreased slightly compared to ENDF/B-VII.0, the more important change is in the population standard deviation which has decreased significantly, from 0.0042 to 0.0019. This is due to the large decrease in calculated eigenvalue for the previously overpredicted W reflected systems and the modest increase in calculated eigenvalues for the previously underpredicted Be reflected systems. C/E  $k_{\text{eff}}$  for bare and uranium reflected systems were accurately calculated with ENDF/B-VII.0 cross sections and they remain so with ENDF/B-VII.1 cross sections.

There are a large suite of U233-SOL experiments in the Handbook that span the INTER and THERM categories. These include unreflected systems as well as one or more of water, polyethylene and beryllium reflectors. As shown in Fig. 19, there is a significant trend in C/E  $k_{\text{eff}}$  when plotted versus energy. This is a characteristic of ENDF/B-VII.0 and earlier cross sections, and remains so with the most recent cross sections. The only difference of note with the ENDF/B-VII.1 cross sections compared to ENDF/B-VII.0 is a small but uniform increase in calculated reactivity. There is a clear trend of decreasing eigenvalue with increasing ATFF that suggest one or more nuclear data deficiencies in the epithermal energy regime. However, it is also true that the multiplication factor attained in many of these experiments is less than 100, a relatively low value compared to most other near critical multiplication factors. Such low factors mean that a large extrapolation to critical is required which in turn implies are large uncertainty in the true critical configuration.

Reactor physicists with an interest in  $^{233}\text{U}$  cross sections will likely also care about  $^{232}\text{Th}$ . There is limited benchmark information in the ICSBEP Handbook to date on such systems. The United States' Naval Reactors Program conducted a successful Light Water Breeder Reactor (LWBR) demonstration experiment from the late 1960s into the early 1980s (see Ref. [10, 11]). Several critical assembly experiments from that program have been evaluated by the ICSBEP - UCT1 and UCT4. We include our C/E  $k_{\text{eff}}$  results for these experiments in Fig. 19. UCT1 is a lattice of fuel rods containing various combinations of  $^{233}\text{UO}_2$ ,  $^{235}\text{UO}_2$  and  $\text{ThO}_2$ . The fuel matrix

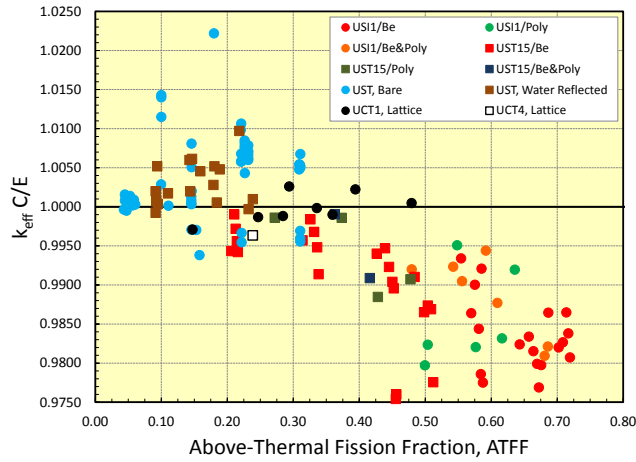


FIG. 19: Calculated eigenvalues for a suite of U233-SOL-THERM and U233-COMP-THERM benchmarks. Moderating materials include one or more of water, polyethylene and beryllium. Accurate eigenvalue predictions are obtained for the most thermal systems, and a bias of less than 0.5% is observed for the Light Water Breeder Reactor Seed-Blanket (UCT1) benchmarks, but otherwise there is a clear trend in calculated eigenvalue versus Above-Thermal Fission Fraction.

also contains significant quantities of zirconium. Collectively these experiments are sometimes referred to as the LWBR SB experiments, where “SB” means “Seed-Blanket”. The C/E  $k_{\text{eff}}$  values for these experiments generally fall within the trend established by the U233-SOL experiments and occur at an average Above-Thermal Fission Fraction value that fortuitously yields calculated  $k_{\text{eff}}$  values near unity. We have previously noted that a FAST system with a Thorium reflector, PMF6 (also known as “Thor”) has a slightly low C/E  $k_{\text{eff}}$ . C/E  $k_{\text{eff}}$  values for this small population of Thorium bearing benchmarks are generally within 200 pcm of unity; a good result. Nevertheless the population size for Thorium bearing benchmarks is very small and there is a clear need to expand this benchmark category. We conclude this discussion noting that the most highly thermalized systems, characterized by ATFF values near 0.05 are accurately calculated and, as summarized in Table VII, a number of FAST systems (whose ATFF values are unity) are also accurately calculated. This suggests that the thermal and high energy (hundreds of keV and higher) cross sections for  $^{233}\text{U}$  are likely accurate. It is deficiencies in  $^{233}\text{U}$  nuclear data over a broad range of intermediate energies that are likely responsible for the observed C/E  $k_{\text{eff}}$  trend.

Finally, we note C/E  $k_{\text{eff}}$  results for zirconium, an important reactor material, both for its superior corrosion resistance and its low neutron absorption cross section. We have assembled a suite of 21 ICSBEP benchmarks that contain significant quantities of zirconium. Eigenvalue calculations have been performed using ENDF/B-VI.8, ENDF/B-VII.0 and ENDF/B-VII.1 cross sections,

as shown in Fig. 20.

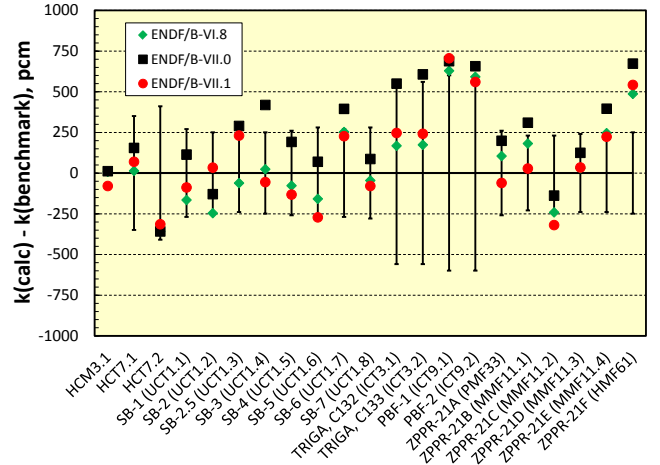


FIG. 20: Calculated eigenvalues for a suite of ICSBEP benchmarks containing zirconium.

Changes in the zirconium cross section evaluation have occurred when moving from ENDF/B-VI.8 to ENDF/B-VII.0 and again in moving from ENDF/B-VII.0 to the new ENDF/B-VII.1 file. The history of this work is summarized in our companion papers [1, 2]. For the 21 benchmark suite the average C/E  $k_{\text{eff}}$  bias was +74 pcm with ENDF/B-VI.8 cross sections and increased by approximately  $\sim 0.2\%$  when ENDF/B-VII.0 cross sections were used. Particularly disturbing was the nearly 0.4% increase in the well characterized Triga (ICT3) benchmark. The latest zirconium cross section revisions have done much to restore the previous, more accurate, C/E  $k_{\text{eff}}$  results, as the ENDF/B-VII.1 based average bias is now +83 pcm. Further evaluation work on the important stable Zr isotopes is planned, as specialized reaction rate ratio experiments (discussed below) suggest further refinements are needed in selected capture cross sections. Particularly disturbing was the nearly 0.4 % increase in the well characterized Triga (ICT3) benchmark [13].

## F. Argonne ZPR Systems

Detailed as-built MCNP models have been developed at ANL for a series of Argonne ZPR/ZPPR critical assemblies. These models represent the physical dimensions and masses of each and every plate, can, drawer and matrix tube and the interstitial gaps among these materials for the as-built material loadings for each of these assemblies. It is now practical to produce high-fidelity models of these assemblies and to calculate these experiments using continuous-energy Monte Carlo methods. Simplified models of most of these experiments are also available in the ICSBEP Handbook and results of performance testing with ENDF/B-VII.1 data for many of these models are also reported in Appendix B of this paper. It should be noted that because only very small corrections or bi-

ases are required with the use of the detailed models of these experiments to account for simplifications of the model, the associated uncertainties (and potential biases) in these models are smaller than those for the simplified benchmark models.

To test the performance of the new ENDF/B-VII.1 evaluations, analyses of these detailed models were performed by ANL using MCNP5 [4] and NJOY [3] with both ENDF/B-VII.0 and -VII.1 data. Four types of experiments (criticality,  $\beta_{eff}$ , sodium-void worth and control rod worth) are analyzed.

### 1. Criticality Measurements

Measurements of criticality (and/or sub-criticality) for 38 Argonne ZPR/ZPPR configurations, including 13 highly enriched uranium configurations, nine intermediate enriched uranium configurations, 14 mixed-(Pu, U) configurations, and two Pu metal configurations have been analyzed. The performance of the new ENDF/B-VII.1 library versus the performance of the ENDF/B-VII.0 are displayed for these four groups - HEU, IEU, mixed-(Pu, U) and Pu-metal in Figs. 21 through 24, respectively. In all of these figures the y-axis, or ordinate, represents  $(C/E - 1) \times 10^5$ , i.e., the fractional deviation between the calculated  $k_{eff}$  and the experimental  $k_{eff}$ , in pcm. The ICSBEP identifier for the critical assembly is displayed on the abscissa. The standard ZPR/ZPPR assembly numbers are displayed as labels with each of the data values. The order of the assemblies, with the exception of the three mixed-(Pu, U) assemblies which are not provided in the ICSBEP Handbook, is always from hardest neutron spectrum (left side) to softest spectrum (right side), as determined by the values of EALF and the fission fraction at energies  $>100$  keV as given in the neutron balance tables in the Handbook.

The results obtained for the HEU-fueled assemblies (see Fig. 21) indicate that all 13 assemblies were overpredicted with ENDF/B-VII.0 data. The average ENDF/B-VII.0  $k_{eff}$  bias is in excess of 1%  $\delta k/k$  (1042 pcm); the largest bias (ZPR-9/4) was almost 2%  $\delta k/k$  (1948 pcm). All 13 C/E  $k_{eff}$  's are reduced with ENDF/B-VII.1 cross sections and the average C/E  $k_{eff}$  bias is now  $<0.5\%$   $\delta k/k$  (461 pcm). Notably, the bias for ZPR-9/4 was reduced by  $>1.2\%$   $\delta k/k$  to  $0.7\%$   $\delta k/k$  with ENDF/B-VII.1 data. The ZPR-9 series includes varying amounts of tungsten. We have already noted the improved C/E  $k_{eff}$  values for tungsten bearing benchmarks and obtaining improved results here further confirms our previous conclusion about the improved tungsten cross sections in ENDF/B-VII.1 Only the bias for the ZPPR-20E assembly, an accident scenario for a space application with an HEU core containing lithium and reflected with beryllium oxide and silicon dioxide, was not significantly reduced (from  $+1685 \pm 800$  pcm to  $+1490 \pm 800$  pcm). The ZPPR-20E experiment was very subcritical and had the largest experimental uncertainty among the full set of 38 configurations. The last

of the experiments displayed in Fig. 21 is for ZPR-9/34, a Uranium/Iron assembly. This is a clean physics benchmark assembly with an intermediate spectrum, having only 40% of the fissions occurring above 100 keV. The overprediction of  $k_{eff}$  for this assembly, almost 1%  $\delta k/k$  (882 pcm) with ENDF/B-VII.0, is reduced to  $+217 \pm 111$  pcm with ENDF/B-VII.1.

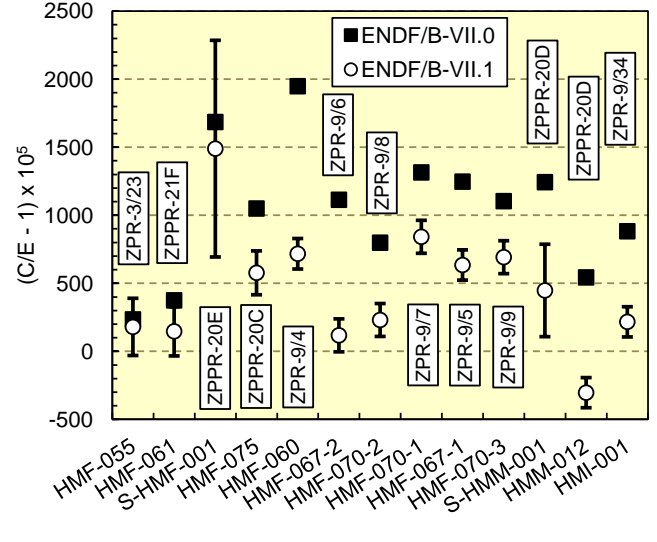


FIG. 21: MCNP calculations with As-Built models for HEU FAST and INTER ZPR/ZPPR Assemblies.

The C/E  $k_{eff}$  results obtained for the IEU-fueled assemblies (see Fig. 22) indicate that seven of the nine assemblies are overpredicted with ENDF/B-VII.0 cross sections. The average ENDF/B-VII.0 C/E  $k_{eff}$  bias is  $0.27\%$   $\delta k/k$  (270 pcm). Eight of the nine C/E  $k_{eff}$  's are reduced and one is unchanged with the ENDF/B-VII.1 data and the average C/E  $k_{eff}$  bias is reduced by one-half ( $134 \pm 115$  pcm). The change in these average values is skewed by the relatively large changes for the two tungsten-bearing assemblies, ZPR-9/2 and ZPR9/3,  $388 \pm 7$  pcm and  $625 \pm 7$  pcm, respectively. The improved C/E  $k_{eff}$  predictions for tungsten bearing benchmarks have already been discussed and so a similar observation for assemblies is to be expected. For the other seven IEU-fueled assemblies ENDF/B-VII.1 cross sections have little effect as these assemblies were well predicted with ENDF/B-VII.0 data and remain so with the ENDF/B-VII.1 data.

Collectively the results obtained for ZPR-9 Assemblies 1-3 (shown in Fig. 22) and for ZPR-9 Assemblies 4-9 (shown in Fig. 21) provide a very strong test for tungsten in the fast energy region. The cleanest test of these data is provided with the first four assemblies. Assembly 1 was a well-characterized reference for these measurements. It contained no tungsten and had an enrichment ( $^{235}\text{U}/\text{U}$ ) of  $\sim 11\%$ . In Assemblies 2, 3 and 4, one-fourth, one-half, and finally all of the depleted uranium diluent in the core unit cell of Assembly 1 was replaced by tungsten, resulting in  $^{235}\text{U}/\text{U}$  enrichments in Assemblies 2

and 3 of  $\sim 16\%$  and  $\sim 21\%$ , respectively. Carbon was added to the core unit cell in Assembly 5 to soften the spectrum. In Assembly 6 some of the tungsten was replaced with perforated aluminum; and in Assemblies 7, 8 and 9 the aluminum reflector was replaced with  $\text{Al}_2\text{O}_3$  and BeO-Al. The improvement in the monotonic (or perhaps, monolithic) increase or trend in the C/E bias for Assemblies 1-4, namely, 215, 533, 897 and 1948 pcm with ENDF/B-VII.0 data, versus 205, 147, 273 and 717 pcm with ENDF/B-VII.1 further support the changes made in the new isotopic tungsten evaluations.

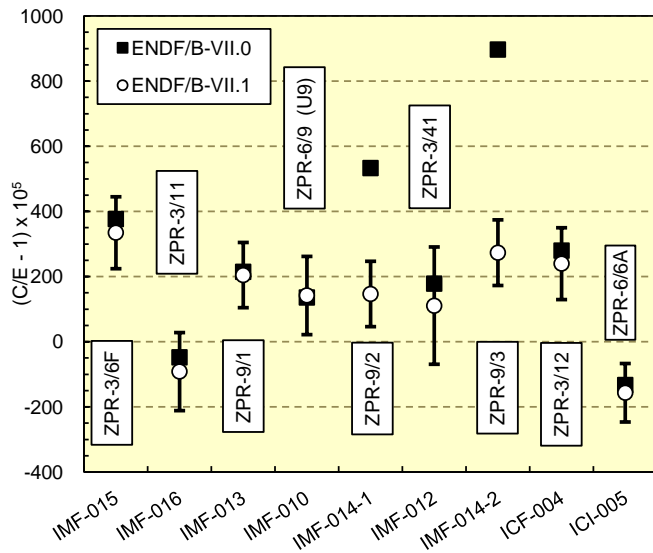


FIG. 22: MCNP calculations with As-Built models for IEU FAST and INTER ZPR/ZPPR Assemblies.

The results shown in Fig. 23 for Mixed-(Pu, U)-fueled assemblies demonstrate that all 14 calculated C/E  $k_{\text{eff}}$ 's are reduced with ENDF/B-VII.1, with individual C/E  $k_{\text{eff}}$  values dropping by approximately 60 to 215 pcm. Two of these 14 assemblies, ZPR-3/53 and ZPR-3/54, have a softer spectrum than the remaining assemblies. We note that the calculated  $k_{\text{eff}}$  C/E biases for the ZPR-3/53 and ZPR-3/54 assemblies are considerably larger than the biases for the other twelve assemblies. The average bias for the 14 assemblies with ENDF/B-VII.0 data is 271 pcm; the average bias with ENDF/B-VII.1 is 144 pcm. The biases for ZPR-3/53 and ZPR-3/54 with ENDF/B-VII.0 data are 855 and 1233 pcm, respectively; and with ENDF/B-VII.1 data are 755 and 1047 pcm, respectively. The average bias for the other 12 assemblies with ENDF/B-VII.0 data is 142 pcm; the average bias with ENDF/B-VII.1 data is 18 pcm. In summary, the new data evaluations improve the results for the 2 softer spectrum assemblies by  $\sim 100 - 200$  pcm; and the new data evaluations essentially remove the average bias for the remaining mixed-(Pu, U)-fueled fast assemblies.

There were only 2 Pu-Metal fueled experiments among the present series of detailed models of ZPR/ZPPR experiments. Their results are shown in Fig. 24. The first is

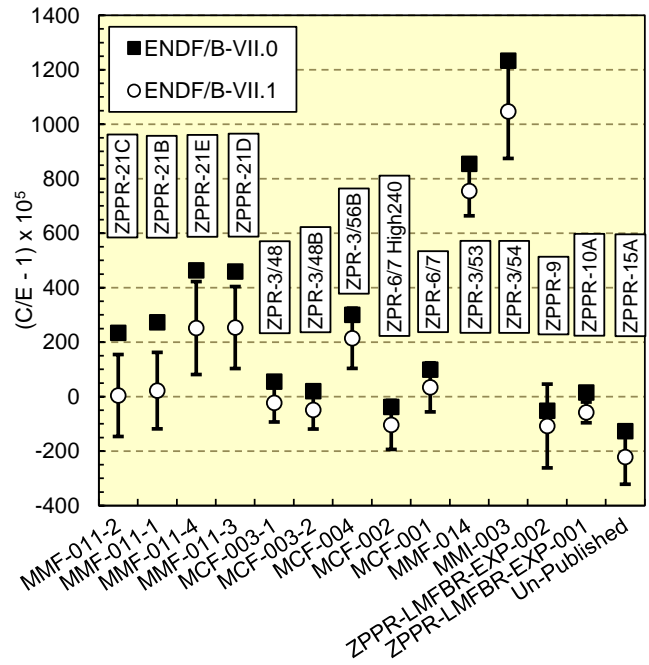


FIG. 23: MCNP Calculations with As-Built models for Mixed (Pu, U) FAST and INTER ZPR/ZPPR Assemblies.

a very fast spectrum assembly, ZPPR-21A, having  $\sim 80\%$  of the fissions occurring above 100 keV. The C/E  $k_{\text{eff}}$  bias for this assembly with ENDF/B-VII.0 cross sections is  $225 \pm 150$  pcm, which is completely eliminated,  $-22 \pm 150$  pcm, with ENDF/B-VII.1. The second of these assemblies, ZPR-6/10, has the softest spectrum among this series of 38 assemblies, with only  $\sim 33\%$  of the fissions occurring above 100 keV. The  $k_{\text{eff}}$  C/E bias for this assembly with ENDF/B-VII.0 data is  $\sim 3.8\% \delta k$  ( $3786 \pm 135$  pcm), and is reduced to  $\sim 2.6\% \delta k$  ( $2648 \pm 135$  pcm) with ENDF/B-VII.1 data. Improvements in the underlying Mn and Cr evaluated files are primarily responsible for these more accurate results.

A summary comparison of the average values of C/E - 1 (in pcm) for ENDF/B-VII.1 according to fuel type for these 38 ZPR/ZPPR assemblies is given in Table VIII. It is seen that the ENDF/B-VII.1 data consistently lower the calculated  $k_{\text{eff}}$ 's for these systems. With the exception of a few unusual assemblies in support of space nuclear (having non-traditional reflector materials) and the three very soft spectrum assemblies (ZPR-3/53, ZPR-3/54 and ZPR6/10) which remain badly overpredicted, the traditional fast reactor assemblies are consistently well-predicted with ENDF/B-VII.1

## 2. Beta-effective ( $\beta_{\text{eff}}$ ) Measurements

Measurements of  $\beta_{\text{eff}}$  were made in three of the 38 ZPR/ZPPR critical assemblies for which detailed as-built

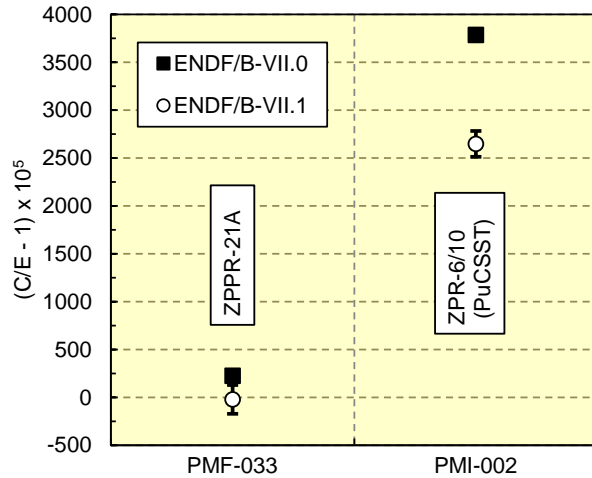


FIG. 24: MCNP Calculations with As-Built models for Pu metal FAST and INTER ZPR/ZPPR Assemblies.

TABLE VIII: Summary of average calculated eigenvalue, given as  $k_{\text{eff}}$  (C/E - 1), in pcm, for ENDF/B-VII.0 and ENDF/B-VII.1. Results are categorized by ZPR/ZPPR Fuel Type.

Fuel Type	# of Expts	ENDF/B-VII.0 (C/E-1)*	ENDF/B-VII.1 (C/E-1)*
Pu Metal	2	2005(143)	1327(143)
Mixed (Pu, U)	14	271(114)	156(114)
HEU	13	1042(201)	463(201)
IEU	9	270(115)	134(115)

\* Values in parenthesis represent the uncertainty in the corresponding least significant digits.

\*\* Mean values are not as meaningful for this fuel type category due to the limited sample size and knowledge that the two assemblies in this category had distinctly different energy spectra.

Monte Carlo models are available. Experimental measurements of  $\beta_{\text{eff}}$  were made in ZPR-9/34, ZPR-6/9 and ZPR-6/10. All 3 of these assemblies were clean, physics benchmark assemblies performed as part of the ANL Diagnostic Core Program. ZPR-9/34 (HEU-MET-INTER-001) was referred to as the Uranium/Iron Benchmark Assembly; ZPR-6/9 (IEU-MET-FAST-010) was referred to as the U9 Benchmark Assembly; and ZPR-6/10 (PU-MET-INTER-002) was referred to as the Pu/C/SST Benchmark Assembly. The  $\beta_{\text{eff}}$  measurements in these assemblies were analyzed using detailed MCNP models with both ENDF/B-VII.0 and -VII.1 data. Results are presented in Table IX. There is very little change in the values calculated for these three assemblies between ENDF/B-VII.0 and ENDF/B-VII.1 data; only the value in ZPR-6/9 is lower by  $\sim 1.5\%$ . The calculated values

are slightly higher (by  $1.5\sigma$ ) than the measured values in ZPR-9/34 and in excellent agreement with the ZPR-6/9 and ZPR-6/10 measurements.

TABLE IX: Comparison of measured and either ENDF/B-VII.0 or ENDF/B-VII.1 calculated  $\beta_{\text{eff}}$  values.

Benchmark	Measured $\beta_{\text{eff}}$ *	ENDF/B Version	Calculated $\beta_{\text{eff}}$ *
HMI1 (ZPR-9/34, U/Fe)	0.00657(13)	VII.0 VII.1	0.00681(6) 0.00682(6)
IMF10 (ZPR-6/9, U9)	0.00706(9)	VII.0 VII.1	0.00716(6) 0.00707(6)
PMI2 (ZPR-6/10, PuC/SS)	0.00222(5)	VII.0 VII.1	0.00224(3) 0.00224(3)

\* Values in parenthesis represent the uncertainty in the corresponding least significant digits.

$\beta_{\text{eff}}$  was also calculated for two additional ICSBEP benchmarks, ZPR-6/6A (IEU-COMP-INTER-005) and ZPR-6/7 (MIX-COMP-FAST-001) using detailed, as-built, Monte Carlo models, even though experimental values of  $\beta_{\text{eff}}$  were not available. For ZPR-6/6A the calculated  $\beta_{\text{eff}}$  value decreased by  $\sim 1.2\%$  with ENDF/B-VII.1 cross sections compared to the ENDF/B-VII.0 result; for ZPR-6/7 the ENDF/B-VII.1 calculated  $\beta_{\text{eff}}$  value decreased by  $\sim 0.9\%$ . Although these calculated values cannot validate either ENDF/B-VII.0 or ENDF/B-VII.1 data, they do verify that the changes from ENDF/B-VII.0 to ENDF/B-VII.1 yield only small changes in predicted  $\beta_{\text{eff}}$  values for typical sodium fast reactors, consistent with the small changes observed for the three assemblies (HMI1, IMF10 and PMI2) tested and discussed above.

### 3. Measurements of Sodium Void Worth ( $\rho_{\text{Na}}$ )

Among the series of 38 ZPR/ZPPR critical assemblies for which detailed as-built Monte Carlo models are available, measurements of sodium-void worth ( $\rho_{\text{Na}}$ ) were made in three, ZPPR-9, ZPPR-10A and ZPPR-15A. These measurements simulated the voiding of sodium by replacing sodium-filled stainless-steel cans with closely-matched empty stainless-steel cans from all core drawers within a specified central region. The worth of the material replacements was obtained by first measuring a sub-critical (sodium-filled) reference configuration, and then successively voiding sodium from specific regions of the core and using the Modified Source Multiplication (MSM) method to measure the sub-criticality of each voiding step. These measured reactivity changes can then be calculated by k-difference calculations using detailed Monte Carlo models of each successive assembly loading.

In order to minimize the contribution of the Monte Carlo statistical uncertainties to the uncertainty in the C/E values, individual eigenvalue calculations were generally run for 250 million histories, yielding  $k_{\text{calc}}$  stochastic uncertainties ( $1\sigma$ ) of 2 to 3 pcm.

Results of analyzing these sodium void worth measurements with ENDF/B-VII.0 and ENDF/B-VII.1 are compared with the measured values in Table X. In the past these experiments have generally been characterized as well calculated. Changes seen in moving to ENDF/B-VII.1 generally lead to smaller C/E's, but there are notable differences, such as the last ZPPR-9 configuration and the first two ZPPR-15A configurations where the C/E deviation exceeds  $2\sigma$ .

#### 4. Worth Measurements of Control Rods and Control Positions

Worth measurements of simulated control rods (CRs) and control rod positions (CRPs) were also made in the ZPPR-9, ZPPR-10A and ZPPR-15A assemblies. As with the measurement of the sodium void worths, these experiments were performed by first measuring a sub-critical reference configuration and then using the MSM method to measure the sub-criticality of subsequent configurations containing simulated CRs and/or CRPs.

Results of analyzing these control rod and control rod position worth measurements with ENDF/B-VII.0 and ENDF/B-VII.1 cross sections are presented in Table XI. As for the sodium void measurements, these control rod experiments are generally well calculated with ENDF/B-VII.0. And again there is very little change in the calculated values with ENDF/B-VII.1, which also are generally in good agreement with the measured data. The ZPPR-10A measurements are slightly overpredicted and the ZPPR-15A measurements are slightly underpredicted. As several of these differences exceed  $2\sigma$  it is clear that further study to understand these differences is needed.

In summary, the analysis of the detailed Monte Carlo models for this series of fast reactor systems with ENDF/B-VII.1 data confirms the analysis performed using the simplified ICSBEP benchmarks for these systems. Prediction of criticality is generally improved with the new data, and select new evaluations such as tungsten are considerably improved. Analyses of  $\beta_{\text{eff}}$ , sodium-void worth and control rod worth measurements confirmed that the new data make only small changes in these parameters, and the generally good performance of ENDF/B-VII.0 will be maintained with ENDF/B-VII.1 data.

#### G. Reaction Rate Studies

Advanced nuclear systems and associated fuel cycles need accurate cross section data to provide a reliable as-

TABLE X: Comparison of sodium void worth ( $\rho_{\text{Na}}$ ) measurements in ZPPR-9, ZPPR-10A and ZPPR-15A with ENDF/B-VII.0 and ENDF/B-VII.1 predictions. Measured and calculated values are in pcm.

ZPPR/Void Region	Measured $\rho_{\text{Na}}$	ENDF/B Version	Calculated $\rho_{\text{Na}}$
ZPPR-9			
20.32 cm axial region, 97 drawers per half	104(2)	VII.0 VII.1	106(4) 100(4)
50.80 cm axial region, 97 drawers per half	112(2)	VII.0 VII.1	109(4) 110(4)
68.58 cm axial region, 97 drawers per half	86(2)	VII.0 VII.1	85(4) 78(4)
ZPPR-10A			
20.32 cm axial region, 88 drawers per half	76(1)	VII.0 VII.1	88(4) 78(4)
20.32 cm axial region, 172 drawers per half	145(2)	VII.0 VII.1	153(4) 148(4)
40.64 cm axial region, 172 drawers per half	187(2)	VII.0 VII.1	194(4) 192(4)
50.80 cm axial region, 172 drawers per half	159(2)	VII.0 VII.1	160(4) 154(4)
ZPPR-15A			
20.32 cm axial region, 148 drawers per half	370(3)	VII.0 VII.1	352(4) 356(4)
35.56 cm axial region, 148 drawers per half	101(1)	VII.0 VII.1	89(4) 80(4)
45.72 cm axial region, 148 drawers per half	-35(1)	VII.0 VII.1	-39(4) -30(4)
78.74 cm axial region, 148 drawers per half	-76(2)	VII.0 VII.1	-75(4) -84(4)

\* Values in parenthesis represent the uncertainty in the corresponding least significant digits.

TABLE XI: Comparison of Control Rod (CR) and Control Rod Position (CRP) measurements in ZPPR-9, ZPPR-10A and ZPPR-15A and ENDF/B-VII.0 and ENDF/B-VII.1 predictions. Measured and calculated values are in pcm.

ZPPR/CR or Measured CRP	$\rho_{CR}$ *	ENDF/B Version	Calculated $\rho_{CR}$ *
ZPPR-9			
6 CRs, row 7	-969(12)	VII.0	-991(4)
		VII.1	-980(4)
6 CRPs, row 7	-6245(73)	VII.0	-6356(5)
		VII.1	-6379(5)
6 CRs in center and middle ring	-6131(74)	VII.0	-6170(5)
		VII.1	-6198(5)
CRs 4 and 7	-2315(28)	VII.0	-2374(4)
		VII.1	-2372(4)
Central 3x3 CR	-1179(14)	VII.0	-1209(4)
		VII.1	-1209(4)
ZPPR-10A			
Central Rod	-886(10)	VII.0	-945(9)
		VII.1	-953(4)
6 CRs, row 4	-4496(48)	VII.0	-4833(4)
		VII.1	-4854(4)
12 CRs, row 7	-7156(105)	VII.0	-7550(5)
		VII.1	-7574(5)
6 row 7 corner rods	-3237(37)	VII.0	-3447(4)
		VII.1	-3458(4)
ZPPR-15A			
Central 2x2 Na CRP	-161(2)	VII.0	-160(4)
		VII.1	-156(4)
Central 2x2 CR, 100% $^{nat}B_4C$	-1306(9)	VII.0	-1265(4)
		VII.1	-1277(4)
Central 2x2 CR, 50% $^{nat}B_4C$	-999(7)	VII.0	-910(4)
		VII.1	-932(4)

\* Values in parenthesis represent the uncertainty in the corresponding least significant digits.

assessment of their performance. Closed fuel cycles with the objective of waste minimization imply, from a physics point of view:

- A high content of minor actinides in the reactor core and in the fuel cycle;
- A high Fissile/Fertile isotope content in the core fuel;
- A variable, and potentially degraded, Pu isotopic vector in the fuel cycle;
- Lower fuel density to achieve lower conversion ratios

Basic data are available for TRU (transuranic) isotopes up to Cf but validation is needed in order to quantify their

reliability. The high amount of minor actinides (MA) foreseen in advanced fuel cycle systems requires specific validation work, especially for capture and fission cross sections of such isotopes.

Such validation is traditionally done through the use of differential and integral experiments, and uncertainty assessment. Information that can be gathered on MA's from experiment comes mostly from small sample irradiation, reactivity oscillation, and fission and capture rate measurements. Separate isotope sample and fuel pin irradiation in power reactors also provides a unique source of measurement data.

Results from analyses of such experiments provide indications to nuclear data evaluators for improving the quality of basic files, and to assess their impact on advanced fuel cycles. Experimental data from the PROFIL irradiation experiments [12], performed at the CEA PHENIX fast reactor, provide clean and precise information on both cross section data and transmutation rates of actinides. These data are essential for the validation of the methods and data to be used in advanced fuel cycles where transmutation systems will be used to reduce the existing inventory of nuclear waste.

During the PROFIL-1 experiment (see Fig. 25 and Fig. 26), performed in 1974, a pin containing 46 samples, including fission products plus major and minor actinides (Uranium, Plutonium, and Americium isotopes) was irradiated in the PHENIX reactor for the first three cycles, corresponding to a total of 189.2 full-power days. The experimental pin was located in the central subassembly of the core, and in the third row of pins inside the subassembly. This location is far away from neutronic perturbations allowing clear irradiation conditions. Following the reactor irradiation, mass spectroscopy was then used, with simple or double isotopic dilution and well-characterized tracers to measure isotopic concentrations. The data are reported as "spectral indices", i.e., as a ratio of the cited reaction to  $^{235}U(n,f)$  cross section. The experimental uncertainty, provided in Tables XII and XIII, is relatively small.

The second part of the PROFIL irradiation campaign took place in 1979. During this experiment two standard pins, each containing 42 separated capsules of fission products plus major and minor actinides (Uranium, Plutonium, Americium and Neptunium isotopes), were irradiated for four cycles (the 17th through 20th) in the PHENIX reactor. As for PROFIL-1, chemical and mass spectrometry analyses were subsequently performed to determine the post-irradiation isotopic concentrations.

MCNP5 models were developed for the analysis of the irradiation experiments. One group cross sections for the samples were calculated by taking batch statistics of several independent calculations with recorded surface sources. For the results obtained using ENDF/B-VII.1 data, the same recorded surface histories obtained with ENDF/B-VII.0 data were used. This assumption is justified as the cross section data for the major actinides comprising the PHENIX reactor fuel did not change sig-

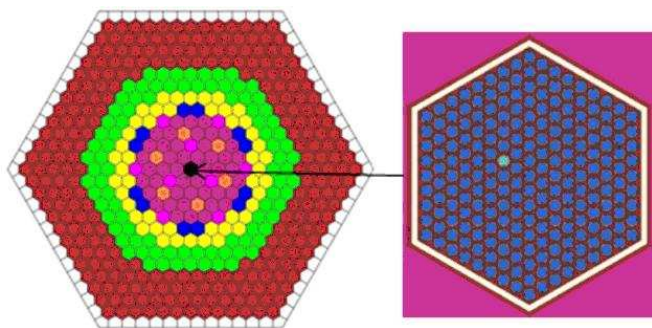


FIG. 25: PROFIL-1 irradiation experiment in the French fast reactor PHENIX - Assembly Overview.

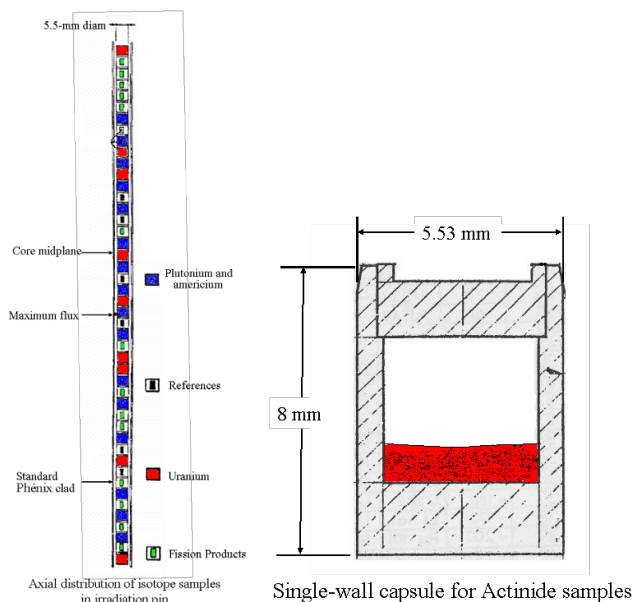


FIG. 26: PROFIL-1 irradiation experiment in the French fast reactor PHENIX - Rod and Sample Overview.

nificantly between ENDF/B-VII.0 and VII.1.

Table XII shows a comparison of the C/E's for the different irradiation experiments. Improvements can be observed for the ENDF/B-VII.1 capture data in  $^{238,242}\text{Pu}$ ,  $^{241,243}\text{Am}$ ,  $^{244}\text{Cm}$ ,  $^{97}\text{Mo}$ ,  $^{151}\text{Sm}$ ,  $^{153}\text{Eu}$ , and for  $^{240}\text{Pu}(n,2n)$ . On the other hand,  $^{95}\text{Mo}$  and  $^{133}\text{Cs}$  capture C/E results exhibit little change, or are slightly worse. For the major actinides  $^{235}\text{U}$  and especially  $^{239}\text{Pu}$  capture C/E's are underestimated. For fission products,  $^{105,106}\text{Pd}$ ,  $^{143,144}\text{Nd}$  and  $^{147,149}\text{Sm}$  are significantly underestimated, while  $^{101}\text{Ru}$  and  $^{151}\text{Sm}$  are overestimated. Other C/E deviations from unity are within the combined experimental and calculated statistical uncertainty.

The PROFIL experiments also provide information on fission cross sections. Experimental results provide the Nd isotope build-up in the actinide samples. If the fission product yield is well known, an estimate can be made for the fission cross section. Nevertheless, the knowledge of

TABLE XII: C/E's for the PROFIL-1 and PROFIL-2 irradiation experiments. Measured data are a ratio of the reaction cited below to  $\sigma_{fis}^{235}\text{U}$ . The spectral index (ratio of  $^{238}\text{U}(n,f)$  to  $^{235}\text{U}(n,f)$ ) is 0.027.

Reaction	PROFIL-1 C/E		
	ENDF/B-VII.0	ENDF/B-VII.1	Expt. Unc.
$\sigma_{capt}^{235}\text{U}$	0.948	0.948	1.7%
$\sigma_{capt}^{238}\text{U}$	0.972	0.972	2.3%
$\sigma_{capt}^{238}\text{Pu}$	1.299	1.135	4.0%
$\sigma_{capt}^{239}\text{Pu}$	0.906	0.906	3.0%
$\sigma_{n,2n}^{239}\text{Pu}$	0.745	0.745	15.0%
$\sigma_{capt}^{240}\text{Pu}$	0.964	0.945	2.2%
$\sigma_{n,2n}^{240}\text{Pu}$	0.779	1.084	15.0%
$\sigma_{capt}^{241}\text{Pu}$	0.950	0.947	4.1%
$\sigma_{capt}^{242}\text{Pu}$	1.061	1.020	3.5%
$\sigma_{capt}^{241}\text{Am}$	0.968	0.980	1.7%
$\sigma_{capt}^{243}\text{Am}$	0.834	0.939	5.0%
$\sigma_{capt}^{95}\text{Mo}$	1.032	1.063	3.8%
$\sigma_{capt}^{97}\text{Mo}$	0.968	0.993	4.4%
$\sigma_{capt}^{101}\text{Ru}$	1.101	1.095	3.6%
$\sigma_{capt}^{105}\text{Pd}$	0.852	0.845	4.0%
$\sigma_{capt}^{133}\text{Cs}$	0.878	0.827	4.7%
$\sigma_{capt}^{145}\text{Nd}$	0.955	0.936	3.8%
$\sigma_{capt}^{149}\text{Sm}$	0.915	0.908	3.1%

Reaction	PROFIL-2 C/E		
	ENDF/B-VII.0	ENDF/B-VII.1	Expt. Unc.
$\sigma_{capt}^{235}\text{U}$	0.967	0.967	1.7%
$\sigma_{capt}^{238}\text{U}$	0.985	0.985	2.3%
$\sigma_{capt}^{237}\text{Np}$	0.944	0.941	3.6%
$\sigma_{capt}^{238}\text{Pu}$	1.341	1.181	4.0%
$\sigma_{capt}^{239}\text{Pu}$	0.922	0.922	3.0%
$\sigma_{n,2n}^{239}\text{Pu}$	0.574	0.745	15.0%
$\sigma_{capt}^{240}\text{Pu}$	0.973	0.961	2.2%
$\sigma_{capt}^{242}\text{Pu}$	1.054	1.022	4.3%
$\sigma_{capt}^{241}\text{Am}$	1.018	1.021	1.7%
$\sigma_{capt}^{244}\text{Cm}$	1.101	0.956	2.0%
$\sigma_{capt}^{106}\text{Pd}$	0.939	0.939	2.0%
$\sigma_{capt}^{143}\text{Nd}$	0.937	0.937	2.0%
$\sigma_{capt}^{144}\text{Nd}$	0.935	0.928	2.0%
$\sigma_{capt}^{147}\text{Sm}$	0.894	0.894	2.0%
$\sigma_{capt}^{151}\text{Sm}$	1.094	1.085	2.0%
$\sigma_{capt}^{153}\text{Eu}$	0.924	0.954	2.0%

the fission yields is based on the fission cross sections, so this can be a tautological situation.

A more accurate way to gather information on fission cross sections from elemental experiments is through the analysis of fission spectral indices. In this case, fission reaction rates of actinides are measured against a standard, in particular  $^{235}\text{U}$  fission. If the measurements are done in the center of a reactor in a well characterized spectrum, indirect effects are minimal and the result can be

directly related to the actinide fission cross section. This is the situation for the COSMO experimental campaign, performed at the French zero power fast spectrum facility MASURCA, where different actinide fission spectral indices were measured. The experiment was analyzed based upon the benchmark specifications provided in Ref. [14] and results are shown in Table XIII. We conclude from these results that ENDF/B-VII.1  $^{238,240}\text{Pu}$  fission cross sections have improved while  $^{242}\text{Pu}$ 's fission cross section has not.

TABLE XIII: C/E's for COSMO fission spectral indices. Measured data are a ratio of the reaction cited below to  $\sigma_{fis}^{235\text{U}}$ . The spectral index (ratio of  $^{238}\text{U}(n,f)$  to  $^{235}\text{U}(n,f)$ ) is 0.042.

Isotope	COSMO C/E		
	ENDF/B-VII.0	ENDF/B-VII.1	Expt. Unc.
$\sigma_{fis}^{238}\text{U}$	0.984	0.981	1.5%
$\sigma_{fis}^{237}\text{Np}$	1.005	1.004	1.5%
$\sigma_{fis}^{238}\text{Pu}$	1.072	1.040	2.5%
$\sigma_{fis}^{239}\text{Pu}$	0.991	0.989	1.3%
$\sigma_{fis}^{240}\text{Pu}$	1.051	1.028	2.3%
$\sigma_{fis}^{241}\text{Pu}$	1.004	1.001	2.0%
$\sigma_{fis}^{242}\text{Pu}$	1.018	1.041	2.3%
$\sigma_{fis}^{241}\text{Am}$	1.089	1.081	2.3 %
$\sigma_{fis}^{243}\text{Am}$	1.010	1.009	2.3%

Additional reaction rate data are available from the ICSBEP Handbook's FUND-IPPE-RR-MULT-RRR-001 benchmark. This is an unmoderated, Pu fueled assembly with a central cavity for sample irradiation. As with any reactor based measurement the flux spectrum seen by the sample covers a broad energy distribution. In these measurements the average energy of that spectrum is near 1.5 MeV. Differences in the "fast" spectra seen at the sample location in the PROFIL, Flattop-25 and this assembly are illustrated in Fig. 27. A number of actinide and structure cross section ratio measurements have been reported. As with the PROFIL and COSMO experiments above the data are given as a spectral index, again to  $^{235}\text{U}(n,f)$ . Measured and calculated results are given in Tables XIV and XV.

Many of the major actinide cross sections are little or unchanged in ENDF/B-VII.1 compared to ENDF/B-VII.0; a notable exception being  $^{236}\text{U}$  whose ENDF/B-VII.0 capture cross section is clearly low. The upward revision found in ENDF/B-VII.1 yields a clearly superior C/E value, as was shown in our companion paper [1].

These results have not been generally available to the evaluation community before. We note that some of these results appear contradictory, with some PROFIL and COSMO C/E values being greater than (or less than) unity while similar data from the FUND-IPPE-RR-MULT-RRR-001 experiment yield the opposite result. Results for  $^{237}\text{Np}$  capture and either  $^{240}\text{Pu}$  or  $^{242}\text{Pu}$  fission are examples. It is beyond the scope of a survey

TABLE XIV: Measured and calculated spectral indices (measured data are a ratio of the reaction cited below to  $^{235}\text{U}(n,f)$ ) for selected actinide cross sections from the FUND-IPPE-RR-MULT-RRR-001 benchmark. Values in parenthesis represent the uncertainty in the corresponding least significant digits.

Reaction	Measured Value	ENDF/B-VII.0	ENDF/B-VII.1
$^{232}\text{Th}(n,f)$	0.0430(13)	0.0398(2)	0.0398(1)
$^{233}\text{U}(n,f)$	1.54(3)	1.5546(7)	1.5545(1)
$^{234}\text{U}(n,f)$	0.790(24)	0.7294(4)	0.7293(2)
$^{236}\text{U}(n,f)$	0.333(10)	0.3215(2)	0.3216(1)
$^{238}\text{U}(n,f)$	0.165(5)	0.1622(1)	0.1622(1)
$^{237}\text{Np}(n,f)$	0.771(23)	0.8135(4)	0.8134(2)
$^{239}\text{Pu}(n,f)$	1.33(4)	1.3603(6)	1.3603(2)
$^{240}\text{Pu}(n,f)$	0.877(26)	0.8234(4)	0.8110(2)
$^{241}\text{Pu}(n,f)$	1.29(4)	1.3222(6)	1.3219(2)
$^{242}\text{Pu}(n,f)$	0.658(20)	0.6704(4)	0.6859(2)
$^{241}\text{Am}(n,f)$	0.825(25)	0.7816(4)	0.7782(3)
$^{232}\text{Th}(n,\gamma)$	0.109(4)	0.1019(1)	0.1029(1)
$^{236}\text{U}(n,\gamma)$	0.123(6)	0.1118(2)	0.1201(1)
$^{238}\text{U}(n,\gamma)$	0.077(3)	0.0778(1)	0.0777(1)
$^{237}\text{Np}(n,\gamma)$	0.240(12)	0.3007(3)	0.3006(1)
$^{232}\text{Th}(n,2n)$	0.00924(50)	0.01084(6)	0.01070(3)
$^{238}\text{U}(n,2n)$	0.00916(50)	0.00954(5)	0.00948(2)

report such as this to resolve such apparent discrepancies, but we note below that there are clear differences in the spectra for what are generically categorized as "fast" assemblies. By highlighting this behavior to the broader technical community we hope to stir interest in further studies to resolve such issues. Poor C/E values are also seen for several mid-Z reactions, such as  $^{48}\text{Ti}(n,p)$  and  $^{94,96}\text{Zr}(n,\gamma)$ . It is our expectation that the results provided herein will be judged useful as revised evaluation efforts are undertaken in the future.

We conclude this section with the presentation of previously unpublished fission reaction rate ratio measurements from LANL's Flattop-25 assembly [15]. Like the PROFIL results presented previously, these data are obtained in a "fast" system. However, "fast" can cover a broad range of energies, as illustrated in Fig. 27. This figure illustrates calculated multigroup spectra at the sample or measurement location for the PROFIL, Flattop-25 and FUND-IPPE-FE-MULT-RRR-001 assemblies. While all of these assemblies are clearly "fast" systems, the average energy is seen to vary by hundreds of keV which then means these measurements test different energy regimes within the more general "fast" category. The Flattop-25 measurements were performed in the early 1970s with data obtained from two radial locations - one near the center of the assembly where the spectrum is hardest, the second in the tamper region where the spectrum is softer. As with many older experiments, quantitative uncertainty information is lacking but recent discussions with the principal experimenter,

TABLE XV: Measured and calculated spectral indices for selected structural element cross sections from the FUND-IPPE-RR-MULT-RRR-001 Benchmark. Values in parenthesis represent the uncertainty in the corresponding least significant digits.

Reaction	Measured Value	ENDF/B-VII.0	ENDF/B-VII.1
<sup>27</sup> Al(n,α)	0.00043(2)	0.00046(1)	0.00045(1)
<sup>54</sup> Fe(n,α)	0.00050(2)	0.00053(1)	0.00053(1)
<sup>59</sup> Co(n,α)	0.000095(4)	0.000096(1)	0.000095(1)
<sup>92</sup> Mo(n,α)	0.000055(5)	0.000086(1)	0.000085(1)
<sup>24</sup> Mg(n,p)	0.00090(4)	0.00102(1)	0.00101(1)
<sup>27</sup> Al(n,p)	0.00221(15)	0.00205(1)	0.00215(1)
<sup>46</sup> Ti(n,p)	0.0066(3)	0.0071(1)	0.0058(1)
<sup>47</sup> Ti(n,p)	0.0097(5)	0.0093(1)	0.0102(1)
<sup>48</sup> Ti(n,p)	0.000180(8)	0.000180(1)	0.000219(1)
<sup>54</sup> Fe(n,p)	0.0447(15)	0.0418(1)	0.0418(1)
<sup>56</sup> Fe(n,p)	0.00061(2)	0.00062(1)	0.00061(1)
<sup>58</sup> Ni(n,p)	0.055(3)	0.0552(1)	0.0553(1)
<sup>59</sup> Co(n,p)	0.00084(4)	0.00078(1)	0.00078(1)
<sup>50</sup> Cr(n,γ)	0.0057(5)	0.0055(1)	0.0052(1)
<sup>55</sup> Mn(n,γ)	0.00297(15)	0.00386(1)	0.00391(1)
<sup>58</sup> Fe(n,γ)	0.00228(9)	0.00302(1)	0.00300(1)
<sup>59</sup> Co(n,γ)	0.0064(3)	0.0059(1)	0.0059(1)
<sup>64</sup> Ni(n,γ)	0.00185(8)	0.00475(1)	0.00353(1)
<sup>63</sup> Cu(n,γ)	0.0114(5)	0.0120(1)	0.0120(1)
<sup>65</sup> Cu(n,γ)	0.0076(6)	0.0075(1)	0.0075(1)
<sup>94</sup> Zr(n,γ)	0.0064(4)	0.0096(1)	0.0098(1)
<sup>96</sup> Zr(n,γ)	0.00306(15)	0.00475(10)	0.00617(1)
<sup>98</sup> Mo(n,γ)	0.0193(8)	0.0271(1)	0.0271(1)
<sup>197</sup> Au(n,γ)	0.105(5)	0.101(1)	0.101(1)

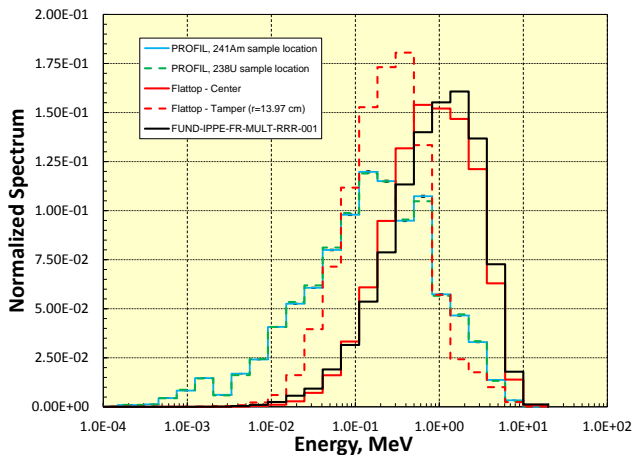


FIG. 27: Calculated multigroup spectra for the PROFIL, Flattop-25 and FUND-IPPE-FR-MULT-RRR-001 benchmark assemblies at locations where reaction rate data were obtained.

now retired, suggest that a 5% uncertainty is not unreasonable and so that is the uncertainty value cited for the

reported C/E values given in Table XVI. The Monte Carlo calculations to produce the C values were run for 250 million histories, or more, and yield a stochastic uncertainty that is a fraction of a per cent.

TABLE XVI: Measured and Calculated Fission Rate Ratios for Selected Actinides in Flattop-25 by Barr *et al.* [15]. Data for the uranium isotopes and <sup>239</sup>Pu are ratioed to <sup>235</sup>U(n,f), the remaining results are ratioed to <sup>239</sup>Pu(n,f). The measurement location for those data given in the top half of the Table are near the center of the assembly (r=1.11 cm), data given in the bottom half of the Table are from the tamper region (r=13.97 cm). As these data have not been published previously, we also include the measured spectral indices in the second column of this Table. A generic 5% uncertainty is judged appropriate for these data, but the values tabulated are given to the precision used in internal LANL documents.

Reaction	Measured Spectral Index	ENDF/B-VII.0 C/E	ENDF/B-VII.1 C/E
<sup>236</sup> U(n,f)	0.3155	0.921(46)	0.922(46)
<sup>237</sup> U(n,f)	0.537	0.832(42)	0.892(45)
<sup>238</sup> U(n,f)	0.1397	1.029(51)	1.030(51)
<sup>239</sup> Pu(n,f)	1.307	1.039(52)	1.039(52)
<sup>238</sup> Pu(n,f)	1.002	0.967(48)	0.950(47)
<sup>240</sup> Pu(n,f)	0.549	1.043(52)	1.026(51)
<sup>241</sup> Pu(n,f)	1.073	0.911(46)	0.911(46)
<sup>242</sup> Pu(n,f)	0.482	0.961(48)	0.984(49)
<sup>241</sup> Am(n,f)	0.577	0.918(46)	0.914(46)
<sup>236</sup> U(n,f)	0.08	0.669(33)	0.672(34)
<sup>237</sup> U(n,f)	0.391	1.018(51)	0.973(49)
<sup>238</sup> U(n,f)	0.02487	0.832(42)	0.832(42)
<sup>239</sup> Pu(n,f)	1.145	0.985(49)	0.985(49)
<sup>238</sup> Pu(n,f)	0.708	0.968(48)	0.946(47)
<sup>240</sup> Pu(n,f)	0.26	0.899(45)	0.870(43)
<sup>241</sup> Pu(n,f)	1.251	0.954(48)	0.953(48)
<sup>242</sup> Pu(n,f)	0.19	0.845(42)	0.871(44)
<sup>241</sup> Am(n,f)	0.184	0.793(40)	0.784(39)

Spectral index data for a number of actinide fission and capture cross sections have been presented in Table XII through Table XVI. Presenting such tabular data is important to allow future data testing by all interested parties, but it is often more beneficial to display these results in graphical form to better demonstrate the level of accuracy attained in these analyses. Therefore we have collected the fission rate spectral index data in Fig. 28 and the actinide capture spectral index data in Fig. 29. Changes in the cross sections of selected actinides between ENDF/B-VII.0 and ENDF/B-VII.1 have been discussed in the companion paper [1], and the new C/E values reported here are consistent with those revisions. That many of the spectral index ratios are within 2σ of unity is encouraging, but other C/E values are clearly far removed from this standard. Further work on these minor actinide cross sections await a future ENDF release.

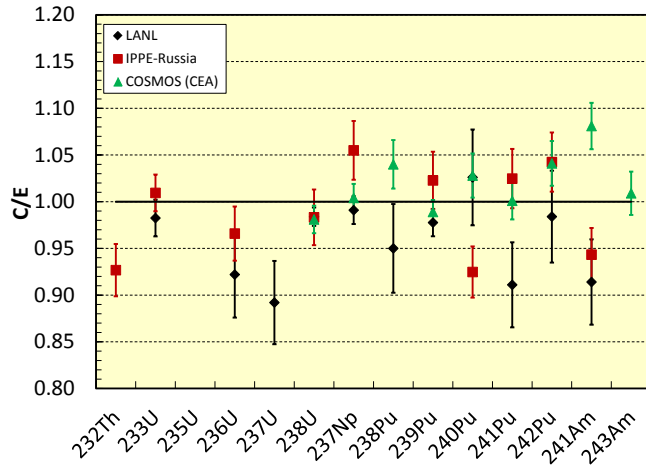


FIG. 28: Fission spectral index  $C/E$  values for selected actinides from LANL (Flattop-25), PROFIL and FUND-IPPE-FR-MULT-RRR-001 assemblies. The spectral index ratio is typically made to  $^{235}\text{U}(n,f)$ , although some LANL ratios are to  $^{239}\text{Pu}(n,f)$ . See Table XVI

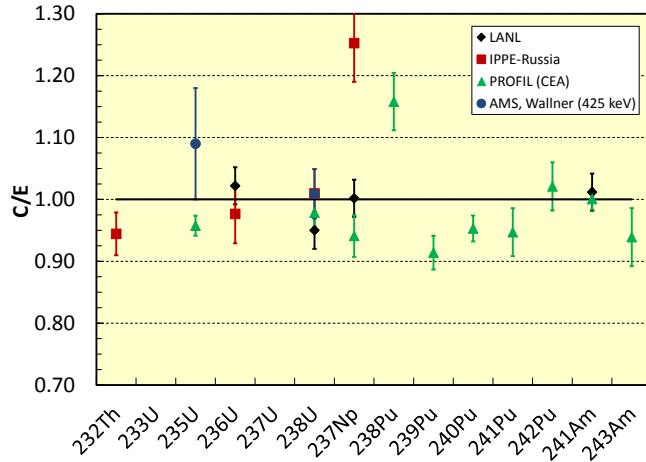


FIG. 29: Capture spectral index  $C/E$  values for selected actinides from LANL (Flattop-25), PROFIL and FUND-IPPE-FR-MULT-RRR-001 assemblies. The spectral index ratio is typically made to  $^{235}\text{U}(n,f)$

### H. Rossi $\alpha$

Rossi- $\alpha$  characterizes the exponential change in the population of prompt neutrons that produce fissions in a system that is close to delayed critical:

$$n_{pf}(t) = n_{pf}(0)e^{\alpha_R t}, \quad (1)$$

where  $\alpha_R$  is Rossi- $\alpha$ ,  $n_{pf}$  is the population of prompt neutrons that produce fissions, and  $t$  is time. By definition, Rossi- $\alpha$  is zero at prompt critical, negative below it, and positive above it. It is straightforward to show that

$$\alpha_R = \frac{(k_p - 1)}{\lambda_{pf}} = -\frac{\beta_{eff}}{\lambda_{pf}}, \quad (2)$$

where  $k_p$  is the prompt neutron multiplication factor,  $\lambda_{pf}$  is the lifetime for prompt neutrons producing fission, and  $\beta_{eff}$  is the effective delayed neutron fraction. A technique to measure Rossi- $\alpha$  using correlated fission chains was developed by Bruno Rossi at Los Alamos in the 1950s [16].

Version 1.60 of the MCNP5 Monte Carlo code, released from RSICC in November 2010, is capable of computing Rossi- $\alpha$  in criticality calculations [17]. As part of the validation of that capability, a Rossi- $\alpha$  validation suite has been developed. This suite includes  $^{233}\text{U}$ , HEU, IEU, and plutonium benchmarks. These benchmarks include systems with thermal, intermediate, and fast spectra. Some of the benchmarks are unreflected, while the others are reflected by normal uranium, depleted uranium, thorium, copper or water. Calculated results using ENDF/B-VII.0 and ENDF/B-VII.1 cross sections are presented in Table XVII. Measured values of Rossi- $\alpha$  for all but five of the benchmarks are taken from the CSEWG Benchmark Book [18]. For STACY-30 (LST7) and STACY-46 (LST4) they are taken from Ref. [19]. The measured value for Zeus-1 (HMI6) is taken from the ICSBEP Handbook while the values for Zeus-5 (HMF73) and Zeus-6 (HMF72) are taken from the logbooks for those experiments.

TABLE XVII: Comparison of measured and calculated values for Rossi- $\alpha$ .

Benchmark	Rossi- $\alpha$ ( $10^4$ generations/second) at Delayed Critical		
	Measured	MCNP5-1.60 Results	
		ENDF/B-VII.0	ENDF/B-VII.1
Jezebel-23	-100(1)	-108(1)	-104(1)
Flattop-23	-26.7(5)	-30.2(4)	-28.6(0.4)
Godiva	-111(2)	-113(2)	-113(2)
Flattop-25	-38.2(2)	-39.7(2)	-39.6(0.2)
Zeus-1	-0.338(8)	-0.363(2)	-0.360(2)
Zeus-5	-7.96(8)	-10.8(1)	-10.8(1)
Zeus-6	-3.73(5)	-4.14(3)	-4.19(3)
Big-Ten	-11.7(1)	-11.8(1)	-11.8(1)
STACY-30	-0.0127(3)	-0.0133(3)	-0.0127(3)
STACY-46	-0.0106(4)	-0.0104(2)	-0.0109(3)
Jezebel	-64(1)	-65(1)	-64(1)
Flattop-Pu	-21.4(5)	-21.0(3)	-20.8(3)
THOR	-19(1)	-20(1)	-21(1)

The changes in calculated Rossi- $\alpha$  values from using ENDF/B-VII.0 to ENDF/B-VII.1 are generally small, as expected because the changes in the underlying actinide data are small. The only changes that are statistically significant, as evidenced by a change of more than two standard deviations are the fast  $^{233}\text{U}$  benchmarks, which are now lower and in better agreement with experiment.

The ENDF/B-VII.1 delayed neutron data are reverted to what is available in ENDF/B-VI.8; however these changes only have a significant impact on the individual precursor fractions and decay constants - the resulting total delayed neutron fractions for the isotopes only change slightly. The resulting changes in the neutron spectra (different precursor groups have different emission spectra, so a change in the precursor fractions changes the overall delayed neutron spectrum) may also cause small differences. The other difference in the  $^{233}\text{U}$  data that may impact these fast benchmarks is the revision of the inelastic scattering cross section below 1 MeV [1].

### I. Bethe Sphere Tritium-Production

We described the Bethe Sphere experiments in Ref. [20] in the context of MCNP validation testing of our iridium and thulium dosimetry cross sections. These same experiments also measured the tritium production from  $^6\text{Li}$  and  $^7\text{Li}$  at various locations within the assemblies, the focus of this subsection. Comparison of simulations with experimental data here provide an integral test of both the lithium isotope tritium production cross sections as well as the calculated neutron spectrum and fluence that is based on MCNP simulations sensitive to various neutron reaction and scattering ENDF data.

The experiments and results of various older simulations are described in detail by Frankle in Refs. [21, 22]. These 1970s experiments consisted of a 14 MeV neutron source from the target chamber of the Cockcroft-Walton accelerator at LANL, surrounded by semi-spherical shells. One of the sets of shells was of  $^6\text{LiD}$  with an inside diameter of 4.44 cm and an outside diameter of 60 cm; the other consisted of an inner shell of HEU with outer shells of  $^6\text{LiD}$ . At various locations at the shell interfaces, quartz ampules were placed containing  $^6\text{LiH}$  and  $^7\text{LiH}$ . After the irradiations, tritium production was measured and compared with MCNP simulated results.

Frankle [21, 22] has described the details of the MCNP simulations of these experiments and noted how more refined MCNP models have been developed over the last few decades to more accurately model these data, including accounting for details of room return, the quartz ampule casings, *etc.*. The MCNP calculated neutron spectra are shown in Figs. 2-5 of Ref. [20] and are not repeated here. For the  $^6\text{LiD}$  sphere, the spectrum consists of a 14 MeV peak together with a broad component of lower energy neutrons, with the relative importance of the 14 MeV peak decreasing at larger radii where more scattering has occurred. For the  $^6\text{LiD-HEU}$  sphere, the 14 MeV spectrum peak is augmented by a significant fission spectrum component, with the details of the spectrum shape varying with location.

Comparisons of our calculated and measured tritium production from  $^6\text{Li}$  and  $^7\text{Li}$  are given in Tables XVIII and XIX. In addition to the statistical measurement uncertainty, a systematic uncertainty of 6% is included in

TABLE XVIII: LiD Bethe sphere results for tritium production from  $^6\text{LiH}$  and  $^7\text{LiH}$  ampules, showing total tritium production calculated with MCNP to experimental ratios and error estimates. The LiD sphere has a 14 MeV source at its center, and the tritium production from Li isotopes is measured in ampules at various locations within the LiD.

LiD sphere	ENDF/B-VII.0	ENDF/B-VII.1
Radius (cm)	C/E, $^6\text{Li}(n, t)$	C/E, $^6\text{Li}(n, t)$
30.0	1.03±0.08	1.03±0.08
20.2	1.00±0.07	1.00±0.07
12.8	0.97±0.07	0.97±0.07
7.72	1.00±0.07	1.01±0.07
5.04	0.95±0.07	0.95±0.07
Radius (cm)	C/E, $^7\text{Li}(n, t)$	C/E, $^7\text{Li}(n, t)$
30.0	0.84±0.07	0.83±0.07
20.1	0.89±0.07	0.89±0.07
15.1	0.92±0.07	0.92±0.07
7.67	0.95±0.07	0.95±0.07
5.05	0.98±0.07	0.98±0.07

TABLE XIX: LiD-HEU Bethe sphere results for tritium production from  $^6\text{LiH}$  and  $^7\text{LiH}$  ampules, showing total tritium production calculated with MCNP to experimental ratios and error estimates. The LiD sphere has a 14 MeV source at its center, and the tritium production from Li isotopes is measured in ampules at various locations within the LiD and HEU.

LiD-HEU sphere	ENDF/B-VII.0	ENDF/B-VII.1
Radius (cm)	C/E, $^6\text{Li}(n, t)$	C/E, $^6\text{Li}(n, t)$
30.0	0.89±0.07	0.88±0.07
20.2	0.91±0.08	0.91±0.08
12.7	0.87±0.07	0.86±0.07
8.37	0.98±0.08	0.99±0.08
Radius (cm)	C/E, $^7\text{Li}(n, t)$	C/E, $^7\text{Li}(n, t)$
30.0	0.81±0.13	0.80±0.13
20.0	0.93±0.08	0.94±0.08

these tritium measurements. Tritium production from  $^6\text{Li}$  is dominantly from neutrons below 1 MeV (owing to the large resonance at 240 keV); for  $^7\text{Li}$ , the tritium production comes from neutrons with energies in the 4-14 MeV range (its threshold is at 2.82 MeV). We note that the calculations of  $^6\text{Li}(n, t)$  are in fairly good agreement with the data. The LiD sphere results cluster around a C/E of unity while the LiD-HEU results vary between 0.98 and 0.87. Calculations with ENDF/B-VII.1 and ENDF/B-VII.0 are essentially identical – even though the  $^6\text{Li}(n, t)$  was changed in VII.1, the change was only above 1 MeV, and most of the tritium is created at lower energies. Of course the  $^6\text{Li}(n, t)$  reaction is thought to be very accurately known below 1 MeV and is a standard, so the accuracy of this simulation is largely a test of MCNP’s ability to accurately model the neutronics in the assembly.

For  $^7\text{Li}(n, t)$ , we observe that for the LiD sphere the

tritium production is accurately calculated at the smallest radii where the spectrum is most 14-MeV-like, but a 10-15% underprediction is seen at the larger radii. A similar underprediction is observed in the LiD-HEU spheres. It is not yet understood why this is the case, though it could point to deficiencies in either the calculated neutron spectrum (which is impacted by neutron transport cross sections for D,  $^6\text{Li}$ , and U isotopes) or  $^7\text{Li}(n, t)$  cross section deficiencies.

### III. CONCLUSIONS

Hundreds of criticality benchmarks from the ICSBEP Handbook have been calculated with one or more of ENDF/B-VI.8, ENDF/B-VII.0 and ENDF/B-VII.1 cross sections in a comprehensive test of the underlying neutron cross section data. These studies have demonstrated that the new cross section library, ENDF/B-VII.1, is an important advance over the predecessor library, ENDF/B-VII.0. Accurate  $k_{\text{eff}}$  predictions are obtained for a wide variety of critical benchmark assemblies for all fissile nuclides of interest under all spectral conditions from bare unmoderated assemblies to highly moderated assemblies. Significant advances in the underlying accuracy of the basic neutron cross section evaluations have occurred with each ENDF/B generation, and we continue to retain the highly accurate results obtained with past ENDF/B files for unmoderated bare and uranium reflected  $^{233,235}\text{U}$  and  $^{239}\text{Pu}$  systems (e.g., Godiva, Jezebel, Flattop's and Big-Ten). Previous highly accurate criticality predictions for HEU solution systems and low-enriched lattices are also retained. Deficiencies identified since the release of ENDF/B-VII.0 for several elements have been eliminated; most notably for unmoderated systems with metallic titanium and tungsten reflectors. Nevertheless, further improvements await future ENDF/B releases. Our benchmark simulations for beryllium and vanadium reflected systems do not yield the same level of accuracy. Beryllium in particular is problematic as different benchmark suites with many common components yield  $k_{\text{eff}}$  C/E values that vary by more than 0.5% - a reasonably accurate standard in the past but with today's computational resources and measurement and evaluation techniques we expect better. New exper-

iments are planned in coming years with the expectation that this issue will be resolved. Other long-standing issues, such as the overpredicted  $k_{\text{eff}}$  C/E values for Pu solution systems and the apparent  $k_{\text{eff}}$  C/E trend in  $^{233}\text{U}$  systems noted above also remain. We close by noting that these are not new deficiencies, rather they have existed in all internationally available evaluated nuclear data files, as well as in earlier ENDF/B libraries. The ENDF/B-VII.1 library represents the most accurate general purpose nuclear data file yet produced by the Cross Section Evaluation Working Group community.

### Acknowledgments

We thank the staff of Brookhaven National Laboratory's National Nuclear Data Center for their tireless efforts to collect and organize the many individual evaluated data files into the final ENDF/B-VII.1 file. We also thank past and present members of the International Criticality Safety Benchmark Evaluation Project for their work that has produced the International Handbook of Evaluated Criticality Safety Benchmark Experiments. This Handbook allows criticality data testing with thousands of potential benchmark experiments. We acknowledge past and present members of the Cross Section Evaluation Working Group and our international colleagues, particularly from the JEFF and JENDL Projects and KAERI, for their efforts that have ultimately lead to the ENDF/B-VII.1 general purpose nuclear data file. Stephen van der Marck (NRG/Petten) has contributed important data testing results, some of which are included in our companion paper [1]. A more comprehensive report of his work will be published separately. Finally, we thank J. H. Conlin (LANL) for technical support in producing this document.

Work at Los Alamos National Laboratory was supported by U. S. Department of Energy (DOE) contract DE-AC52-06NA25396, at Argonne National Laboratory under DOE contract W-31-109-ENG-38, at Brookhaven National Laboratory under DOE contract DE-AC02-98H10886, at Idaho National Laboratory under DOE contract DE-AC07-05ID14517, at Oak Ridge National Laboratory under DOE contract DE-AC05-00OR22725 and at the Culham Centre for Fusion Energy under RCUK Energy Programme grant EP/I501045.

- 
- [1] M. B. Chadwick *et al.*, "ENDF/B-VII.1 Nuclear Data for Science and Technology: Cross Sections, Covariances, Fission Product Yields and Decay Data," *Nuclear Data Sheets*, **112**, 2887 (2011).
- [2] M. B. Chadwick *et al.*, "ENDF/VII.0: Next Generation Evaluated Nuclear Data Library for Nuclear Science and Technology," *Nuclear Data Sheets*, **107**, 2931-3060 (2006).
- [3] R. E. MacFarlane and A. C. Kahler, "Methods for Processing ENDF/B-VII with NJOY," *Nuclear Data Sheets*, **111**, 2739-2890 (2010).
- [4] X-5 Monte Carlo Team, "MCNP - A General Monte Carlo Transport Code, Version 5," Los Alamos National Laboratory report LA-UR-03-1987 (April 2003).
- [5] J. B. Briggs, editor, "International Handbook of Evaluated Criticality Safety Benchmark Experiments," Technical Report NEA/NSC/DOC(95)03, Nuclear Energy Agency, OECD, Paris, France, 2010. This handbook was first published in the mid-1990s and is updated annually. The benchmark models used herein com from the 2005

and later editions.

- [6] C. R. Lubitz, "Neutron Cross Sections for Uranium-235 (ENDF/VI Release 3)," KAPL-4825 (DOE/TIC-4500-R75), 1996.
- [7] Y. Danon, R. C. Block, M. J. Rapp, F. J. Saglime, G. Leinweber, D. P. Barry, N. J. Drindak and J. G. Hoole, "Beryllium and Graphite High Accuracy Total Cross Section Measurements in the Energy Range from 24 to 900 keV," *Nucl. Sci. and Eng.*, **161**, 321-330 (2009).
- [8] G. Leinweber, D. P. Barry, J. Trbovich, J. A. Burke, N. J. Drindak, H. D. Knox, R. V. Ballard, R. C. Bloch, Y. Danon and L. I. Severnyak, "Neutron Capture and Total Cross Section Measurements and Resonance Parameters of Gadolinium," *Nucl. Sci. and Eng.*, **154**, 261-279 (2006).
- [9] R. Capote, "Summary Report on a Consultants Meeting to Review Benchmarking of Nuclear Data for the Th/U Fuel Cycle," INDC-NDS-0586, 2011.
- [10] H. C. Hecker, "Summary of the Nuclear Design and Performance of the Light Water Breeder Reactor (LWBR)," WAPD-TM-1326, June 1979.
- [11] R. Atherton, "Water Cooled Breeder Program Summary Report," WAPD-TM-1600, October 1987.
- [12] A. D'Angelo, F. Cleri, P. Marimbeau, M. Salvatores and J. P. Grouiller, "Analysis of Sample and Fuel Pin Irradiation in PHENIX for Basic Nuclear Data Validation," *Nucl. Sci. and Eng.*, **105**, 244.
- [13] L. Snoj, G. Žerovnik, A. Trkov, "Analysis of Cross-Section Libraries on Zirconium Benchmarks," Proceedings of the International Conference on Nuclear Criticality 2011, Edinburgh, 19 - 22 September 2011.
- [14] "Benchmark on Computer Simulation of MASURCA Critical and Subcritical Experiments," NEA/NSC/DOC(2005)23.
- [15] D. W. Barr, private communication to M. B. Chadwick.
- [16] J. Orndoff, "Prompt Neutron Periods of Metal Critical Assemblies," *Nucl. Sci. and Eng.*, **2**, 450-460 (July 1957).
- [17] B. C. Kiedrowski, F. B. Brown and P. P. H. Wilson, "Adjoint-Weighted Tallies for k-Eigenvalue Calculations with Continuous-Energy Monte Carlo," *Nucl. Sci. and Eng.*, **168**, 226-241 (2011).
- [18] "Cross Section Evaluation Working Group Benchmark Specifications," Brookhaven National Laboratory report BNL-19302 (ENDF-202) (Rev., September 1986).
- [19] K. Tonoike, Y. Miyoshi, T. Kikuchi, and T. Yamamoto, "Kinetic Parameter  $\beta_{eff}/l$  Measurement on Low Enriched Uranyl Nitrate Solution with Single Unit Cores of STACY," *J. Nucl. Sci. Tech.*, **39**, 11, 1227-1236 (November 2002).
- [20] M. B. Chadwick, S. C. Frankle, H. Trelle, P. Talou, T. Kawano, P. G. Young, R. E. MacFarlane, and C. W. Wilkerson, "Evaluated Iridium, Yttrium, and Thulium Cross Sections and Integral Validation Against Critical Assembly and Bethe Sphere Measurements," *Nuclear Data Sheets* **108**, 2716-2741 (2007).
- [21] A. Hemmendinger *et al.*, "Tritium Production in a Sphere of  $^6\text{LiD}$  Irradiated by 14-MeV Neutrons," *Nucl. Sci. and Eng.*, **70**, 274-280 (1979).
- [22] S. C. Frankle and J. M. Harp, "Tritium Production in  $^6,7\text{Li}$  from 14 MeV Neutrons," Los Alamos National Laboratory Report LA-UR-04-3976 (2004). Also Transactions of the American Nuclear Society, **91**, 568-569 (2004).

## Appendix A

Tabulated below are the calculated eigenvalues for a subset of the ICSBEP Benchmarks discussed elsewhere in this paper. These results were obtained after independent benchmark model development, independent cross section processing into the appropriate application library and with independently developed transport codes MCNP and Tripoli.

This comparison was performed using a pre-release version of the ENDF/B-VII.1 library, ENDF/B-VII.1 $\beta$ 3. As such some of these  $k_{eff}$  values differ from those appearing elsewhere in this paper. However for purposes of performing a code comparison the essential point is that the same cross section evaluation source files be used to create the respective MCNP5.1.51 and Tripoli4.7 application libraries. That is the case here, shown in Table XX. The high degree of agreement in these calculations provides added confidence in the general conclusions on the strengths and weaknesses of the ENDF/B-VII.1 library that were presented in the main body of this paper.

TABLE XX: Comparison of  $k_{eff}$  results for ENDF/B-VII.1 $\beta$ 3.

Benchmark	Model $k_{eff}$	MCNP5	Tripoli-4.7
		Calculated $k_{eff}$	Calculated $k_{eff}$
HEU-MET-FAST-001 (Godiva)	1.0000(10)	0.99980(8)	1.00014(11)
HEU-MET-FAST-028 (Flattop)	1.0000(30)	1.00298(9)	1.00325(11)
PU-MET-FAST-001 (Jezebel)	1.0000(20)	0.99988(8)	0.99960(15)
PU-MET-FAST-002	1.0000(20)	1.00002(8)	0.99975(15)
IEU-MET-FAST-001.2	1.0000(12)	1.00047(9)	0.99850(12)
IEU-MET-FAST-001.3	1.0000(10)	1.00099(9)	1.00056(12)
IEU-MET-FAST-001.4	1.0000(10)	1.00159(9)	1.00132(12)
IEU-MET-FAST-002	1.0000(30)	0.99883(8)	0.99912(10)
IEU-MET-FAST-007 (Big-10) (detailed and CSEWG model)	1.0045(7)	1.00440(7)	1.00479(13)
IEU-MET-FAST-010	0.9948(13)	0.99502(7)	0.99515(13)
IEU-MET-FAST-010	0.9954(24)	0.99624(10)	0.99710(13)

*Continued*

TABLE XX: Comparison of  $k_{\text{eff}}$  results (cont.)

Benchmark	Model $k_{\text{eff}}$	MCNP5	Tripoli-4.7
		Calculated $k_{\text{eff}}$	Calculated $k_{\text{eff}}$
IEU-MET-FAST-012	1.0007(27)	1.00329(10)	1.00370(13)
HEU-SOL-THERM-001.1	1.0004(60)	0.99794(15)	0.99965(16)
HEU-SOL-THERM-001.2	1.0021(72)	0.99595(15)	0.99766(16)
HEU-SOL-THERM-001.3	1.0003(35)	1.00193(15)	1.00304(16)
HEU-SOL-THERM-001.4	1.0008(53)	0.99841(15)	0.99958(16)
HEU-SOL-THERM-001.5	1.0001(49)	0.99871(13)	0.99966(16)
HEU-SOL-THERM-001.6	1.0002(46)	1.00202(13)	1.00292(16)
HEU-SOL-THERM-001.7	1.0008(40)	0.99793(15)	0.99878(16)
HEU-SOL-THERM-001.8	0.9998(38)	0.99803(15)	0.99961(16)
HEU-SOL-THERM-001.9	1.0008(54)	0.99428(15)	0.99549(16)
HEU-SOL-THERM-009.1	0.9990(43)	1.00297(14)	1.00316(16)
HEU-SOL-THERM-009.2	1.0000(39)	1.00306(14)	1.00338(16)
HEU-SOL-THERM-009.3	1.0000(39)	1.00242(14)	1.00294(16)
HEU-SOL-THERM-009.4	0.9986(35)	0.99669(14)	0.99726(16)
HEU-SOL-THERM-011.1	1.0000(23)	1.00466(12)	1.00527(16)
HEU-SOL-THERM-011.2	1.0000(23)	1.00100(11)	1.00182(16)
HEU-SOL-THERM-012	0.9999(58)	1.00084(8)	1.00102(15)
HEU-SOL-THERM-032	1.0015(26)	0.99933(5)	0.99892(16)
PU-SOL-THERM-001.1	1.0000(50)	1.00612(13)	1.00645(12)
PU-SOL-THERM-001.2	1.0000(50)	1.00761(13)	1.00819(12)
PU-SOL-THERM-001.3	1.0000(50)	1.01049(13)	1.01104(12)
PU-SOL-THERM-001.4	1.0000(50)	1.00443(13)	1.00520(12)
PU-SOL-THERM-001.5	1.0000(50)	1.00863(13)	1.00920(12)
PU-SOL-THERM-001.6	1.0000(50)	1.00957(13)	1.01055(12)
PU-SOL-THERM-009.3	1.0003(33)	1.01928(6)	1.01923(11)

*Continued*

TABLE XX: Comparison of  $k_{\text{eff}}$  results (cont.)

Benchmark	Model $k_{\text{eff}}$	MCNP5	Tripoli-4.7
		Calculated $k_{\text{eff}}$	Calculated $k_{\text{eff}}$
PU-SOL-THERM-011 (16.1)	1.0000(52)	1.01020(13)	1.01017(13)
PU-SOL-THERM-011 (16.5)	1.0000(52)	1.00628(13)	1.00665(13)
PU-SOL-THERM-011 (18.1)	1.0000(52)	0.99462(11)	0.99449(13)
PU-SOL-THERM-011 (18.6)	1.0000(52)	1.00024(12)	1.00044(13)
LEU-COMP-THERM-006.1	1.0000(20)	1.00004(10)	1.00074(12)
LEU-COMP-THERM-006.3	1.0000(20)	1.00034(10)	1.00114(9)
LEU-COMP-THERM-006.4	1.0000(20)	0.99989(10)	1.00092(12)
LEU-COMP-THERM-006.8	1.0000(20)	1.00004(10)	1.00086(12)
LEU-COMP-THERM-006.9	1.0000(20)	1.00003(10)	1.00053(12)
LEU-COMP-THERM-006.13	1.0000(20)	0.99954(10)	1.00010(12)
LEU-COMP-THERM-006.14	1.0000(20)	0.99952(10)	1.00052(12)
LEU-COMP-THERM-006.18	1.0000(20)	0.99961(10)	1.00005(12)
LEU-COMP-THERM-007.1	1.0000(16)	0.99761(11)	0.99851(10)
LEU-COMP-THERM-007.2	1.0000(16)	0.99880(11)	0.99984(10)
LEU-COMP-THERM-007.3	1.0000(16)	0.99766(10)	0.99842(10)
LEU-COMP-THERM-007.5	1.0000(16)	0.99714(11)	0.99843(10)
LEU-COMP-THERM-007.6	1.0000(16)	0.99883(10)	1.00003(10)
LEU-COMP-THERM-007.7	1.0000(16)	0.99834(10)	0.99942(10)
LEU-COMP-THERM-039.1	1.0000(14)	0.99722(11)	0.99815(12)
LEU-COMP-THERM-039.4	1.0000(14)	0.99635(11)	0.99746(12)
LEU-COMP-THERM-039.6	1.0000(14)	0.99729(11)	0.99824(12)
LEU-COMP-THERM-027.1	1.0000(11)	1.00418(11)	1.00338(12)

**Appendix B**

Criticality calculations have been performed for nearly one thousand ICSBEP benchmarks as part of the ENDF/B-VII.1 cross section validation and verification process. Although only a subset of these benchmark results have been discussed in detail in this paper, we tabulate the model eigenvalue and both ENDF/B-VII.0 and ENDF/B-VII.1 calculated eigenvalues for all of these systems below. Calculated values given to 5 significant figures represent 50 million neutron history (or more) calculations and have a typical stochastic uncertainty of 15 pcm or less; values given to 4 significant digits were typically run for several, but less than ten, million neutron histories and have a stochastic uncertainty of 250 pcm or less. Model uncertainties are typically several hundred pcm, although values approaching 1000 pcm or less than 100 pcm are sometimes reported. The reader should consult the ICSBEP Handbook for more details. This Handbook was first released in the mid-1990s with annual updates since then. The models used herein come from the 2005 or later editions.

Model and calculated eigenvalues ( $k_{\text{eff}}$ ) for selected ICSBEP benchmarks are compared in Table XXI.

TABLE XXI: Comparison of  $k_{\text{eff}}$  results.

Benchmark	Model $k_{\text{eff}}$	ENDF/B-VII.0 Calculated $k_{\text{eff}}$	ENDF/B-VII.1 Calculated $k_{\text{eff}}$
HEU-MET-FAST-001	1.0000	0.99984	0.99992
HEU-MET-FAST-002	1.0000	1.00225	1.00236
	1.0000	1.00035	1.00034
	1.0000	0.99972	0.99970
	1.0000	1.00004	0.99985
	1.0000	1.00121	1.00129
HEU-MET-FAST-003	1.0000	0.99505	0.99495
	1.0000	0.99457	0.99451
	1.0000	0.99918	0.99929
	1.0000	0.99733	0.99720
	1.0000	1.00139	1.00139
	1.0000	1.00193	1.00167
	1.0000	1.00190	1.00198
	1.0000	1.00836	1.00132
	1.0000	1.00927	1.00154
	1.0000	1.01262	1.00519
	1.0000	1.01677	1.00974
	1.0000	1.00837	1.00876
HEU-MET-FAST-004	1.0020	1.00314	1.00314
HEU-MET-FAST-005	1.0000	0.99551	0.99524
	1.0007	0.99571	0.99803
	0.9996	0.99668	1.00060
	0.9989	0.99002	0.99437

*Continued*

TABLE XXI: Comparison of  $k_{\text{eff}}$  results (cont.)

Benchmark	Model $k_{\text{eff}}$	ENDF/B-VII.0 Calculated $k_{\text{eff}}$	ENDF/B-VII.1 Calculated $k_{\text{eff}}$
	0.9980	0.99634	0.99898
	0.9987	0.99598	0.99761
HEU-MET-FAST-007	0.9950	0.99314	0.99303
	0.9964	0.99877	0.99883
	0.9990	1.00022	1.00028
	0.9948	0.99812	0.99844
	0.9978	1.00035	1.00029
	1.0006	1.00567	1.00587
	0.9974	1.00128	1.00151
	0.9973	0.99945	0.99939
	0.9995	1.00340	1.00338
	0.9981	0.99917	0.99892
	0.9958	0.99798	0.99783
	0.9932	0.99306	0.99288
	0.9990	1.00050	1.00025
	0.9964	0.99712	0.99687
	0.9959	0.99672	0.99679
	0.9969	0.99763	0.99760
	0.9953	0.99607	0.99592
	0.9972	0.99864	0.99829
	0.9956	0.99689	0.99667
	0.9950	0.99811	0.99831
	0.9956	0.99912	0.99866
	0.9963	0.99960	0.99965
	0.9962	0.99949	0.99930
	0.9970	0.99990	0.99966
	0.9959	0.99865	0.99848
	0.9966	0.99854	0.99861
	1.0003	1.00252	1.00216
	0.9999	1.00373	1.00340
	0.9988	1.00178	1.00173
	1.0000	1.00282	1.00286
	1.0018	1.00481	1.00474
	1.0013	1.00607	1.00584
	0.9994	1.00099	1.00083
	1.0016	1.00303	1.00303
	0.9998	1.00082	1.00041
HEU-MET-FAST-008	0.9989	0.99586	0.99580
HEU-MET-FAST-009	0.9992	0.99503	0.99740
	0.9992	0.99541	0.99655
HEU-MET-FAST-010	0.9992	0.99744	0.99844
	0.9992	0.99740	0.99789
HEU-MET-FAST-011	0.9989	0.99915	0.99902
HEU-MET-FAST-012	0.9992	0.99835	0.99835
HEU-MET-FAST-013	0.9990	0.99745	0.99745
HEU-MET-FAST-014	0.9989	0.99774	0.99780
HEU-MET-FAST-015	0.9996	0.99470	0.99445

*Continued*

TABLE XXI: Comparison of  $k_{\text{eff}}$  results (cont.)

Benchmark	Model $k_{\text{eff}}$	ENDF/B-VII.0 Calculated $k_{\text{eff}}$	ENDF/B-VII.1 Calculated $k_{\text{eff}}$
HEU-MET-FAST-016	0.9996	0.99868	1.00190
	0.9996	1.00136	1.00243
HEU-MET-FAST-017	0.9993	0.99715	1.00057
HEU-MET-FAST-018	1.0000	1.00016	1.00018
HEU-MET-FAST-019	1.0000	1.00708	1.00702
HEU-MET-FAST-020	1.0000	1.00087	1.00067
HEU-MET-FAST-021	1.0000	0.99748	0.99739
HEU-MET-FAST-022	1.0000	0.99769	0.99769
HEU-MET-FAST-024	0.9990	0.99859	0.99838
HEU-MET-FAST-025	0.9987	0.99811	0.99882
	0.9990	1.00002	1.00104
	0.9991	1.00247	1.00369
	0.9995	1.00448	1.00550
	0.9991	1.00459	1.00564
HEU-MET-FAST-026	1.0000		1.0030
HEU-MET-FAST-027	1.0000	1.00070	1.00085
HEU-MET-FAST-028	1.0000	1.00297	1.00271
HEU-MET-FAST-029	1.0000	1.00566	1.00569
HEU-MET-FAST-030	1.0000	0.99906	1.00196
HEU-MET-FAST-031	1.0000	1.00526	1.00500
HEU-MET-FAST-032	1.0000	1.00436	1.00413
	1.0000	1.00485	1.00475
	1.0000	1.00015	1.00011
	1.0000	1.00112	1.00094
HEU-MET-FAST-033	0.9991	0.99908	0.99920
	0.9991	0.99757	0.99750
HEU-MET-FAST-034	0.9990	0.99950	0.99711
	0.9990	0.99849	0.99885
	0.9990	0.99743	0.99727
HEU-MET-FAST-036	0.9993	0.99885	0.99879
	0.9993	0.99840	0.99835
HEU-MET-FAST-037	0.9997	1.00233	1.00199
	0.9997	0.99805	0.99801
HEU-MET-FAST-038	0.9999	1.00049	1.00301
	0.9999	1.00048	1.00212

*Continued*TABLE XXI: Comparison of  $k_{\text{eff}}$  results (cont.)

Benchmark	Model $k_{\text{eff}}$	ENDF/B-VII.0 Calculated $k_{\text{eff}}$	ENDF/B-VII.1 Calculated $k_{\text{eff}}$
HEU-MET-FAST-040	0.9991	1.00310	1.00449
HEU-MET-FAST-041	1.0013	1.00279	1.00675
	1.0022	1.00024	1.00523
	1.0006	1.00234	1.00239
	1.0006	1.00732	1.00726
	1.0006	1.00300	1.00294
	1.0006	1.00428	1.00436
HEU-MET-FAST-043	0.9995	0.99905	0.99904
	0.9995	0.99737	0.99803
	0.9995	0.99866	0.99871
	0.9995	0.99810	0.99734
	0.9995	0.99905	0.99852
HEU-MET-FAST-044	0.9995	0.99999	0.99994
	0.9995	0.99958	0.99949
	0.9995	0.99980	0.99998
	0.9995	0.99946	0.99934
	0.9995	1.00000	0.99995
HEU-MET-FAST-047	1.0007	1.00166	1.00213
HEU-MET-FAST-049	0.9990	0.99986	0.99781
	0.9994	1.00356	0.99956
	0.9994	1.00420	0.99857
HEU-MET-FAST-050	0.9990	1.00504	0.99789
HEU-MET-FAST-051	0.9971	0.99512	0.99524
	0.9968	0.99555	0.99538
	0.9974	0.99505	0.99550
	0.9969	0.99527	0.99516
	0.9982	0.99487	0.99495
	0.9996	0.99884	0.99868
	0.9998	0.99810	0.99822
	0.9981	0.99642	0.99634
	0.9969	0.99551	0.99556
	0.9984	0.99388	0.99392
HEU-MET-FAST-055	0.9955	0.99876	0.99832
	1.0013	1.00396	1.00343
HEU-MET-FAST-057	1.0000	0.98933	0.98928
	1.0000	0.99804	0.99833
	1.0000	1.01703	1.01728
	1.0000	0.98781	0.98796
	1.0000	1.02149	1.02173
	1.0000	0.99652	0.99667
HEU-MET-FAST-058	1.0000	0.99971	1.00343
	1.0000	1.00001	1.00490
	1.0000	0.99848	1.00290
	1.0000	0.99841	1.00186
	1.0000	0.99810	1.00089

*Continued*

TABLE XXI: Comparison of  $k_{\text{eff}}$  results (cont.)

Benchmark	Model $k_{\text{eff}}$	ENDF/B-VII.0 Calculated $k_{\text{eff}}$	ENDF/B-VII.1 Calculated $k_{\text{eff}}$	
HEU-MET-FAST-060	0.9955	1.01563	1.00268	
	1.0013	1.02070	1.00848	
HEU-MET-FAST-061	0.9998	1.00618	1.00502	
	1.0006	1.00431	1.00257	
HEU-MET-FAST-063	0.9993	1.00079	1.00046	
	0.9988	1.00073	1.00071	
HEU-MET-FAST-064	0.9996	0.99514	0.99545	
	0.9996	0.99525	0.99567	
	0.9996	0.99326	0.99370	
HEU-MET-FAST-065	0.9995	0.99810	0.99806	
HEU-MET-FAST-066	1.0030	0.99797	1.00336	
	1.0023	0.99670	1.00189	
	1.0023	1.00013	1.00447	
	1.0043	0.99935	1.00508	
	1.0030	0.99831	1.00421	
	1.0028	0.99804	1.00356	
	1.0048	0.99937	1.00557	
	1.0039	0.99873	1.00441	
	1.0027	0.99641	1.00262	
	HEU-MET-FAST-067	0.9959	1.00936	1.00291
1.0023		1.01604	1.00852	
HEU-MET-FAST-072	1.0000	1.00890	1.00874	
HEU-MET-FAST-073	1.0004	1.01148	1.01134	
HEU-MET-FAST-077	1.0001	0.99513	1.00068	
	0.9995	0.99583	1.00068	
	0.9995	0.99325	0.99793	
	0.9998	0.99310	0.99849	
	0.9994	0.99469	1.00001	
	0.9996	0.99430	0.99983	
	0.9994	0.99587	1.00055	
	0.9994	0.99251	0.99843	
	HEU-MET-FAST-078	0.9995	0.99474	0.99465
		0.9994	0.99610	0.99573
0.9991		0.99626	0.99625	
1.0000		0.99864	0.99855	
0.9997		0.99588	0.99554	
0.9995		0.99589	0.99575	
1.0000		0.99731	0.99745	
0.9991		0.99670	0.99670	
0.9995		0.99655	0.99660	
0.9992		0.99814	0.99808	
0.9992		0.99760	0.99744	
0.9992		0.99602	0.99597	
1.0000		1.00218	1.00216	
0.9994	0.99507	0.99525		

*Continued*

TABLE XXI: Comparison of  $k_{\text{eff}}$  results (cont.)

Benchmark	Model $k_{\text{eff}}$	ENDF/B-VII.0 Calculated $k_{\text{eff}}$	ENDF/B-VII.1 Calculated $k_{\text{eff}}$
	0.9996	0.99615	0.99619
	0.9991	0.99438	0.99447
	0.9986	0.99646	0.99622
	0.9989	0.99680	0.99690
	0.9992	0.99685	0.99703
	1.0000	0.99761	0.99766
HEU-MET-FAST-079	0.9996	1.00105	0.99979
	0.9996	1.00114	0.99919
	0.9996	1.00339	1.00035
	0.9996	1.00513	1.00089
HEU-MET-FAST-082	0.9996	1.00413	0.99986
	0.9992	0.99647	0.99628
	0.9989	0.99611	0.99604
	0.9989	0.99846	0.99816
HEU-MET-FAST-084	0.9994	0.99908	0.99907
	0.9994	0.99948	0.99957
	0.9993	0.99686	1.00006
	0.9994	0.99873	0.99877
	0.9993	1.00513	1.00500
	0.9994	0.99872	0.99864
	0.9995	0.99753	0.99742
	0.9994	1.00833	1.00843
	0.9993	1.00278	1.00258
	0.9993	1.00137	1.00130
	0.9995	1.00148	1.00153
	0.9994	1.00324	0.99746
	0.9994	0.99914	0.99904
0.9994	1.00540	0.99959	
0.9995	0.99801	0.99808	
0.9994	0.99744	0.99896	
0.9995	1.00035	1.00037	
0.9995	0.99768	0.99757	
0.9996	0.99750	0.99770	
0.9995	1.00300	1.00281	
0.9995	1.00024	1.00027	
0.9994	0.99827	0.99834	
0.9993	0.99957	0.99938	
0.9996	0.99884	0.99879	
0.9995	1.00149	0.99816	
0.9993	0.99840	1.00043	
0.9994	0.99547	0.99756	
HEU-MET-FAST-085	0.9998	1.00038	0.99992
	0.9997	1.00442	1.00442
	0.9995	0.99622	0.99626
	0.9996	0.99643	0.99993
	0.9995	1.00071	1.00061
	0.9997	1.01383	1.00565
	HEU-MET-FAST-087	0.9991	0.99859
HEU-MET-FAST-089	0.9991	1.00012	1.00004

*Continued*

TABLE XXI: Comparison of  $k_{\text{eff}}$  results (cont.)

Benchmark	Model $k_{\text{eff}}$	ENDF/B-VII.0 Calculated $k_{\text{eff}}$	ENDF/B-VII.1 Calculated $k_{\text{eff}}$
HEU-MET-FAST-091	0.9996	0.99962	0.99963
HEU-MET-INTER-001	0.9966	1.00802	1.00107
HEU-MET-INTER-006	0.9977	0.99295	0.9937
	1.0001	0.99712	0.9964
	1.0015	1.00082	1.0012
	1.0016	1.00737	1.0067
HEU-COMP-INTER-003	1.0000	1.0066	1.00678
	1.0000	1.00679	1.00705
	1.0000	1.00236	1.00268
	1.0000	1.00461	1.00425
	1.0000	0.99650	0.99731
	1.0000	0.99520	0.9964
	1.0000	0.99706	0.99706
HEU-MET-MIXED-001	0.9995	1.00493	1.00216
HEU-MET-MIXED-002	1.0000	1.00692	1.00671
HEU-MET-MIXED-003	1.0000	1.00774	1.00755
HEU-MET-MIXED-004	0.9999	1.00296	1.00243
HEU-MET-MIXED-015	0.9996	0.99926	0.99709
HEU-MET-MIXED-016	0.9995	1.00123	1.00159
HEU-MET-MIXED-017	0.9995	1.00240	1.00256
HEU-MET-THERM-012	0.9956	1.00937	1.00922
HEU-MET-THERM-014	0.9931	1.00814	1.00783
HEU-MET-THERM-031	1.0037	1.00906	1.00851
HEU-MET-THERM-033	0.9939	1.00365	1.00345
HEU-SOL-THERM-001	1.0004	0.99830	0.99808
	1.0021	0.99610	0.99583
	1.0003	1.00140	1.00146
	1.0008	0.99820	0.99823
	1.0001	0.99868	0.99885
	1.0002	1.00191	1.00214
	1.0008	0.99813	0.99768
	0.9998	0.99814	0.99808
	1.0008	0.99437	0.99429
	0.9993	0.99224	0.99245

*Continued*

TABLE XXI: Comparison of  $k_{\text{eff}}$  results (cont.)

Benchmark	Model $k_{\text{eff}}$	ENDF/B-VII.0 Calculated $k_{\text{eff}}$	ENDF/B-VII.1 Calculated $k_{\text{eff}}$
HEU-SOL-THERM-004	1.0000	0.98577	0.98609
	1.0000	0.98126	0.98273
	1.0000	0.98803	0.98983
	1.0000	0.99051	0.99246
	1.0000	0.98887	0.99098
	1.0000	0.98580	0.98785
HEU-SOL-THERM-006	0.9973	0.98258	0.98182
	0.9986	0.98686	0.98681
	1.0000	0.99850	0.99846
	1.0000	1.00097	1.00084
	1.0000	1.00790	1.00763
	1.0000	0.99927	0.99885
	1.0000	1.00075	1.00082
	0.9973	0.98178	0.98165
	0.9986	0.98652	0.98657
	1.0000	0.99785	0.99768
	1.0000	1.00096	1.00102
	0.9973	0.98122	0.98083
	0.9986	0.98505	0.98460
	1.0000	0.99924	0.99934
	1.0000	1.00681	1.00674
	1.0000	0.99914	0.99906
	1.0000	1.00089	1.00060
	1.0000	0.99957	0.99975
	1.0000	1.00747	1.00727
	1.0000	0.99896	0.99883
	1.0000	1.00089	1.00096
	1.0000	0.99881	0.99862
	1.0000	1.00087	1.00066
	1.0000	1.00791	1.00766
HEU-SOL-THERM-009	0.9990	1.00192	1.00190
	1.0000	1.00253	1.00269
	1.0000	1.00202	1.00216
	0.9986	0.99654	0.99651
HEU-SOL-THERM-010	1.0000	1.00128	1.00121
HEU-SOL-THERM-011	1.0000	1.00460	1.00474
	1.0000	1.00062	1.00070
HEU-SOL-THERM-012	0.9999	1.00104	1.00086
HEU-SOL-THERM-013	1.0012	0.99852	0.99843
	1.0007	0.9975	0.9973
	1.0009	0.9942	0.9942
	1.0003	0.9957	0.9953
HEU-SOL-THERM-020	0.9966	0.99104	0.99294
	0.9956	0.99669	0.99825
	0.9957	1.00510	1.00705
	0.9955	1.00448	1.00639
	0.9959	1.01297	1.01495

*Continued*

TABLE XXI: Comparison of  $k_{\text{eff}}$  results (cont.)

Benchmark	Model $k_{\text{eff}}$	ENDF/B-VII.0 Calculated $k_{\text{eff}}$	ENDF/B-VII.1 Calculated $k_{\text{eff}}$
HEU-SOL-THERM-032	1.0015	0.99932	0.99946
HEU-SOL-THERM-042	0.9957	0.99665	0.99659
	0.9965	0.99657	0.99652
	0.9994	1.00082	1.00064
	1.0000	1.00218	1.00214
	1.0000	1.00006	1.00019
	1.0000	1.00042	1.00031
	1.0000	1.00126	1.00131
	1.0000	1.00201	1.00196
HEU-SOL-THERM-043	0.9986	0.99456	0.99464
	0.9995	1.00542	1.00525
	0.9990	1.00094	1.0009
HEU-SOL-THERM-049	1.0012	0.99917	0.9989
	1.0012	0.98993	0.9908
	1.0012	0.99597	0.9981
	1.0012	0.99526	0.9996
	1.0012	0.99607	1.0029
	1.0012	1.00000	1.0047
	1.0012	1.00023	1.0051
	1.0012	0.99868	1.0041
	1.0012	0.99760	0.9976
	1.0012	0.98907	0.9894
	1.0012	0.99081	0.9919
	1.0012	0.99239	0.9957
	1.0012	0.99189	0.9972
	1.0012	0.99230	0.9982
	1.0012	0.99411	1.0002
	1.0012	0.99211	0.9993
	1.0012	0.99148	0.9977
	1.0012	0.99360	0.9995
	1.0012	0.99388	1.0006
	1.0012	0.99184	0.9989
HEU-SOL-THERM-050	0.9953	1.00778	1.00723
	0.9987	1.00274	1.00277
	0.9984	1.00480	1.00469
	0.9987	1.00449	1.00411
	0.9985	1.00073	1.00090
	0.9985	1.00907	1.00910
	0.9978	0.99817	0.99807
	0.9975	0.99797	0.99806
	0.9966	0.99704	0.99727
	0.9960	0.97979	0.98011
	0.9964	0.99142	0.99150
IEU-MET-FAST-001	0.9989	1.0009	1.0002
	0.9997	1.0013	1.0006
	0.9993	1.0014	1.0012
	1.0002	1.0015	1.0010
IEU-MET-FAST-002	1.0000	0.99914	0.99881

*Continued*

TABLE XXI: Comparison of  $k_{\text{eff}}$  results (cont.)

Benchmark	Model $k_{\text{eff}}$	ENDF/B-VII.0 Calculated $k_{\text{eff}}$	ENDF/B-VII.1 Calculated $k_{\text{eff}}$
IEU-MET-FAST-003	1.0000	1.00228	1.00230
IEU-MET-FAST-004	1.0000	1.00755	1.00734
IEU-MET-FAST-005	1.0000	1.00196	1.00172
IEU-MET-FAST-006	1.0000	0.99616	0.99610
IEU-MET-FAST-007d	1.0045	1.00456	1.00455
IEU-MET-FAST-008	1.0000	1.00557	1.00541
IEU-MET-FAST-009	1.0000	1.01050	1.01064
IEU-MET-FAST-010	0.9954	0.99647	0.99624
	1.0014	1.00287	1.00266
IEU-MET-FAST-012	1.0007	1.00348	1.00329
	1.0014	1.00325	1.00294
IEU-MET-FAST-013	0.9941	0.99721	0.99721
	1.0022	1.00433	1.00410
IEU-COMP-FAST-001	0.9939	0.99319	0.99285
	1.0017	0.99824	0.99486
IEU-COMP-THERM-002	1.0017	1.0032	1.0040
LEU-MET-THERM-002	1.0000	1.01386	1.10457
LEU-COMP-THERM-001	0.9998	0.99987	0.99957
	0.9998	0.99923	0.99901
	0.9998	0.99881	0.99830
	0.9998	0.99938	0.99913
	0.9998	0.99720	0.99712
	0.9998	0.99917	0.99895
	0.9998	0.99837	0.99827
	0.9998	0.99748	0.99743
LEU-COMP-THERM-002	0.9997	0.99854	0.99865
	0.9997	0.99975	0.99997
	0.9997	0.99922	0.99932
	0.9997	0.99902	0.99873
	0.9997	0.99801	0.99776
LEU-COMP-THERM-005	1.0000	1.00350	1.00277
	1.0000	1.00050	0.99946
	1.0000	0.99890	0.99819
	1.0000	0.99820	0.99749
	1.0000	1.00500	1.00504
	1.0000	1.00540	1.00537

*Continued*

TABLE XXI: Comparison of  $k_{\text{eff}}$  results (cont.)

Benchmark	Model $k_{\text{eff}}$	ENDF/B-VII.0 Calculated $k_{\text{eff}}$	ENDF/B-VII.1 Calculated $k_{\text{eff}}$
	1.0000	1.00160	1.00144
	1.0000	1.00160	1.00137
	1.0000	1.00200	1.00196
	1.0000	1.00120	1.00151
	1.0000	1.00200	1.00151
LEU-COMP-THERM-006	1.0000	1.00003	0.99994
	1.0000	1.00047	1.00040
	1.0000	1.00029	1.00033
	1.0000	1.00035	0.99992
	1.0000	0.99990	0.99970
	1.0000	1.00035	1.00035
	1.0000	1.00006	1.00002
	1.0000	0.99992	1.00010
	1.0000	1.00012	0.99997
	1.0000	0.99988	0.99998
	1.0000	0.99994	0.99976
	1.0000	0.99983	0.99983
	1.0000	0.99957	0.99969
	1.0000	1.00016	0.99970
	1.0000	0.99983	0.99965
	1.0000	0.99985	0.99961
	1.0000	0.99957	0.99951
	1.0000	0.99981	0.99944
LEU-COMP-THERM-007	1.0000	0.99763	0.99739
	1.0000	0.99890	0.99889
	1.0000	0.99790	0.99743
	1.0000	0.99836	0.99812
	1.0000	0.99710	0.99690
	1.0000	0.99911	0.99888
	1.0000	0.99874	0.99845
	1.0000	0.99853	0.99802
	1.0000	0.99855	0.99825
	1.0000	0.99886	0.99852
LEU-COMP-THERM-008	1.0007	1.00091	1.00067
	1.0007	1.00118	1.00108
	1.0007	1.00146	1.00154
	1.0007	1.00087	1.00085
	1.0007	1.00011	1.00077
	1.0007	1.00074	1.00093
	1.0007	1.00070	1.00034
	1.0007	0.99968	1.00012
	1.0007	1.00035	1.00007
	1.0007	1.00073	1.00065
	1.0007	1.00164	1.00158
	1.0007	1.00110	1.00085
LEU-COMP-THERM-010	1.0000	1.00571	1.00477
	1.0000	1.00585	1.00494
	1.0000	1.00489	1.00394
	1.0000	0.99703	0.99675
	1.0000	0.99943	0.99957
	1.0000	1.00012	1.00033
	1.0000	1.00102	1.00122

*Continued*

TABLE XXI: Comparison of  $k_{\text{eff}}$  results (cont.)

Benchmark	Model $k_{\text{eff}}$	ENDF/B-VII.0 Calculated $k_{\text{eff}}$	ENDF/B-VII.1 Calculated $k_{\text{eff}}$
	1.0000	0.99807	0.99773
	1.0000	0.99992	0.99989
	1.0000	1.00055	1.00033
	1.0000	1.00063	1.00040
	1.0000	0.99988	0.99973
	1.0000	0.99776	0.99763
LEU-COMP-THERM-011	1.0000	0.99865	0.99845
	1.0000	0.99831	0.99829
	1.0000	0.99855	0.99848
	1.0000	0.99842	0.99825
	1.0000	0.99640	0.99637
LEU-COMP-THERM-017	1.0000	1.00185	1.00149
	1.0000	1.00179	1.00098
	1.0000	1.00034	0.99979
	1.0000	0.99810	0.99803
	1.0000	0.99985	0.99985
	1.0000	1.00022	0.99985
	1.0000	0.99990	1.00000
	1.0000	0.99860	0.99825
	1.0000	0.99767	0.99781
	1.0000	0.99838	0.99822
	1.0000	0.99852	0.99834
	1.0000	0.99878	0.99835
	1.0000	0.99891	0.99874
	1.0000	0.99931	0.99906
LEU-COMP-THERM-022	1.0000	1.00289	1.00263
	1.0000	1.00701	1.00696
	1.0000	1.00739	1.00750
	1.0000	1.00814	1.00794
	1.0000	1.00344	1.00318
	1.0000	1.00148	1.00157
	1.0000	1.00399	1.00414
LEU-COMP-THERM-024	1.0000	1.00131	1.00132
	1.0000	1.00842	1.00873
LEU-COMP-THERM-025	1.0000	0.98829	0.98815
	1.0000	0.99563	0.99567
	1.0000	1.00027	1.00050
	1.0000	1.00236	1.00274
LEU-COMP-THERM-027	1.0014	1.00519	1.00416
	1.0014	1.00735	1.00650
	1.0014	1.00790	1.00729
	1.0014	1.00990	1.00950
LEU-COMP-THERM-035	1.0000	0.99995	0.99972
	1.0000	0.99919	0.99899
	1.0000	0.99537	0.99508
LEU-COMP-THERM-039	1.0000	0.99742	0.99711
	1.0000	0.99827	0.99789
	1.0000	0.99744	0.99745

*Continued*

TABLE XXI: Comparison of  $k_{\text{eff}}$  results (cont.)

Benchmark	Model $k_{\text{eff}}$	ENDF/B-VII.0 Calculated $k_{\text{eff}}$	ENDF/B-VII.1 Calculated $k_{\text{eff}}$
	1.0000	0.99647	0.99636
	1.0000	0.99787	0.99750
	1.0000	0.99746	0.99723
	1.0000	0.99725	0.99703
	1.0000	0.99718	0.99721
	1.0000	0.99689	0.99690
	1.0000	0.99768	0.99741
LEU-COMP-THERM-079	0.9999	0.99879	0.99820
	1.0002	0.99884	0.99866
	1.0005	0.99943	0.99912
	1.0004	0.99929	0.99934
	1.0004	0.99910	0.99956
	0.9994	0.99880	0.99829
	1.0003	0.99797	0.99775
	1.0008	0.99864	0.99886
	1.0003	0.99844	0.99822
	1.0009	0.99904	0.99939
LEU-SOL-THERM-002	1.0038	1.0000	0.9998
	1.0024	0.9959	0.9957
LEU-SOL-THERM-004	0.9994	1.00038	1.00026
	0.9999	1.00153	1.00163
	0.9999	0.99973	0.99959
	0.9999	1.00203	1.00185
	0.9999	1.00197	1.00183
	0.9994	1.00128	1.00107
	0.9996	1.00142	1.00133
LEU-SOL-THERM-007	0.9961	0.99497	0.99503
	0.9973	0.99728	0.99743
	0.9985	0.99614	0.99604
	0.9988	0.99872	0.99869
	0.9983	0.99745	0.99734
LEU-SOL-THERM-020	0.9995	0.99991	0.99987
	0.9996	0.99974	0.99950
	0.9997	0.99896	0.99895
	0.9998	0.99982	0.99997
LEU-SOL-THERM-021	0.9983	0.99772	0.99761
	0.9985	0.99833	0.99810
	0.9989	0.99754	0.99743
	0.9993	0.99957	0.99956
PU-MET-FAST-001	1.0000	0.99996	0.99988
PU-MET-FAST-002	1.0000	1.00000	0.99999
PU-MET-FAST-003	1.0000	0.9981	0.9982
PU-MET-FAST-005	1.0000	1.00940	1.00074

*Continued*

TABLE XXI: Comparison of  $k_{\text{eff}}$  results (cont.)

Benchmark	Model $k_{\text{eff}}$	ENDF/B-VII.0 Calculated $k_{\text{eff}}$	ENDF/B-VII.1 Calculated $k_{\text{eff}}$
PU-MET-FAST-006	1.0000	1.00123	1.00106
PU-MET-FAST-008	1.0000	0.99814	0.99770
	1.0000		0.99836
PU-MET-FAST-009	1.0000	1.00498	1.00505
PU-MET-FAST-010	1.0000	0.99974	0.99968
PU-MET-FAST-011	1.0000	1.00012	1.00023
PU-MET-FAST-018	1.0000	0.99657	0.99939
PU-MET-FAST-019	0.9992	0.99795	1.00074
PU-MET-FAST-020	0.9993	0.99801	0.99791
PU-MET-FAST-021	1.0000	0.99161	1.0044
	1.0000	0.99284	0.9929
PU-MET-FAST-022	1.0000	0.99846	0.99831
PU-MET-FAST-023	1.0000	0.99989	0.99981
PU-MET-FAST-024	1.0000	1.00187	1.00188
PU-MET-FAST-025	1.0000	0.99887	0.99869
PU-MET-FAST-026	1.0000	0.99853	0.99859
PU-MET-FAST-027	1.0000	1.00294	1.00288
PU-MET-FAST-028	1.0000	0.99913	0.99917
PU-MET-FAST-029	1.0000	0.99555	0.99554
PU-MET-FAST-030	1.0000	1.00284	1.00278
PU-MET-FAST-031	1.0000	1.00440	1.00456
PU-MET-FAST-032	1.0000	0.99851	0.99871
PU-MET-FAST-033	0.9967	0.99843	0.99681
	1.0023	1.00266	1.00097
PU-MET-FAST-035	1.0000	0.99782	0.99774
PU-MET-FAST-036	1.0000	1.00645	1.00651
PU-MET-FAST-039	1.0000	0.99231	0.99230
PU-MET-FAST-040	1.0000	0.99670	0.99671
PU-MET-FAST-041	1.0000	1.00594	1.00568
PU-MET-FAST-044	0.9977	1.00535	1.00532

*Continued*

TABLE XXI: Comparison of  $k_{\text{eff}}$  results (cont.)

Benchmark	Model $k_{\text{eff}}$	ENDF/B-VII.0 Calculated $k_{\text{eff}}$	ENDF/B-VII.1 Calculated $k_{\text{eff}}$	
PU-MET-FAST-045	0.9980	0.99995	1.00001	
	0.9977	0.99788	0.99952	
	0.9979	0.99991	0.99997	
	0.9977	0.99909	0.99935	
	1.0000	0.99984	1.00141	
	1.0000	1.01142	1.01251	
	1.0000	1.00644	1.00772	
	1.0000	1.00901	1.01016	
	1.0000	1.00520	1.00629	
	1.0000	1.01279	1.01480	
	1.0000	1.00559	1.00685	
	1.0000	1.01279	1.01379	
	1.0000	1.00638	1.00707	
	1.0000	1.00507	1.00579	
1.0000	1.00427	1.00527		
PU-MET-INTER-002	1.0016	1.02699	1.01481	
PU-COMP-INTER-001	1.0000	1.0120	1.0120	
PU-SOL-THERM-001	1.0000	1.00566	1.00614	
	1.0000	1.00747	1.00771	
	1.0000	1.01067	1.01053	
	1.0000	1.00484	1.00467	
	1.0000	1.00868	1.00852	
	1.0000	1.00955	1.00971	
PU-SOL-THERM-002	1.0000	1.00386	1.00402	
	1.0000	1.00474	1.00458	
	1.0000	1.00378	1.00384	
	1.0000	1.00653	1.00651	
	1.0000	1.00917	1.00939	
	1.0000	1.00524	1.00543	
	1.0000	1.00739	1.00755	
	PU-SOL-THERM-003	1.0000	1.00257	1.00282
		1.0000	1.00217	1.00260
		1.0000	1.00495	1.00481
1.0000		1.00451	1.00448	
1.0000		1.00532	1.00552	
1.0000		1.00573	1.00591	
1.0000		1.00665	1.00679	
1.0000		1.00559	1.00567	
PU-SOL-THERM-004		1.0000	1.00389	1.00385
		1.0000	0.99870	0.99875
	1.0000	1.00066	1.00110	
	1.0000	0.99871	0.99885	
	1.0000	0.99971	0.99990	
	1.0000	1.00152	1.00164	
	1.0000	1.00558	1.00554	
	1.0000	1.00127	1.00135	

*Continued*

TABLE XXI: Comparison of  $k_{\text{eff}}$  results (cont.)

Benchmark	Model $k_{\text{eff}}$	ENDF/B-VII.0 Calculated $k_{\text{eff}}$	ENDF/B-VII.1 Calculated $k_{\text{eff}}$	
PU-SOL-THERM-005	1.0000	1.00044	1.00074	
	1.0000	1.00229	1.00204	
	1.0000	1.00044	1.00063	
	1.0000	1.00320	1.00294	
	1.0000	1.00025	1.00026	
	1.0000	1.00226	1.00239	
	1.0000	1.00268	1.00311	
	1.0000	1.00337	1.00334	
	1.0000	1.00498	1.00539	
	1.0000	1.00628	1.00629	
	1.0000	1.00585	1.00581	
	1.0000	1.00418	1.00432	
	1.0000	0.99919	0.99931	
	1.0000	1.00208	1.00205	
PU-SOL-THERM-006	1.0000	1.00058	1.00079	
	1.0000	1.00171	1.00183	
	1.0000	1.00145	1.00162	
PU-SOL-THERM-007	1.0000	1.00927	1.00945	
	1.0000	1.00367	1.00376	
	1.0000	1.00934	1.00945	
	1.0000	1.00330	1.00324	
	1.0000	1.00531	1.00553	
	1.0000	0.99839	0.99866	
PU-SOL-THERM-009	1.0000	0.99721	0.99731	
	1.0000	1.00110	1.00073	
	PU-SOL-THERM-010	1.0000	1.01920	1.01925
		1.0000	1.01790	1.01820
	1.0000	1.01456	1.01443	
	1.0000	1.00846	1.00853	
	1.0000	1.01236	1.01274	
	1.0000	1.01018	1.01028	
	1.0000	1.00927	1.00956	
	1.0000	1.00248	1.00242	
1.0000	1.00377	1.00379		
PU-SOL-THERM-011	1.0000	1.01500	1.01486	
	1.0000	1.00279	1.00280	
	1.0000	1.00984	1.01011	
	1.0000	1.00954	1.00985	
	1.0000	1.01589	1.01617	
	1.0000	1.00951	1.00956	
	1.0000	1.00990	1.00997	
	1.0000	1.01477	1.01467	
	1.0000	1.01694	1.01676	
	1.0000	1.00929	1.00926	
1.0000	1.00630	1.00644		
1.0000	0.99427	0.99435		
1.0000	1.00041	1.00017		
1.0000	0.99697	0.99688		
1.0000	0.99362	0.99342		
1.0000	1.00342	1.00386		

*Continued*

TABLE XXI: Comparison of  $k_{\text{eff}}$  results (cont.)

Benchmark	Model $k_{\text{eff}}$	ENDF/B-VII.0 Calculated $k_{\text{eff}}$	ENDF/B-VII.1 Calculated $k_{\text{eff}}$
	1.0000	1.00005	1.00041
	1.0000	0.99959	0.99968
PU-SOL-THERM-012	1.0000	1.00560	1.00544
	1.0000	1.00640	1.00587
	1.0000	1.00762	1.00725
	1.0000	1.00768	1.00769
	1.0000	1.00977	1.00966
	1.0000	1.00700	1.00671
	1.0000	1.00576	1.00506
	1.0000	1.00514	1.00458
	1.0000	1.00996	1.00989
	1.0000	1.00440	1.00421
	1.0000	1.00697	1.00658
	1.0000	1.00711	1.00715
	1.0000	1.00977	1.00964
PU-SOL-THERM-018	1.0000	1.00883	1.00839
	1.0000	1.01205	1.01170
	1.0000	1.00994	1.00909
	1.0000	1.00775	1.00743
	1.0000	1.00665	1.00668
	1.0000	1.00502	1.00478
	1.0000	1.00422	1.00380
	1.0000	1.00400	1.00378
	1.0000	1.00244	1.00204
PU-SOL-THERM-021	1.0000	1.0043	1.0036
	1.0000	1.0044	1.0047
PU-SOL-THERM-022	1.0000	1.00006	0.99950
	1.0000	1.00263	1.00213
	1.0000	1.00132	1.00110
	1.0000	1.00166	1.00171
	1.0000	1.00250	1.00219
	1.0000	1.00296	1.00283
	1.0000	1.00457	1.00429
	1.0000	1.00511	1.00463
	1.0000	1.00371	1.00371
PU-SOL-THERM-028	1.0000	1.00795	1.00797
	1.0000	1.00739	1.00734
	1.0000	1.00905	1.00931
	1.0000	1.00879	1.00872
	1.0000	1.00987	1.00976
	1.0000	1.01081	1.01074
	1.0000	1.00821	1.00793
	1.0000	1.00808	1.00830
	1.0000	1.00997	1.00978
PU-SOL-THERM-032	1.0000	0.99613	0.99592
	1.0000	1.00168	1.00143
	1.0000	1.00289	1.00271
	1.0000	1.00250	1.00226
	1.0000	1.00448	1.00462
	1.0000	1.00447	1.00454

*Continued*

TABLE XXI: Comparison of  $k_{\text{eff}}$  results (cont.)

Benchmark	Model $k_{\text{eff}}$	ENDF/B-VII.0 Calculated $k_{\text{eff}}$	ENDF/B-VII.1 Calculated $k_{\text{eff}}$
	1.0000	1.00501	1.00521
	1.0000	1.00454	1.00455
	1.0000	1.00320	1.00329
	1.0000	1.00495	1.00535
	1.0000	1.00439	1.00474
	1.0000	1.00327	1.00350
	1.0000	1.00214	1.00217
	1.0000	1.00196	1.00190
	1.0000	1.00391	1.00429
	1.0000	1.00379	1.00383
	1.0000	1.00383	1.00396
PU-SOL-THERM-034	1.0000	1.00033	1.00010
	1.0000	1.00167	1.00157
	1.0000	0.99935	0.99942
	1.0000	1.00240	1.00264
	1.0000	0.99994	0.99994
	1.0000	1.00147	1.00126
	1.0000	0.99903	0.99869
	1.0000	0.99948	0.99917
	1.0000	0.99824	0.99766
	1.0000	0.99741	0.99722
	1.0000	0.99922	0.99877
	1.0000	0.99864	0.99855
	1.0000	0.99762	0.99702
	1.0000	0.99730	0.99689
	1.0000	0.99785	0.99743
U233-MET-FAST-001	1.0000	0.99964	0.99990
U233-MET-FAST-002	1.0000	0.99907	0.99894
	1.0000	1.00050	1.00024
U233-MET-FAST-003	1.0000	0.99450	0.99928
	1.0000	1.00016	0.99970
U233-MET-FAST-004	1.0000	1.00459	0.99841
	1.0000	1.00500	0.99536
U233-MET-FAST-005	1.0000	0.99427	0.99611
	1.0000	0.99248	0.99537
U233-MET-FAST-006	1.0000	0.99928	0.99862
U233-SOL-INTER-001	1.0000	0.98453	0.98646
	1.0000	0.98031	0.98201
	1.0000	0.98135	0.98267
	1.0000	0.99311	0.99440
	1.0000	0.98477	0.98649
	1.0000	0.98638	0.98771
	1.0000	0.98201	0.98381
	1.0000	0.98173	0.98317
	1.0000	0.97925	0.98094
	1.0000	0.97922	0.98073

*Continued*

TABLE XXI: Comparison of  $k_{\text{eff}}$  results (cont.)

Benchmark	Model $k_{\text{eff}}$	ENDF/B-VII.0 Calculated $k_{\text{eff}}$	ENDF/B-VII.1 Calculated $k_{\text{eff}}$
	1.0000	0.98056	0.98213
	1.0000	0.98102	0.98240
	1.0000	0.98178	0.98339
	1.0000	0.99102	0.99234
	1.0000	0.97999	0.98153
	1.0000	0.98190	0.98236
	1.0000	0.98926	0.99049
	1.0000	0.97850	0.97991
	1.0000	0.97552	0.97689
	1.0000	0.98097	0.98205
	1.0000	0.97340	0.97482
	1.0000	0.97865	0.97975
	1.0000	0.99062	0.99196
	1.0000	0.99201	0.99340
	1.0000	0.98498	0.98639
	1.0000	0.98892	0.99003
	1.0000	0.99097	0.99200
	1.0000	0.98364	0.98439
	1.0000	0.97762	0.97860
	1.0000	0.97886	0.97972
	1.0000	0.99126	0.99209
	1.0000	0.97622	0.97751
	1.0000	0.99410	0.99508
U233-SOL-THERM-001	1.0005	1.00130	1.00139
	1.0010	1.00139	1.00131
	1.0011	1.00087	1.00078
	1.0003	1.00089	1.00070
	1.0004	1.00025	1.00019
U233-SOL-THERM-005	1.0000	1.00192	1.00171
	1.0000	1.00515	1.00518
U233-SOL-THERM-008	1.0006	1.00153	1.00139
U233-SOL-THERM-009	0.9966	0.99612	0.99611
	0.9981	0.99930	0.99920
	0.9989	1.00058	1.00047
	0.9998	0.99934	0.99945
U233-SOL-THERM-012	1.0000	1.00085	1.00098
	1.0000	1.00010	0.99970
	1.0000	1.00962	1.00971
	1.0000	1.00269	1.00280
	1.0000	1.00491	1.00455
	1.0000	1.00599	1.00599
	1.0000	1.00194	1.00199
	1.0000	0.99908	0.99923
U233-SOL-THERM-013	0.9992	1.00532	1.00519
	0.9992	1.00545	1.00543
	0.9992	1.00578	1.00586
	0.9992	1.00637	1.00629
	0.9992	1.00694	1.00705
	0.9992	1.00617	1.00614

*Continued*

TABLE XXI: Comparison of  $k_{\text{eff}}$  results (cont.)

Benchmark	Model $k_{\text{eff}}$	ENDF/B-VII.0 Calculated $k_{\text{eff}}$	ENDF/B-VII.1 Calculated $k_{\text{eff}}$
	0.9992	1.00631	1.00631
	0.9992	1.00734	1.00695
	0.9992	1.00759	1.00734
	0.9992	1.00799	1.00767
	0.9992	1.00524	1.00530
	0.9992	1.00620	1.00599
	0.9992	1.00357	1.00351
	0.9992	1.00684	1.00669
	0.9996	1.02136	1.02178
	0.9996	0.99380	0.99342
	0.9996	0.99678	0.99664
	0.9996	1.00036	1.00008
	0.9996	0.99657	0.99667
	0.9996	0.99995	0.99974
	0.9996	1.00229	1.00247
U233-SOL-THERM-015	1.0000	0.98983	0.99103
	1.0000	0.98518	0.98652
	1.0000	0.98640	0.98737
	1.0000	0.99007	0.99088
	1.0000	0.98623	0.98690
	1.0000	0.97695	0.97756
	1.0000	0.98795	0.98847
	1.0000	0.97362	0.97435
	1.0000	0.96906	0.96971
	1.0000	0.99018	0.99073
	1.0000	0.99289	0.99401
	1.0000	0.99348	0.99470
	1.0000	0.99165	0.99231
	1.0000	0.99832	0.99906
	1.0000	0.98965	0.99040
	1.0000	0.98864	0.98957
	1.0000	0.99818	0.99859
	1.0000	0.97477	0.97542
	1.0000	0.97514	0.97600
	1.0000	0.99491	0.99571
	1.0000	0.99770	0.99840
	1.0000	0.99604	0.99679
	1.0000	0.99402	0.99482
	1.0000	0.99078	0.99138
	1.0000	0.99845	0.99861
	1.0000	0.99398	0.99434
	1.0000	0.99864	0.99903
	1.0000	0.99673	0.99719
	1.0000	0.99550	0.99560
	1.0000	0.99492	0.99524
	1.0000	0.99440	0.99421
U233-SOL-THERM-016	0.9987	1.00391	1.00398
	0.9983	1.00482	1.00504
	0.9992	1.00450	1.00422
	0.9993	0.99611	0.99622
	1.0008	0.99696	0.99678
	1.0011	0.99642	0.99666
	1.0000	1.00488	1.00478
	0.9992	1.00458	1.00461

*Continued*

TABLE XXI: Comparison of  $k_{\text{eff}}$  results (cont.)

Benchmark	Model $k_{\text{eff}}$	ENDF/B-VII.0 Calculated $k_{\text{eff}}$	ENDF/B-VII.1 Calculated $k_{\text{eff}}$
	0.9992	1.00469	1.00461
	0.9993	1.00500	1.00509
	1.0000	1.00551	1.00579
	1.0000	1.00669	1.00678
	0.9994	1.01001	1.01004
	1.0000	0.99533	0.99546
	0.9988	0.99576	0.99546
	1.0000		0.99557
	1.0000	1.00976	1.00979
	1.0000	1.00965	1.00979
	1.0000	1.00988	1.00993
	0.9981	1.00042	1.00011
	0.9980	1.00571	1.00607
	0.9988	1.00375	1.00386
	0.9986	0.99924	0.99945
	0.9985	0.99990	0.99980
	0.9993	0.99951	0.99963
	0.9990	1.01074	1.01049
	0.9985	1.01249	1.01277
	0.9986	1.01258	1.01259
U233-SOL-THERM-017	0.9997	1.00447	1.00449
	1.0000	1.00045	1.00055
	1.0001	1.00533	1.00528
	0.9994	1.00565	1.00553
	1.0000	1.00198	1.00197
	1.0000	1.00088	1.00070
	1.0000	1.00045	1.00037
U233-COMP-THERM-001	1.0006	1.00183	0.99942
	1.0015	1.00486	1.00198
	1.0000	1.00459	1.00223
	1.0007	1.00269	1.00054
	1.0015	1.00233	1.00018
	1.0015	1.00017	0.99859
	0.9995	1.00367	1.00210
	1.0004	1.00162	0.99940
U233-COMP-THERM-004	1.0017		0.99804
MIX-MET-FAST-001	1.0000	0.99938	0.99926
MIX-MET-FAST-002	1.0000	1.00561	1.00527
	1.0000	1.00536	1.00550
	1.0000	1.00537	1.00559
MIX-MET-FAST-003	0.9993	1.00058	1.00072
MIX-MET-FAST-004	0.9993	0.99944	1.00062
	0.9993	0.99909	0.99952

TABLE XXI: Comparison of  $k_{\text{eff}}$  results (cont.)

Benchmark	Model $k_{\text{eff}}$	ENDF/B-VII.0 Calculated $k_{\text{eff}}$	ENDF/B-VII.1 Calculated $k_{\text{eff}}$
MIX-MET-FAST-005	0.9990	1.00393	1.00386
MIX-MET-FAST-007	1.0000	1.00046	1.00342
	1.0000	1.00497	1.00831
	1.0000	1.00260	1.00639
	1.0000	1.00190	1.00536
	1.0000	0.99991	1.00259
	1.0000	0.99938	1.00084
	1.0000	1.00295	1.00615
	1.0000	1.00187	1.00513
	1.0000	1.00166	1.00522
	1.0000	1.00156	1.00519
	1.0000	1.00063	1.00359
	1.0000	1.00072	1.00250
	1.0000	1.00007	1.00085
	1.0000	1.00448	1.00787
	1.0000	1.00407	1.00763
	1.0000	1.00297	1.00615
	1.0000	1.00350	1.00589
	1.0000	1.00651	1.00790
	1.0000	1.00416	1.00691
	1.0000	1.00300	1.00483
	1.0000	1.00424	1.00490
	1.0000	1.00161	1.00393
	1.0000	1.00203	1.00349
MIX-MET-FAST-008	1.0030	1.0191	1.0195
MIX-MET-FAST-009	1.0000	1.00012	1.00034
MIX-MET-FAST-010	1.0000	0.99994	1.00001
MIX-MET-FAST-011	1.0007	1.00343	1.00092
	0.9998	1.00214	0.99984
	1.0018	1.00640	1.00434
	1.0012	1.00584	1.00372
MIX-COMP-FAST-001	0.9866	0.98781	0.98751
	1.0006	1.00594	1.00346
MIX-COMP-THERM-002	1.0024	1.0010	1.0007
	1.0009	1.0022	1.0021
	1.0042	1.0032	1.0024
	1.0024	1.0079	1.0061
	1.0038	1.0046	1.0033
	1.0029	1.0068	1.0053

*Continued*